PREPARATION OF NANOCRYSTALLINE TITANIUM DIOXIDE PARTICLES FROM NEW-ZEALAND ILMENITE

by

RANJEETH KUMAR RAJASHEKAR R

A Thesis Submitted in

Fulfillment of the

Requirements for the Degree of

Master of Engineering

In Chemical Engineering and Nanotechnology

At

Massey University, New Zealand

May 2011

Acknowledgements

I would like to take this opportunity to express my special gratitude to my supervisor, Prof. Richard Haverkamp, not only for giving me once in a lifetime opportunity to go further distance, but also for his invaluable guidance, encouragement and inspiration in my academic life. His willingness to provide me with technical training on some instruments is deeply appreciated, not to mention his advice and unsurpassed knowledge in the field of Chemical Engineering and Nanotechnology. I had almost lost track in thesis work but he got me back to my groove and gave me a chance even though he was tied up with his busy schedule, for which I am extremely grateful. Thank you very much for believing in me sir.

I would like to acknowledge my appreciation to technical staff of School of Engineering and Advanced Technology, in particular Mrs. Ann-Marie Jackson and Mr. John Sykes for their endless assistance with all technical issues I faced during the course of the project. I would like to say special thanks to Mr. Doug Hopcroft from MMIC Electron Microscopy for getting my samples analyzed within the specified time frame. Further I would like to extend my thankfulness to administration staffs, Mrs. Linda Lowe and Mrs. Michele Wagner for their commendable support and assistance.

I am thankful to my family for being very supportive and understanding throughout the research period. They have always inspired me to show positive attitude at rough times. Last but not least I thank Massey University for giving me this wonderful opportunity. I am greatly indebted to all people who are directly and indirectly involved in my research work.

Abstract

Titanium dioxide being one of the most important composite precursors has wide range of application due to the unique properties that it exhibits. TiO_2 with varying amount of anatase and rutile phases were prepared by controlled hydrolysis of dissolved liquor (Ti—Fe—Cl solution) from dissolution of New Zealand ilmenite followed by calcination of the hydrate sample at different temperatures. The kinetics of ilmenite digestion is examined based on the factors affecting the ilmenite dissolution rate such as acid/ilmenite ratio, additive (iron powder) and optimum dissolution temperature. In hydrolysis, the use of structure determining agents (SDA) that alters the morphology of TiO_2 fine particles is analyzed. Samples without SDA have resulted in rutile phase formation at 110°C, while samples with SDA (phosphoric acid/tri-sodium citrate/citric acid) resulted in either anatase phase or mixed phase (both anatase and rutile) at 110°C. The phosphate and citrate ions (0.35% P_2O_5 and 0.4% citrate) helps in promoting an anatase phase of TiO_2 particles. Along with SDA, parameter such as hydrolysis temperature and percentage seed also affects the intermediate product.

The influence of calcination temperature ranging from 925°C—1000°C on anatase-rutile phase transformation and variation in crystallite size was studied. X-ray diffraction (XRD) and scanning electron microscopy (SEM) were employed to characterize the resultant TiO_2 phase, crystallite size and particle size and shape. The degree of conversion to rutile was higher at higher calcination temperature. Introducing potassium additive (0—2 mass% K_2O) in the hydrate sample enhanced the anatase-rutile phase transformation at higher calcination temperature. However, the potassium content in the hydrate sample has a negligible effect on the crystallite

size of anatase and rutile after calcination. The XRD pattern shows an increase in the rutile peak intensity and a decrease in the anatase peak intensity with higher calcination temperature. SEM images show that the particle size of the calcined product at 975°C with 1% K_2O ranges from 230nm—300nm.

Table of Contents

List of Figures

List of Tables

List of Graphs

List of Abbreviations

1D- one dimensional

2D- two dimensional

$2\theta_A$ – Braggs angle of anatase peak

$2\theta_R$ – Braggs angle of rutile peak

3D- three dimensional

AAM - anodic alumina membrane

ALD - atomic-layer deposition

CF-CVC – combustion flame-chemical vapor condensation

CMC – critical micelle concentration

CVD – Chemical vapor deposition

d_A – crystallite size of anatase sample

d_R – crystallite size of rutile sample

DSSC – dye-sensitized solar cell

EPA – Environmental protection agency

ESEM – Environmental scanning electron microscopy

Et-OH – Ethanol

FWHM – Full width at half maximum

GENS – Green earth nano science

HF – Hydrogen fluoride

I_A – Intensity of anatase peak

I_R - Intensity of rutile peak

MOCVD – metal organic chemical vapor deposition

OA - oleic acid

PDMAEMA-b-PFOMA - dimethyl amino ethyl methacrylate-block-1H,1H,2H,2H-perflourooctyl methacrylate

PTCB – peroxo-titanium solution chemical bath

PVC – Poly vinyl chloride

PVD – physical vapor deposition

RBF – Round bottom flask

SDA – Structure determining agent

SEM - scanning electron microscopy

TEOA – triethanolamine

THyCA – transfer hydrolytic crystallization in alcohols

TOPO – trioctylphosphine oxide

TTIP - titanium tetraisopropoxide

UV – Ultra violet

XRD – X-Ray powder diffraction

β_A – FWHM of anatase peak

β_R – FWHM of rutile peak

1 Outline of Research

1.1 Research Aim

This study aims to produce titanium dioxide fine particles from New Zealand ilmenite by controlled hydrolysis using hydrochloric acid and structure determining agents (SDA).

1.2 Key Questions Guiding Research

- What is the scope of this project?
- Is this method readily applicable for industrial purposes?
- Why is concentrated hydrochloric acid used in this procedure?
- Why is iron powder used during dissolution of ilmenite?
- What is the significance of the resultant product?
- Why does addition of phosphoric acid, sodium citrate and citric acid lead to anatase formation?
- What role does potassium play in calcination?
- What role does calcination temperature play on crystallite size and phase of the product?
- How is this method economical?

1.3 Research Objectives

- To produce highly efficient titanium di oxide particles utilizing natural resources from Barrytown, West Coast of South Island (New Zealand).
- To develop a process flow sheet.
- To investigate the role played by structure determining agents (phosphoric acid, tri- sodium citrate and citric acid) in hydrolysis.
- To investigate the effect of calcination on TiO_2 hydrate.
- To examine the effect of potassium additive on calcination.
- To investigate the effect of calcination temperature on TiO_2 phase and crystallite size of TiO_2 particles.
- To obtain TiO_2 particles with desired size and shape.

1.4 Scope of the Project

Titanium dioxide is a material which is being used since long time in a wide range of common and high technique applications because of its moderate price, chemical stability and non-toxicity. Titanium dioxide is reckoned as safe material for human beings and animals. Titanium dioxide is regarded as the strong contender in the field of green chemistry, in photocatalytic systems for the purification of polluted water(Anpo, 2000), the decomposition of offensive atmospheric odors as well as toxins, the fixation of CO_2, and the decomposition of NO/NO_2 and chlorofluorocarbons on a huge global scale.

This project will investigate **Preparation of Titanium Dioxide fine particles** by controlled hydrolysis of dissolved liquor (Ti—Fe—Cl solution) from dissolution of

New Zealand ilmenite (Barrytown, West Coast of South Island) followed by calcination. The method employed in this project has a lower production cost on long-scale and makes a continuous-possible process. The raw materials required for this project are readily available. Concentrated hydrochloric acid used in this method during dissolution can be recovered at the end. This method may also help in producing profitable byproducts (hematite and metal silicates), thus making the wastage disposal effluent free. To the best of my knowledge, there has been no previous reports of this procedure been performed. So this project could be first of its kind. This could lead to an industrial growth in the field of TiO_2 production in New Zealand. In recent years the cost of natural rutile has increased due to scarcity of exploitable deposits, an efficient and cheaper product is produced by using this method. This project also investigates the role of structure determining agents (SDA) like phosphoric acid, tri-sodium citrate and citric acid which helps in producing highly crystalline anatase particles. It is interesting to know the behavior of potassium additive on rutile transformation during calcination. Structural behavior of TiO_2 under elevated temperatures are also studied

2 Literature Review

2.1 Introduction

Titanium is found to be the ninth most abundant element on earth's crust. Earth's crust covers up about 0.57 % of titanium (Seagle, 2000). Titanium (IV) is also called titanium dioxide or titania (named after Greek mythology from word "titans"). Titanium dioxide (TiO_2) naturally occurs in 3 main types of minerals: Rutile, anatase and brookite. The most stable and common form of mineral among them is rutile. On heating anatase hydrates to higher calcination temperatures, anatase phase TiO_2 transforms to rutile phase TiO_2 (Ovenstone & Yanagisawa, 1999). Each contains 6 coordinated titanium components. Rutile and anatase has tetragonal crystal system, whereas brookite has orthorhombic crystal system. The crystal structure of the rutile, anatase and brookite is shown in the following Figure 1.

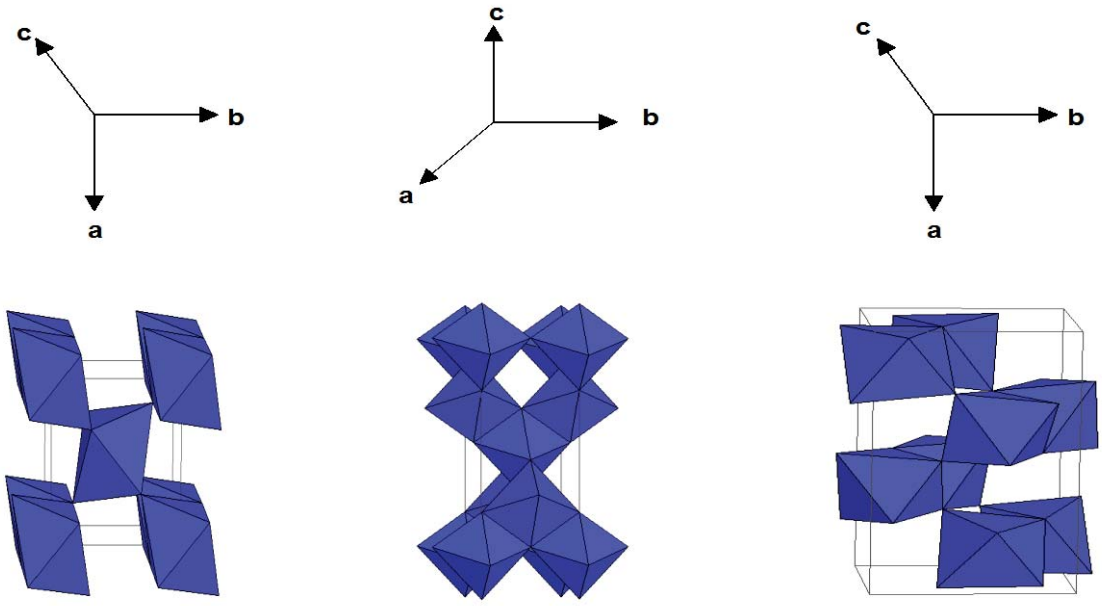

Figure 1: Rutile (left), Anatase (Center), Brookite (right)

TiO_2 is produced in a demanding scale, as approximately 4 million tons of titanium dioxide pigment is consumed annually worldwide (West, Beran, Green, & Kraft, 2007). Titanium dioxide is a commercial product, and it is being widely used in various day to day needs to human life. It has many physical, chemical and biological properties which is a challenge to future technologies. Due to its high refractive index and brightness, it is reckoned as the most widely used white pigment (it has E number E171) on earth which is used in sunscreen, paints, ointments, skimming milk and toothpaste (Wen, Jiang, Qiao, Yang, & Lu; Wikipedia, 2009b). EPA has approved titanium dioxide as the food additive over 42 years ago, hence widely used in food manufacturers, cosmetics, pharmaceutical and other industry. The most interesting fact about titanium dioxide is, it acts as a photo catalyst and can break down organic matter when exposed to UV rays. Hence enormous efforts have been devoted towards TiO_2 materials because of its application, ranging from photocatalytic and photovoltaic properties to photo electrochromic and sensors.

2.1.1 Submicron structured Titanium Dioxide

In most cases, the size of the titanium dioxide particle influences the performance of the materials (B. Li, Wang, Yan, & Li, 2002). Now, increasing demands are emphasized on TiO_2 particle at submicron scale in the field of cosmetic products, ceramics, ultraviolet light absorber and photocatalyst (BIN XIA, WEIBIN LI, BIN, & XIE, 1999). Submicron particles exhibit a distinctive and enhanced physical, chemical, mechanical and biological properties compared to macro or larger particle size, which make them suitable for many technological applications (Anal K. Jha, K. Prasad, & Kulkarni, 2009). TiO_2 has excellent optical transmittance, high refractive index, photo activity, chemical stability, semi conductivity, hydrophillicity, biocompatibility, corrosion resistance, etc. In photochemical solar cell application, submicron TiO_2 has

unique properties such as high incident-photo-to-current conversion efficiency (Jianshu Lu, et al., 2009).

TiO_2 is considered as the efficient heterogeneous photocatalyst because it is highly photoactive, stable, non-toxic and inexpensive. Many studies have shown that anatase form of TiO_2 is more photoactive than rutile form (Mohammad, Modirshahla, Mohammad Shokri, & Zeininezhad, 2008). Several preparation methods are being examined to develop the best method of producing titanium dioxide powders, as it comprises of many favorable properties such as small particle size, high surface area, controlled porosity and tailored-designed pore size distribution (J. Zhu, et al., 2007).

Some of the common methods that are being followed in production of submicron titanium dioxide are sol-gel process, hydrothermal synthesis, chemical vapor deposition (CVD), solvothermal method, vapor phase hydrolysis, peroxo-titanium solution chemical bath (PTCB) route, combustion flame-chemical vapor condensation (CF-CVC) method, microbial method. The preparation methods play a vital role in obtaining highly significant morphological, structural, surface physicochemical and electronic properties that are directly proportional to photo activity (Maurizio Addamo, Vittorio Loddo, & Leonardo Palmisano, 2004). Titanium dioxide fine particles exhibits some unique properties such as antimicrobial, self-cleaning and air purification properties which are breakthrough to coating technology adopted by GENS nano Inc (GENS Nano Inc, 2010).

2.2 Properties of Titanium Dioxide

2.2.1 Photocatalytic Property

Photocatalysis is the process which uses light to activate a semiconductor material which can modify the rate of chemical reaction without being involved itself (TiPE,

2003-2008). Chlorophyll of the plant has a habitual nature. A difference between chlorophyll and a semiconductor material which acts as a photo-catalyst is that, usually chlorophyll captures sunlight to turn water and carbon dioxide into oxygen and glucose (Lichtenthaler, 1988), but on the contrary semiconductor material creates strong oxidation agent and electronic holes to breakdown the organic matter to CO_2 and H_2O in the presence of sun light, which is more than or equal to its band gap (T. Aarthi, Prashanthi Narahari, & Madras, 2007). The above explanation is shown in the following figure 2.

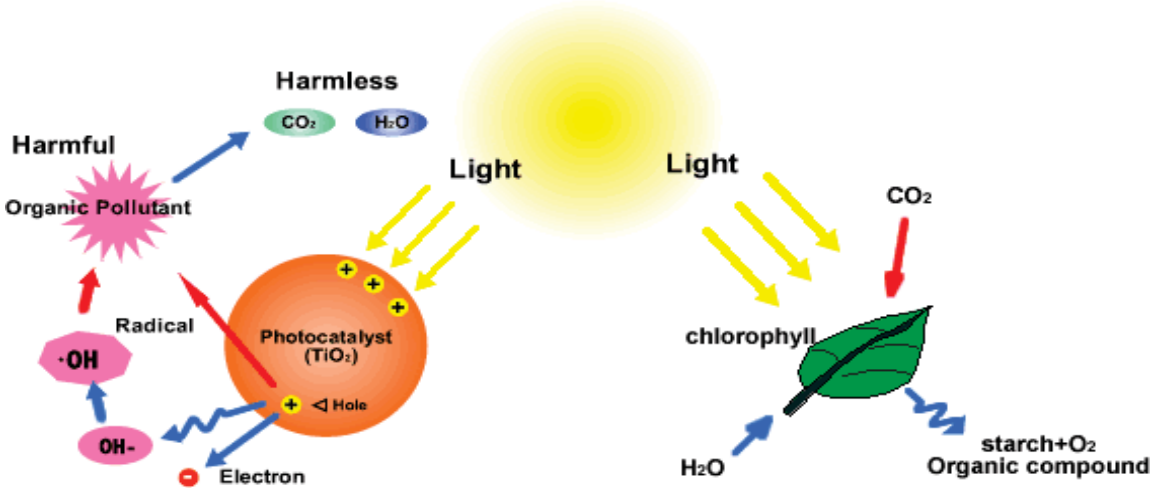

Figure 2: TiO_2 Photo-catalyst (H. A. Lim, 2003) and Chlorophyll

The mechanism of TiO_2 photo-catalyst is that, it absorbs UV radiation from sunlight or illuminated light source (fluorescent lamps), which will produce a pair of electron and holes. The illuminated light excites the electron of the valence band of TiO_2. The excited electron produces excess energy to promote the electron to the conduction band of TiO_2 thus creating positive hole (h+) and negative electron (e-), which is known as semiconductor's 'photo-excitation' state (TiPE, 2003-2008). Band gap is the energy difference between the valence and conduction band. For photo-excitation, the light wavelength required is 1240 (Planck's constant, h)/3.2 eV (band gap energy) =

388nm. H_2 gas and hydroxyl radical (powerful oxidant) are formed from the water molecule by positive-hole (A Fujishima & Honda, 1972) while super-oxide anion is formed by negative-electron with O_2. This cycle continues till the availability of sunlight. The above explanation is shown in the following figure 3. The above photocatalyst can be employed in the form of colloid or as an immobilized film (Wen-Yu Wang, 2008).

Chemical Reactions:

$$TiO_2 + 4H_2O + Air\ flow + UV\ light \longrightarrow Ti(OH)_3 + 2H_2 + OH^- + O_2^-$$

(Stable) (Reactive) (Reactive)

"Recycling Effect"

$$Ti(OH)_3 + O^-_2 \rightarrow TiO_2 + H_2\ (g)$$

$$Ti(OH)_3 + 2H_2 + OH^- + O_2 \rightarrow TiO_2 + 4H_2O$$

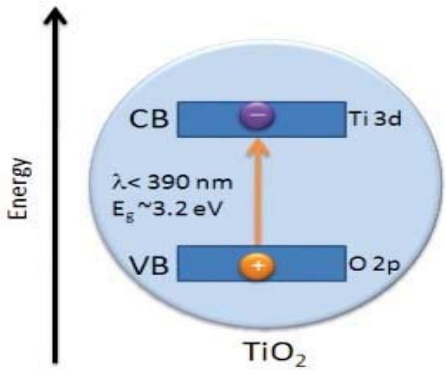

Process	Name
$TiO_2 + h\upsilon \rightarrow h_{VB}^+ + e_{CB}^-$	Charge Separation
$h_{VB}^+ + H_2O \rightarrow OH^\bullet$	$OH^\bullet$ Generation (VB)
$e_{CB}^- + O_2 \rightarrow O_2^{\bullet-} + H_2O \rightarrow OH^\bullet$	$OH^\bullet$ Generation (CB)

Figure 3: Band energy level diagram of TiO_2 photocatalyst (Bahnemann, D et.al 2004)

TiO_2 photocatalyst is commonly used in oxidizing organic pollutants and decolorizing dyes. Some organic pollutants are degraded and completely mineralize under UV radiation on TiO_2 catalyst (Mohammad, et al., 2008). A number of researches are being conducted to optimize the performance of TiO_2 photocatalyst with high surface area (L. Zhang, Zhu, He, Li, & Sun, 2003). Eventually one would like to have a material which can absorb full solar spectrum with highest specific surface area on to the smallest foot print (F Di Fonzo, et al., 2009).

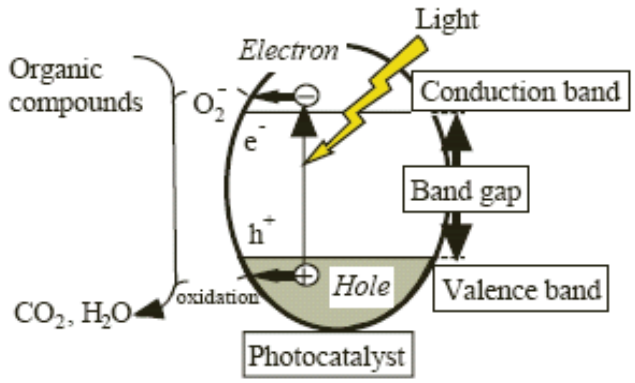

Figure 4: The schematic representation of the mechanism of photocatalysis (Kathirvelu, S., D'Souza, L., & Dhurai, B. 2008)

A multistage organization with hierarchical structure and with large and accessible surface area is suitable for photocatalytic application just like a forest assembly starting from a single tree, with trunk, branches and leaves which has a hierarchical and organized structure where the gaseous exchange is maximized with atmosphere by maximizing the leaf area at the same time optimizing the exposure of leaf to the sunlight (F Di Fonzo, et al., 2009).

2.2.2 Super-Hydrophilic Property

When the surface of photocatalytic TiO_2 film is exposed to light, the contact angle of the photo-catalyst surface with water is reduced gradually. After enough exposure to light, the surface reaches its super-hydrophilic state(Boi Shield Inc, 1999-2009). In other words, it does not repel water at all. So water cannot exist in the shape of a drop, but spreads flatly on the surface of the substrate and the water takes the form of a highly uniform thin film, which behaves optically like a clear sheet of glass. If the water-surface angle is greater than 130° or less than 5°, then the surface is said to be super- hydrophobic or super-hydrophilic respectively (X. Chen & Mao, 2007). The mechanism of super-hydrophilicity is explained when TiO_2 surface is irradiated to UV light. The photogenerated hole reacts with lattice oxygen to form surface oxygen vacancies. On this surface the water tends to spread out flat with a contact angle of about 0° instead of moulding up. The photogenerated hole weakens the binding energy between Ti atom and the lattice oxygen, thus the adsorbed water molecules breaks the $Ti-O-Ti$ bond to form 2 new $Ti-OH$ bonds making them super hydrophilic. This surface not only adsorbs polar but also non polar liquids.

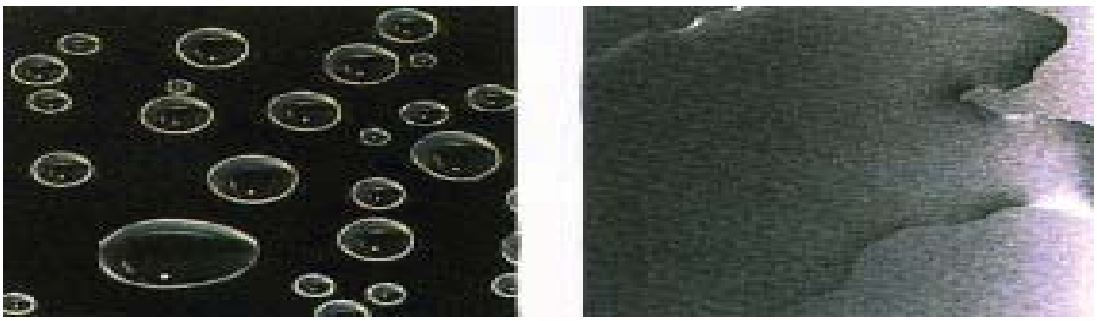

Figure 5: Hydrophilic mechanism (T. Hashimoto, Yoko, & Sakka, 1994)

When the water is rinsed over the surface, the contaminants like oil and dust are washed away. The films when placed in dark, the adsorbed hydroxyl groups were

steadily replaced by atmospheric oxygen resulting in the surface evolving back to its original state. The hydrophilic nature of titanium dioxide, coupled with the gravity, will enable the dust particles to be swept away following the water stream, thus making the product self-cleaning (J. Chen & Poon, 2009).

2.2.3 Electrocatalytic Property

TiO_2 has great importance for electrocatalytic application because of oxidizing power of its holes. It is observed that TiO_2 with larger surface area exhibits high electrocatalytic efficiency than TiO_2 with smaller surface area. The reason being large surface area enhances the electron transfer thus increasing the electrocatalytic activity. A number of researches are being carried out to improve the electrocatalytic properties by enhancing the surface area (D. Chu, et al., 2008). There has been a lot of focus on the use of mesoporous semiconductor as a support for large surface area catalyst (D. V. Bavykin, 2006). Some of the examples in which submicron particles are used as mesoporous catalyst support are as follows:

Pd/ TiO_2 used in oxidation of methanol fuel cell: Compared to TiO_2 particles or pure palladium as substrate, palladium dispersed on TiO_2 tubes was most effective electrocatalyst with respect to the high surface-volume ratio which might act as a hopeful catalyst in direct oxidation of methanol fuel cells. In an experiment perfomed by Wang and coworkers, electro-oxidation of methanol in sulfuric acid solution was studied using palladium well-dispersed on TiO_2 tubes. Pd dispersed on TiO_2 showed excellent catalaytic activity due to high surface area substrate. The TEM results obtained showed the diameter of TiO_2 hydrolyzed from $TiCl_4$ and $Ti(OBu)_4$ are about 10nm and 30nm repectively. These particles have uniform morphologies and the phenomenon of reuniting is not visible. Of all catalyst examined, it was found that Nafion supported 3wt% Pd-TiO_2 tubes give the best oxidation activity due to its

morphological TiO_2 accessibility, optimum combination of catalytic activity, proton conductivity and stabilization of catalysts (M. Wang, Guo, & Li, 2005).

RuO_2/ TiO_2 used in CO_2 reduction: RuO_2/TiO_2 submicron particles were prepared by lining RuO_2 on TiO_2 submicron particles repectively. The continuous potentiostatic electrolysis of CO_2 led to formation of methanol even under low overpotential. The conversion of CO_2 to methanol showed current efficiency upto 60.5% on RuO_2/ TiO_2 modified Pt electrode. By dispersing RuO_2 on TiO_2 surface with higher surface area can increase the effective area of the electrode, enhancing the utilization of RuO_2 for CO_2 reduction and creating more active sites which is then introduced on a Pt electrode, which makes them stable for long time electrolysis. This appeared to be the promising electrocatalyst for electrochemical reduction of CO_2 to methanol (Qu, Zhang, Wang, & Xie, 2005).

Nb-doped TiO_2 as Pt support in DSSC (Dye-Sensitized Solar Cell):

Mesoporous nobium (Nb)-Doped TiO_2 was prepared by sol-gel method on a transparent conducting FTO glass, which was examined as a stable Pt support in DSSC electrode. In this experiment, Pt submicron particles were impregnated in the mesoporous TiO_2 support substrate and tested for counter electrode in dye-sensitized solar cell (DSSCs). The use of Nb is necessary to increase the conductivity of the film to allow its use in electrocatalytic reactions. By fabricating Pt/Nb doped TiO_2 electrode, the charge transfer resistance and exchange current density can be controlled. The impregnation of Pt in mesoporous TiO_2 can also improve the mechanical rigidity and stability of electrocatalyst against abrasion. Nb increases the conductivity of the film in electrocatalytic applications. Pt with large surface area in Pt/Nb-doped TiO_2, it is observed that there is an increase in exchange current density

and less charge transfer heat. Hence Pt loading is directly proportional to the exchange current density of Pt/Nb-doped TiO_2 electrode (Hasin, Alpuche-Aviles, Li, & Wu, 2009)

2.2.4 Structural Property

Unit cell structure of rutile and anatase can be best described in terms of TiO_6 octahedra chains in which octahedron of six O^{2-} ions surround every Ti^{4+} ion. In anatase structure, each octahedron is in contact with 8 neighboring octahedron (4 sharing an edge and 4 sharing a corner), while in rutile structure each octahedron is in contact with 10 neighboring octahedron (2 sharing edge O_2 pairs and 8 sharing corner O_2 atoms) (X. Chen & Mao, 2007). The variation in mass densities and electronic band structures are due to different lattice structure exhibited by the 2 forms of TiO_2 (Linsebigler, Lu, & Yates, 2002). Anatase and rutile crystal structure varies by their grouping pattern of octahedral chains and deformation of each octahedron. In anatase, the octahedron is largely distorted so that its orthorhombic evenness is less than rutile, while in rutile there is little orthorhombic distortion in octahedron. The Ti-O distance is larger in rutile, whereas Ti-Ti distance is shorter than those in anatase (Y. Q. Wang, Yu, & Sun, 2007).

Swamy et al concluded that anatase is metastable and is a function of pressure dependent on size, defending the structure to high pressure with small crystallite size. Pressure induced phase transition of anatase is witnessed by 3 size system; an anatase-amorphous transition system (smallest crystallite size), an anatase-baddeleyite transition system (intermediate crystallite size) and an anatase-αPbO_2 transition system (large submicron crystals) (Swamy, et al., 2005). Submicron crystalline morphology and phase stability was influenced by surface passivation (Barnard & Curtiss, 2005; Barnard & Zapol, 2004; Barnard, Zapol, & Curtiss, 2004,

2005). They found that shape of rutile submicron crystals were changed by stimulating surface hydrogenation but had little or no effect on anatase. From the results obtained by Barnard et al it is evident to say that, below cross point anatase phase was more stable than rutile. They also found that the phase transition size in water (15.1 nm) was greater than that under vacuum (9.6nm) when TiO_2 submicron particles subjected to vacuum or water environments.

2.2.5 Thermodynamic Property

Among the 3 phases of TiO_2, rutile is the most thermodynamically stable phase, while anatase and brookite are metastable at higher temperature, transforming to rutile when they are heated. This doesn't mean anatase and brookite is not stable, infact they are stable at small particle sizes (H. Zhang & Banfield, 1998, 2000). Following transformation is commonly observed on heating: anatase to brookite to rutile; brookite to anatase to rutile; anatase to rutile and brookite to rutile(X. Chen & Mao, 2007). Based on the preparation method of TiO_2 submicron particles its crystal structure was classified (Hwu, Yao, Cheng, Tung, & Lin, 1997). For smaller TiO_2 submicron particles (<50nm) anatase appeared more stable and transformed to rutile at a temperature higher than 700°C. It is evident from the experiment conducted by Banfield et al that anatase and brookite transforms to rutile after reaching certain particle size. He also showed that anatase with particle size >14nm is less stable than rutile, as rutile formation was initiated it grew much faster than anatase (H. Zhang & Banfield, 2000). Ye et al concluded that brookite could not transform directly to rutile but had to first transform to anatase (Ye, Sha, Jiao, & Zhang, 1997). But Kominami et al showed that direct transformation of brookite to rutile is possible above 700°C (Kominami, et al., 1999).

The transition of anatase to rutile occurs at temperature ranging from 600°C–1100°C depending on the presence of impurities in anatase which tends to enhance the transition rate such as Cu^{2+}, Co^{2+}, Fe^{2+} etc and impurities such as SO_4^{2-}, PO_4^{3-} etc tend inhibit the transition rate to some extent. In rutile there are straight chains if octahedral; in anatase zig-zag chains. In both structures TiO_2 is present as TiO_6 octahedra which shares edges and corners, due to requirement of electroneutrality equal number of empty oxygen octahedral are present. Due to high activation energy at higher temperature substantial rearrangement of structure occurs during transition. Hence the kinetics of anatase to rutile transition is observed as a result of shrinkage of oxygen structure and a cooperation movement of ions(Shannon & Pask, 1965). Higher temperature not increases rutilization but also increases the crystallite size and particle size and particle size which leads to rearrangement of photo-generated holes and electrons, thus inhibits the photocatalytic activities. With better transition rate, the product exhibits higher refractive index and lower porosity. This transition is irreversible due to expansion of crystal lattice, recrystallization followed by formation of rutile nuclie and crystallite growth. In anatase to rutile transition, rutile nucleates at the interface, on the surface and in the bulk. The predominant mode may change from interface nucleation at low temperature to surface nucleate, ion at intermediate temperature and to bulk nucleation at very high temperature (B. Grzmil et al., 2004).

Zhang and Banfield concluded that, in an evenly size submicron materials, anatase was thermodynamically stable for sizes <11nm; brookite was stable for sizes between 11nm and 35nm and rutile was stable for size >35nm (H. Zhang & Banfield, 2000). Ranade et al investigated that, the lack of course-grained anatase was steady for its phase change to rutile with larger driving force (Ranade, et al., 2002). Rutile phase

transformation from anatase seems to occur at the temperature range of 700-800°C (W. Li, Ni, Lin, Huang, & Shah, 2004). Growth rate of rutile was higher than anatase. As a result of nucleation, rutile particle grew rapidly, while anatase showed no change. Hence the growth rate of anatase is inhibited at 800°C. With the increase in activation energy, size related surface enthalpy and less stress energy results in good thermal stability in submicron TiO_2 particle (W. Li, et al., 2004).

2.2.6 Electronic Property

Electronic property of n-TiO_2 has been studied with various experimental techniques like X-ray photoelectron, X-ray absorption and emission spectroscopes (H. C. Choi, et al., 2004; Finkelstein, et al., 1999; Hwu, et al., 1997; Luca, Djajanti, & Howe, 1998; Z. Y. Wu, Ouvrard, Gressier, & Natoli, 1997; Zimmermann, Steiner, Claessen, Reinert, & Hüfner, 1998). In TiO_2, density of states is composed of Ti t_{eg}, Ti t_{2g} (d_{yz}, d_{zx} and d_{xy}), Op_σ (in the Ti_3O cluster plane), and Op_π (out of Ti_3O cluster plane) as shown in the following figure. The upper valence band can be divided into mainly 3 regions: the σ bonding in the lower energy region due to Op_σ bonding; the π bonding in the middle of energy region; Op_π states in the higher energy region due to Op_π non-bonding states at the top of the valence bands. Here, the contribution of σ bonding is much stronger than that of π bonding (X. Chen & Mao, 2007). The conduction band were also divided into of Ti_{eg} (>5eV) and Ti t_{2g} bands (<5eV) where the bottom of the conduction band are dominated by d_{xy} states and t_{2g} band antibond with p states (Asahi, Taga, Mannstadt, & Freeman, 2000).

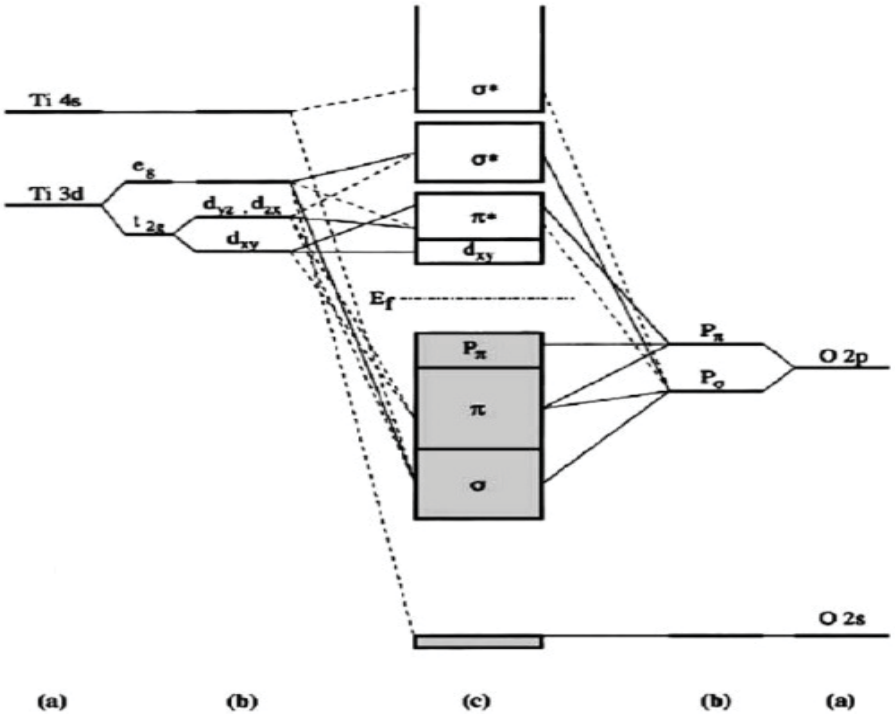

Figure 6: Molecular-orbital bonding structure for anatase TiO_2: (a) atomic levels, (b) crystal-field split levels, and (c) final interaction states. The thin-solid and dashed lines represent large and small contributions, respectively (Asahi, R et.al 2000)

The Molecular orbital bonds in case of anatase shows the nonbonding O_{pp} orbital at the top of the valence band and the nonbonding d_{xy} states at the bottom of the conduction band. A similar but less prominent feature is observed in rutile where each octahedron shares corners with 8 neighbors and shares edges with 2 other neighbors forming a linear chain with high density (4.50g/cm^3) (X. Chen & Mao, 2007). Whereas in case of anatase each octahedron shares corner with 4 neighbors and shares edges with 4 other neighbors resulting in zigzag chain with the screw axis, which is less dense (3.89 g/cm^3) than rutile. The metal–metal distance in rutile is small (2.96 A°) which are provided by t_{2g} orbital at the bottom of the conduction band. Whereas metal- metal distance is large (5.35 A°) as a result of isolation of Ti d_{xy} orbital at the bottom of the conduction band (Sorantin & Schwarz, 2002).

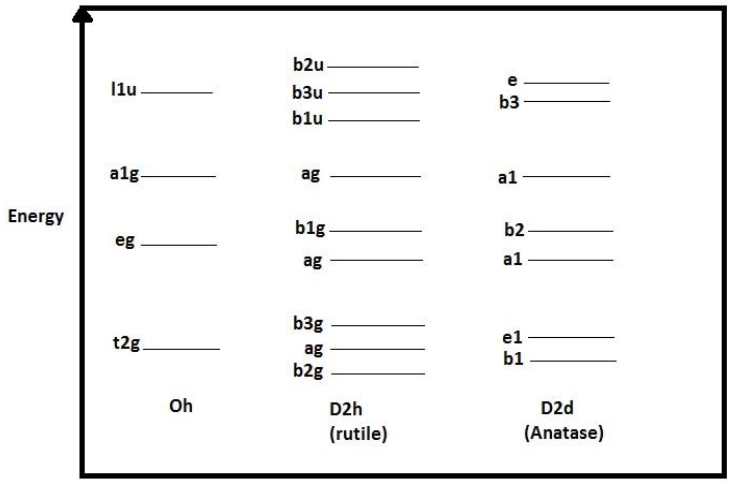

Figure 7: Schematic energy level diagram of the lowest unoccupied MOs of a $[TiO_6]^{8-}$ cluster with O_h, D_2h (rutile), and D_2d (anatase) symmetry (Wu, Z.Y et.al 1997)

Hwu et al found that the difference in Ti 2p and O1s X-ray absorption edges of bulk and crystalline TiO_2 is due to the structural difference between anatase and rutile. In this procedure, soft X-ray absorption spectroscopy was used to explore the electronic structure of TiO_2. Spectral features (high energy spectra of Ti 2p absorption edge) similar to titanium in anatase were revealed. Thus, approximating Ti in +4 valence state (Hwu, et al., 1997). In another experiment performed, the measured absorption spectra of anatase and rutile by Tang et al concludes that the excitons in rutile are free, while in anatase are trapped which is similar to previous photoluminescence studies by Tang (H. Tang, Lévy, Berger, & Schmid, 1995).

2.2.7 Optical Property

In case of optical properties, the photon networks with the system to fabricate an electron-hole pair. Besides polarization clouds, excitons and above threshold resonances are obtained with the strong interaction of electron and hole (Benedict & Shirley, 1999). It is also understood that there properties can only be modeled with 2

particle state and not with effective one particle state. Recently few studies are based on developing metal oxide semiconductor material with advantageous optical properties such as photoluminescence, electro luminescence and nonlinear optical properties (Ramakrishna & Ghosh, 2003). Hence TiO_2 is a large band gap semiconductor. Its transparency to visible light is due to its high refractive index (@ λ=550nm, n=2.54 for anatase or 2.75 for rutile).

The TiO_6 octahedron structures, which are the building block of rutile and anatase helps in deciding the refractive index (Z. Wang, Helmersson, & Käll, 2002). Inter band electron transitions are the result of light absorption mechanism in pure semiconductors, which are very small in indirect semiconductors like TiO_2. This is because crystal symmetry of TiO_2 that prohibits the direct electron transition between band centers. An enhancement of absorption is observed in large interface atoms like TiO_2 submicron crystals, porous and microcrystalline semiconductor. Due to lower dimensionality ($3D \longrightarrow 2D$ transition), band gap of bulk TiO_2 were smaller than the band gap of TiO_2 (Sakai, Ebina, Takada, & Sasaki, 2004; Sato, Ono, Sasaki, & Yamagishi, 2003).

Several effort have been put forth to produce a semiconductor material with optically high refractive index. Desirable optical quality of TiO_2 is still difficult (Aarik, Aidla, Kiisler, Uustare, & Sammelselg, 1997). In an experiment conducted by Aarik et al, an amorphous titanium films having high refractive (up to 2.65) with optical band gap of 3eV are obtained by atomic-layer deposition (ALD) of titania. In this experiment, the optical property can be tuned by varying the temperature from 100°C—300°C (Aarik, et al., 1997). The particle size also influences the optical properties of a material. Energy bands are split into discrete quantized energy level, as a result of diameter of crystallite approaching the exciton Bohr diameter. This effect is called quantum size.

This effect is relatively small, as only microscopic particles can acquire an increased band gap(Kormann, Bahnemann, & Hoffmann, 2002).

Splitting of energy bands into distinct quantized energy level occurs, as the diameter of crystallite approaches the exciton bohr diameter. This is so called quantum size effect. Size quantization leads to a blue shift in the absorption spectrum due to increased band gap, nonlinear optical properties and unusual luminescence. Ultrafine and fine TiO_2 particles have comparatively small band gap blue shift (Madhusudan Reddy, Gopal Reddy, & Manorama, 2001). The particles showed a concomitant blue shift in absorption spectrum with decrease in particle size. Size quantization causes the absorption edge to be shifted to higher energies. The size dependent shift in bandgap is found to be 0.1eV–0.2eV. In another experiment performed by Serpone et al. it was suggested that quantum confinement effect was not responsible for the small blue shift, this was actually due to direct electronic transitions for microscopic particles (Serpone, Lawless, Khairutdinov, & Pelizzetti, 2002).

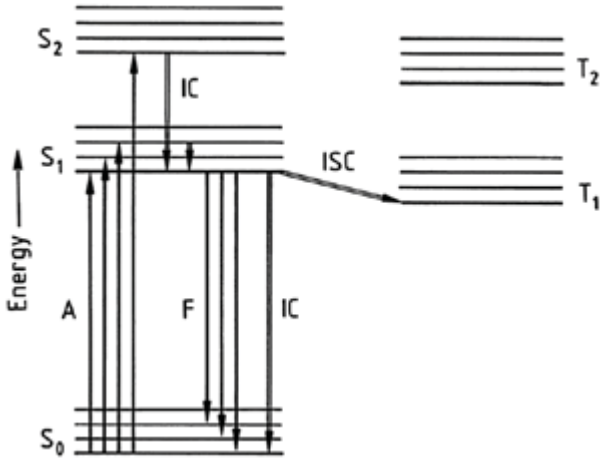

Figure 8: Energy diagram of optical brighteners and transitions (Siegrist, A.E et.al 2003) A = absorption; F = fluorescence; IC = internal conversion; ISC = intersystem crossing; S = singlet state; T = triplet state

Absorption (A) of light quanta by the TiO_2 molecules induces transitions from the singlet ground state S_0 to vibrational levels of the electronically excited singlet states S_1 and S_2. The electronic state and vibrational level reached depend on the wavelength of the absorbed light. Absorption occurs within ca. 10^{-15} s and results in a gain in energy E and a change in the electron distribution within the TiO_2 molecule. TiO_2 molecules that have been excited to a higher electronic state such as S_2 or into a higher vibrational level of S_1 relax by a nonradiative process within ca. 10^{-12} s to the vibrational ground state of S_1 (internal conversion, IC), which has a lifetime of ca. 10^{-9} s. This time is sufficient for the brightener geometry to adapt to the electron distribution in the S_1 state.

Bavykin proved that the optical properties of TiO_2 submicron particles were similar with different inner diameter ranging from 2.5nm—5nm. This study was based on absorption and photoluminescence of colloidal TiO_2 submicron particles (Bavykin, Gordeev, Moskalenko, Lapkin, & Walsh, 2005).

2.3 Preparation methods

A number of preparation methods that have been developed over years for the manufacture of submicron TiO_2 particles for its photocatalytic, superhydrophilic, electrocatalytic properties. Hence most economical and efficient methods are being adopted for manufacture of sub-micron structured TiO_2 on a large scale. Some of which are explained below.

2.3.1 The sulphate process

Though sulphate process is complex in operation, it depends on a series of simple chemical reaction as shown below.

$$FeTiO_3 + 2H_2SO_4 \longrightarrow TiOSO_4 + FeSO_4 + 2H_2O$$

$TiOSO_4 \longrightarrow TiO_2.nH2O + H_2SO_4$

$TiO_2.nH_2O \longrightarrow TiO_2 + nH_2O$

The chemical reactions involved in sulphate process are conversion of the ilmenite ore, using sulphuric acid to form titanyl sulphate which, through hydrolysis, is converted to hydrated titanium dioxide. The ilmenite ore, previously dried and ground is digested with sulphuric acid. The strength of the acid is usually 85-92% but is adjusted according to the composition of the ore. Digestion may be a continuous or batch operation. The mixture of ground ore and sulphuric acid is agitated by compressed air and superheated steam is blown in. When the temperature reaches about 100°C a vigorous exothermic reaction starts and the mixture is converted to a porous cake which may contain ferrous, ferric and titanium sulphates. This cake is dissolved in water or dilute acid to form black liquor. The liquor is then clarified by sedimentation to remove unwanted residues.

Hydrolysis of the liquor is performed to produce a precipitate of hydrous titanium dioxide. Through boiling for several hours precipitation occurs. Appropriate nuclei, prepared from titanium tetrachloride can be added at this stage, or later during calcination. Hydrolysis of industrial titanyl sulfate solution ($TiOSO_4$ solution, black liquor) is the essential step of the process. Hydrolysis undergoes 3 steps, i.e. grain formation of crystallization, nuclei growth and hydrated titania precipitation, aggregation of hydrated titania and composition changes of the precipitation. Hydrolysis of hydrous titanium ion is a rapid reaction, but can be inhibited by acidity. Higher acidity may reduce the nucleation rate, and accelerate the crystal growth rate, leading to larger microcrystal, then aggregate smaller colloidal particle.

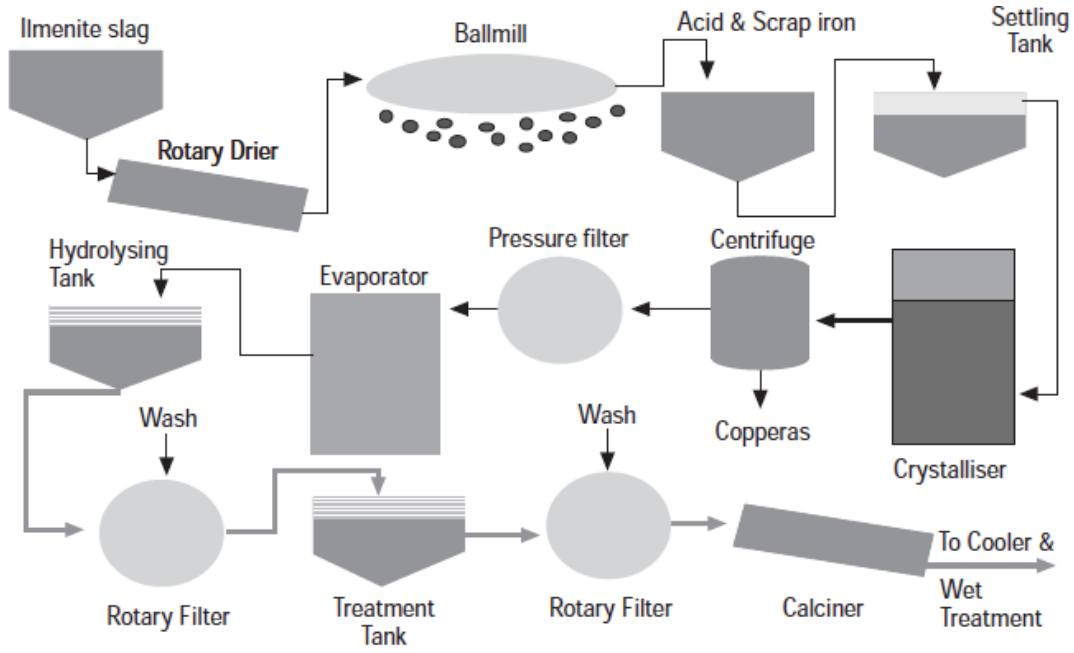

Figure 9: Schematic diagram of the sulphate process (Reck and Richard 1999)

Ideally, no ferric iron should be present so any ferric ion present is reduced to ferrous through addition of scrap iron. The precipitate formed at this stage is in the anatase form depending on the type of nuclei added, either rutile or anatase will be formed during calcination. The precipitated pulp is leached under reducing conditions to remove any remaining iron and is then calcined. During calcination, the wet pulp is dried rotary kiln, This process removes water, SO_2 and SO_3 which are driven off. The acidic, gaseous effluent is washed to remove the SO_3 and then passed through a bed of activated carbon where the SO_2 is converted to sulphuric acid. The growth of crystals and conversion to rutile occurs in the calciner in which the temperature of 1000°C is maintained.

2.3.2 Sol-Gel Method

Sol-gel method is used mainly in manufacturing ceramic materials (X. Chen & Mao, 2007; Hench & West, 1990; Pierre & Pajonk, 2002; Schwarz, Contescu, & Contescu,

1995; Wight & Davis, 2002). Precursors used in sol-gel are usually metal organic compounds or inorganic metal. In sol-gel process, formation of colloidal substance or sol is a result of hydrolysis and polymerization of precursor. The change of phase from liquid sol into solid gel phase is a result of loss of solvents and complete polymerization. Further wet gel is transformed into dense ceramic by drying and heat treatment (X. Chen & Mao, 2007). This method is adopted for the preparation of submicron TiO_2.

The initial stage of hydrolysis of Ti(IV)-alkoxide can be decribed by the following reaction.

Hydrolysis:

$$\equiv Ti{-}OR + HOH \longrightarrow \equiv Ti{-}OH + R{-}OH.$$

The mechanism of this reaction can be considered in terms of (a) nucleophilic attack of Ti by a water oxygen, (b) transfer of water proton to the OR group of Ti and (c) release of resulting ROH. In the next stage the co-ordination of titanium is increased through the reaction but partially hydrolysed oligomers (olation reaction). The formation of oxo-bridges $\equiv Ti-O-Ti \equiv$, can be described by the following oxolation reaction.

Polymerisation:

Oxolation reaction:

$$\equiv Ti{-}OX + HO{-}Ti \equiv \longrightarrow \equiv Ti{-}O{-}Ti \equiv + XOH$$

(X = H or R).

Acid catalyzed hydrolysis of titanium alkoxide followed by condensation are the steps involved in the production of submicron TiO_2 (Barringer & Bowen, 1985; Yassine Bessekhouad, Robert, & Weber, 2003; X. Chen & Mao, 2007; O'Regan & Gratzel, 1991; Oskam, Nellore, Penn, & Searson, 2003; Vorkapic & Matsoukas, 1999). Ti—O—Ti chain developed is favored by low content of water and reduced hydrolysis rate. $Ti(OH)_4$ is favored by high hydrolysis rate and medium content of water. Hence development of a three dimensional polymeric Ti—O—Ti chains with excess water results in closely packed first order particles (Barringer & Bowen, 1985; Yassine Bessekhouad, et al., 2003; X. Chen & Mao, 2007; O'Regan & Gratzel, 1991; Oskam, et al., 2003; Vorkapic & Matsoukas, 1999). Rate constant of coarsening is directly proportional to temperature because of the temperature dependence of the viscosity of solution and the equilibrium solubility of TiO_2 (X. Chen & Mao, 2007; Oskam, et al., 2003) by using titanium tetraisopropoxide (TTIP) as a precursor in the study of growth kinetics of submicron TiO_2 particles. .

2.3.3 Micelle and Inverse Micelle Method

Colloidal particles formed by the aggregation of surfactant molecules are called micelles, and when concentration of surfactants exceeds a certain value the critical micelles are formed, and this concentration is called critical micelle concentration (CMC) (X. Huang, Yang, Zhang, Zhang, & An, 1999). A distinctive normal phase micelle in an aqueous medium forms an aggregate with hydrophilic group of surfactant in contact with surrounding solvent, sequestering the hydrophobic hydrocarbon chains of surfactant in the micelle centre (X. Chen & Mao, 2007). An inverse or reverse micelle phase are formed in non-aqueous media, hydrophilic group (head) is centered towards the core of the micelle, while the hydrophobic group (tail) is extended outward towards non aqueous media (X. Chen & Mao, 2007).

Zhang et al came up with synthesis of TiO_2 fine particles by hydrolysis of titanium tetrabutoxide with acids (hydrochloric acid, nitric acid, sulfuric and phosphoric acid) in NP-5 - cyclohexane reverse micelle at room temperature. It was found that the reaction parameters control the crystal structure and particle size of TiO_2 ultra-fine particles. The type of acid used determines the formation of rutile at room temperature. An increased $[H_2O]$/ [NP-5] and $[H_2O]$/[$(TiOC_4H_9)_4$] ratios agglomerates particles. Round shaped TiO_2 submicron particles were obtained by supplementing suitable acid (X. Chen & Mao, 2007).

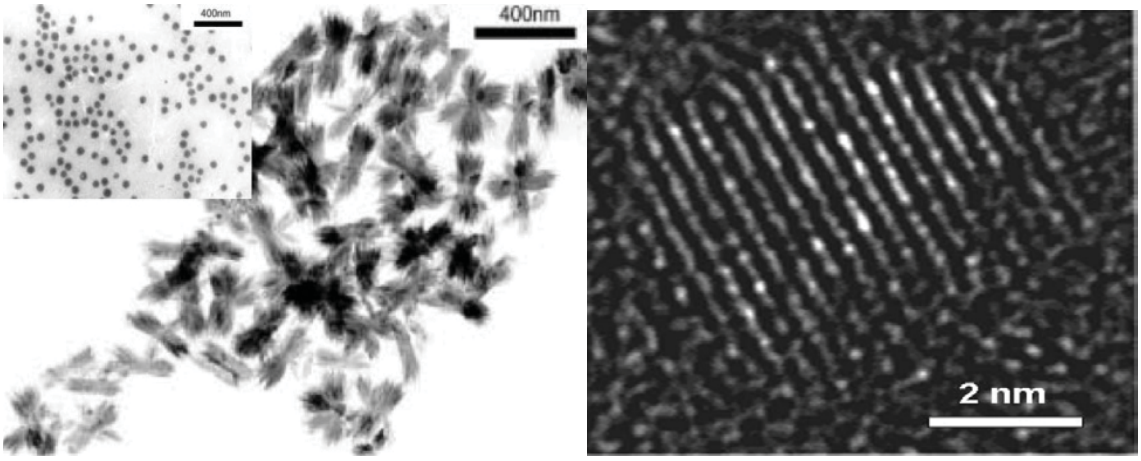

Figure 10: TEM and HRTEM images of TiO_2 particles shuttle-like and round-shaped after annealing by micelle and inverse micelle method (Zhang, D et.al 2002; Lin, J et.al 2002)

In an experiment, conducted by Lim and Hwang which demonstrates the production of TiO_2 particles by controlled hydrolysis of titanium tetraisopropoxide (TTIP) in reverse micelle formed in CO_2 with the surfactant ammonium carboxylate perfluoro polyether ($PFPECOO^-NH_4^+$) and poly (dimethyl amino ethyl methacrylate-block-1H,1H,2H,2H-perflourooctyl methacrylate) (PDMAEMA-b-PFOMA) (X. Chen & Mao, 2007; K. T. Lim, Hwang, Ryoo, & Johnston, 2004). It was found that crystallite size prepared in the presence of reverse micelle is directly proportional or dependent on the molar ratio of water to surfactant and precursor to surfactant ratio (Wo/R)

indicating the importance of surfactant stabilization (K. T. Lim, et al., 2004). The crystallinity of TiO_2 particles can be improved by annealing in the presence of micelle at lower temperature than a calcination treatment in solid state (X. Chen & Mao, 2007).

2.3.4 Sol Method

A non-hydrolytic sol-gel process is referred to sol method, which involves the reaction of different oxygen donor molecules with titanium chloride (Arnal, Corriu, Leclercq, Mutin, & Vioux, 1997; Hay & Raval, 1998, 2001; Lafond, Mutin, & Vioux, 2004; Niederberger, Bartl, & Stucky, 2002; J. Tang, et al., 2005; Trentler, Denler, Bertone, Agrawal, & Colvin, 1999)

Chemical Reactions:

$$TiX_4 + Ti(OR)_4 \longrightarrow 2TiO_2 + 4RX$$

$$TiX_4 + 2ROR \longrightarrow TiO_2 + 4RX$$

Ti—O—Ti bridge is developed by condensation between Ti—X and Ti—OR. The alkoxide group can be provided in first place by the reaction of $TiCl_4$ with alcohols/ ethers or by titanium alkoxides. In a method put forth by Trentler and Colvin, a solution containing titanium halide and trioctylphosphine oxide (TOPO) at 300°C was injected by metal alkoxide in a heptadecane and protected by dry inert gas. The reaction was complete in 5 minutes. It was found with greater distribution of R, the reaction rate of alkyl substituent including methyl, ethyl, isopropyl and tert-butyl also increased. The variation in halide resulted in a noticeable increase in average particle size but not the noticeable increase in reaction rate. As a result of nucleophilicity of halide, smaller anatase crystals ranging from 9.2nm for TiF_4 to

3.8nm for TiI_4 were formed. It is observed that the reaction with pure TOPO was slower and yielded small particles, while a much quicker reaction with a mixture of brookite, rutile and anatase with particle size of 10nm was produced without TOPO in the reaction (Trentler, et al., 1999).

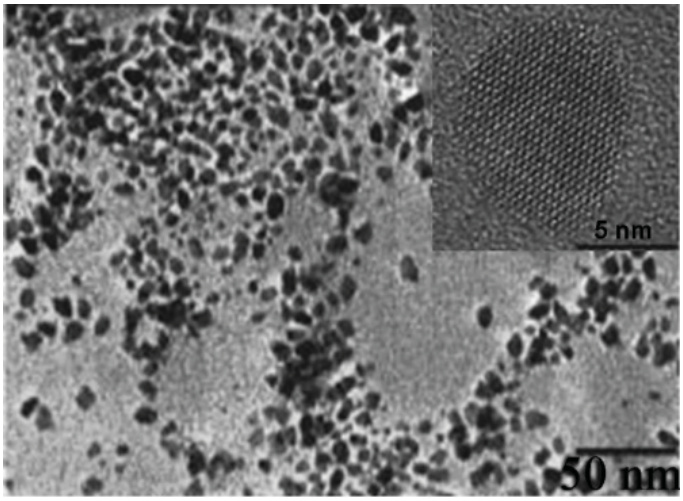

Figure 11: TEM image of TiO_2 particles derived from reaction of $TiCl_4$ and TTIP in TOPO/heptadecane at 300 °C (Trentler, T.J et al 1999)

Different particles are prepared by using surfactants which results in good particle size distribution and dispersity (Burda, Chen, Narayanan, & El-Sayed, 2005; Murray, Kagan, & Bawendi, 2000). By using a mixture of surfactants such as acetic acid and acetyl acetone (capping agents), monodispersed TiO_2 particles can be obtained (Cozzoli, Comparelli, Fanizza, Curri, & Agostiano, 2003; Cozzoli, Kornowski, & Weller, 2003; Scolan & Sanchez, 1998). In a typical procedure, titanium butoxide was hydrolyzed with acetylacetone and p-toluenesulfonic acid at 60°C(Scolan & Sanchez, 1998). The resultant particles called xerosol was dispersed in alcohol solution whose concentration is greater than 1M without aggregation, which results in binding of surface by acetylacetone ligand and by an adsorbed organic-inorganic layer made of acetylacetone, p-toluenesulfonic acid and water (Scolan & Sanchez, 1998). Thus,

producing a mono dispersed non-aggregated TiO_2 particles. TiO_2 of different size and shape can be synthesized with the help of surfactant (Buonsanti, et al., 2006; Cozzoli, Comparelli, et al., 2004; Cozzoli, Fanizza, et al., 2004; Cozzoli, Fanizza, Curri, Laub, & Agostiano, 2005; P. Davide Cozzoli, et al., 2003; Joo, et al., 2005; Zhihua Zhang, 2005). In an experiment, conducted by Cozzoli and coworker, at a growth of higher-aspect-ratio anatase TiO_2 were formed by controlled hydrolysis of TTIP in oleic acid (OA) (Buonsanti, et al., 2006; Cozzoli, Comparelli, et al., 2004; Cozzoli, Fanizza, et al., 2004; Cozzoli, et al., 2005; P. Davide Cozzoli, et al., 2003).

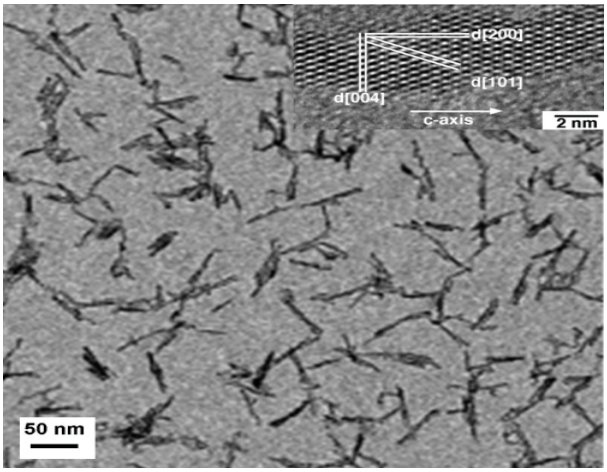

Figure 12: TEM of TiO_2 particles (Cozzoli, P. D et.al 2003)

In this method, a dried OA TTIP was added to a dried OA at 80—100°C with nitrogen flow of dry inert gas protection and stirred for 5 minutes. To the above solution a concentration of 0.1—2M was supplied, and the temperature was maintained around 80—100°C with continuous stirring for 6—12hrs. The base used here included organic amines, like trimethylamino-N-oxide, trimethylamine, tertramethyl ammonium hydroxide, tetrabutyl ammonium hydroxide, triethylamine and tributylamine. The hydrolysis rate of titanium precursor was controlled by chemical modification of titanium precursor with carboxylic acid. Use of appropriate catalyst (tertiary amines

or quaternary ammonium hydroxide) resulted in rapid crystallization, even at mild condition. Hence TiO_2 obtained by this method were the result of kinetically overdriven growth mechanism (P. Davide Cozzoli, et al., 2003).

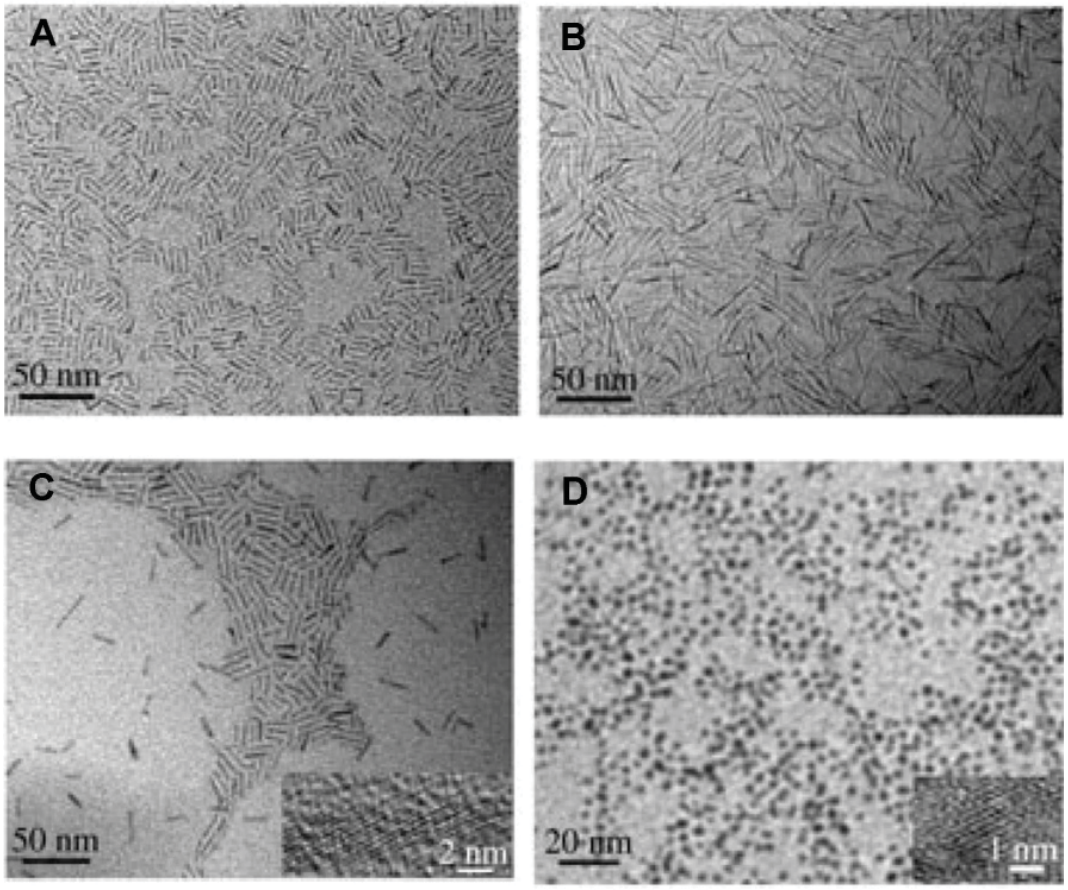

Figure 13: TEM images of TiO_2 rods with lengths of (A) 12 nm, (B) 30 nm, and (C) 16 nm. (D) 2.3 nm TiO_2 particles (Zhang, Z et.al 2005)

Addition of chemical modifiers such as carboxylic acids leads to different molecular structure, geometry and reactivity of a precursor. Polynuclear oxocarboxyalkoxides have been reported upon modification of precursor with carboxylic acid. These molecular species typically comprise a compact Ti-O-Ti framework of hexa-coordinated Ti atoms, surrounded by a hydrocarbon periphery. Because of the existence of Ti- O-Ti linkages even before hydrolysis, the modified precursor

molecules act as “monomers” for the development of an extended Ti-O-Ti network. The modified molecular precursor itself has a potential “anisotropic” reactivity, as the accessibility of -OR a group toward water depends on their spatial orientation in the starting oxocarboxyalkoxide. The directions, in which cross-linking of Ti-O-Ti bonds can occur, can thus be limited. The carboxylic chains can effectively hinder the attack of water at metal centers, allowing only the most exposed -OR groups to be primarily hydrolyzed, thus decelerating hydrolysis rate. In recent research TiO_2 were obtained without the use of catalyst (Joo, et al., 2005; Zhihua Zhang, 2005). In a typical procedure, OA complexes of titanium were generated at 80°C in 1-octadecene using TTIP and OA mixture. The use of the predetermined amount of oleylamine at 260 resulted in different sized TiO_2 with diameter of 2.3 nm were also produced by this method (Zhihua Zhang, 2005).

2.3.5 Hydrothermal Method

Hydrothermal Method is widely used in production of different submicron materials in the ceramic field. It is also employed in producing TiO_2 particles (Chae, et al., 2003; Cot, Larbot, Nabias, & Cot, 1998; Juan Yang, 2000, 2001; J. Yang, Mei, & Ferreira, 2001). It is normally performed in a steel pressure vessel called autoclaves under controlled temperature/pressure in aqueous solution irrespective of Teflon liners. The internal pressure produced is determined by the temperature and the amount of solution added. In a typical procedure, a precipitate of titanium precursor prepared by the addition of 0.5M iso-propanol solution of titanium butoxide into de ionized water ($[H_2O]/[Ti]=150$). The resultant mixture was peptized at 70°C for 1hr in the presence of tetra-alkyl-ammonium hydroxide (peptizer). The so formed precipitate was then filtered and treated at 240°C for 2hrs. The powder obtained was washed with de-ionized water and then processed for drying at 60°C (J. Yang, et al., 2001).

Hence hydrothermal treatment of peptized precipitate of titanium precursor with water results in TiO_2 particles. The morphology of the particles were greatly influenced by peptizer and their concentration (J. Yang, et al., 2001).

In another method, hydrothermal reaction of titanium precursor in an acidic ethanol water solution yields TiO_2 particles (Chae, et al., 2003) with only anatase phase (primary structure) with no secondary structure. The particles sizes were greatly influenced by concentration of Ti precursor and composition of the solvent. In a mixed ethanol water solution at pH 0.7 with nitric acid, TTIP was added drop wise and reacted at 240°C for 4hrs, thus yielding anatase phase TiO_2 particles. The sizes of particles have been controlled to the range of 7-25 nm by adjusting the concentration of Ti precursor and the composition of the solvent system. Hydrothermal method is also used in preparing TiO_2 submicron material (Q. Huang & Gao, 2003; Xinjian Feng, 2005; S. Yang & Gao, 2005a, 2005b, 2005c; Q. Zhang & Gao, 2003). In a typical procedure, dilute $TiCl_4$ solution is treated with acid or an inorganic salt for 12hrs at 60—150°C (Q. Huang & Gao, 2003; S. Yang & Gao, 2005a, 2005b, 2005c; Q. Zhang & Gao, 2003).

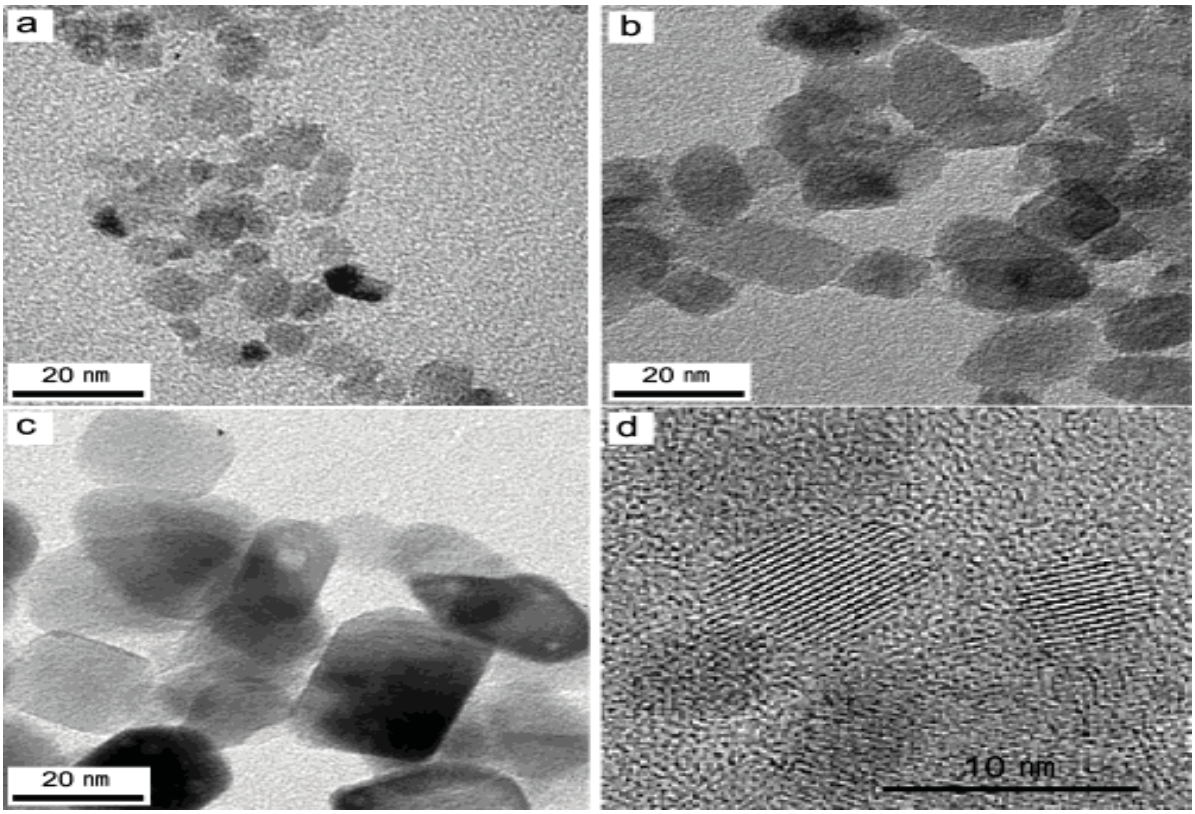

Figure 14: TEM images of 7-nm-sized TiO_2 particles prepared from 0.10 M titanium isopropoxide in 4:1 ethanol/ water (a), 15-nm particles prepared from 0.04 M titanium isopropoxide in 1:2 ethanol/water (b), 25-nm particles prepared from 0.02 M titanium isopropoxide in 1:8 ethanol/water (c), and a high-resolution TEM image for a 7-nm particle (d) (Chae S, Y et.al 2003)

The morphology of TiO_2 was greatly influenced by solvent composition or surfactants (S. Yang & Gao, 2005a). In another method, TiO_2 with uniform diameter of 30 to 60 nm were obtained at 160°C by hydrothermal treatment of titanium trichloride solution supersaturated with NaCl (Xinjian Feng, 2005).

Submicron particles were also obtained by hydrothermal method (A. Robert Armstrong, 2004; Nian & Teng, 2006; Yoshida, Suzuki, & Yoshikawa, 2005; Y. X. Zhang, et al., 2002). In a solution of 10—15M aqueous NaOH TiO_2 white powders were treated for 24—72hrs at 150—200°C in an autoclave. The results showed that highly crystalline TiO_2 with diameter ranging from 30 to 45 nm and length in several

micrometers were obtained (Y. X. Zhang, et al., 2002). Submicron material can also be prepared by hydrothermal treatment of layered titanate particles (M. Wei, Konishi, Zhou, Sugihara, & Arakawa, 2004). In this procedure, $Na_2Ti_3O_7$ was dispersed in 0.05—0.1M HCl solution, aged for 3—7days in an autoclave at 140—170°C. The product was then washed with water and dried forming TiO_2 material.

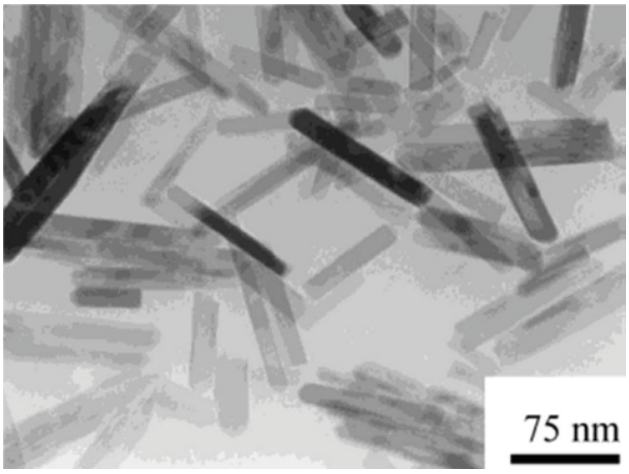

Figure 15: TEM image of TiO_2 material prepared with the hydrothermal method (Zhang, Q et.al 2003)

Submicron TiO_2 materials are widely prepared by using hydrothermal method (Dmitry V. Bavykin, Sergey N. Gordeev, et al., 2005; Bavykin, Lapkin, Plucinski, Friedrich, & Walsh, 2005a, 2005b; D. V. Bavykin, et al., 2005; Bavykin, Parmon, Lapkin, & Walsh, 2004; Chien, Liou, & Kuo, 2005; D. V. Bavykin, 2006; Gundiah, et al., 2003; Kasuga, Hiramatsu, Hoson, Sekino, & Niihara, 1998; Kukovecz, Hodos, Kónya, & Kiricsi, 2005; Ma, Fukuda, Sasaki, Osada, & Bando, 2005; Qian, Du, Yang, & Jin, 2005; Seo, Lee, & Kim, 2001; T. Kasuga, 1999; Tian, Voigt, Liu, Mckenzie, & Xu, 2003; Y. Q. Wang, Hu, Duan, Sun, & Xue, 2002; Y. Lan, 2005; Yao, et al., 2003; Yuan & Su, 2004). In a standard procedure, TiO_2 powders were added to the solution of 2.5—20M aqueous NaOH and were aged for 20hrs at 20—110°C in an autoclave. A thorough wash of the mixture with dilute HCl and distilled water resulted in TiO_2 material. TiO

submicron tubes with inner diameters of approximately 5 nm and outer diameters of approximately 8 nm with length of approximately 100nm were produced by this method. (T. Kasuga, 1999).

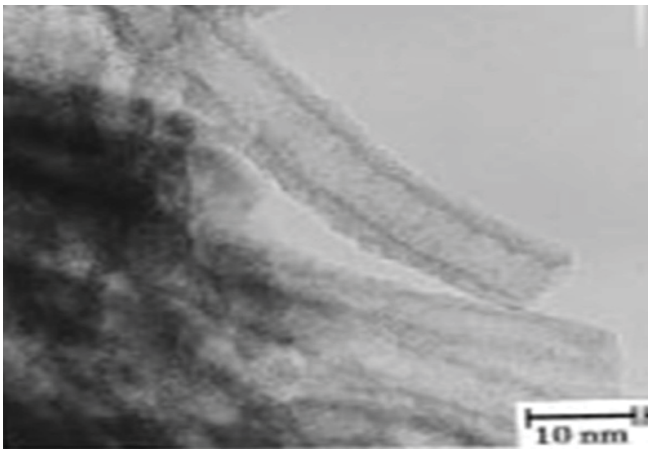

Figure 16: TEM image of TiO_2 submicron tubes (Kasuga, T. 1998)

The mechanism is as follows. When TiO_2 was treated with aq. NaOH solution, the Ti—O—Ti bonds broke forming Ti—O—Na and Ti—OH. A new Ti—O—Ti bond is formed after Ti—O—Na and Ti—OH come under the influence of acid and water (when reaction mixture was treated with dilute HCl and distilled water). Ti—OH bonds were readily being able to form sheet. Ti—O—H—O—Ti hydrogen bonds were obtained by dehydration of Ti—OH in HCl aqueous solution. Ti bond distance reduces on the surface which resulted in folding of sheets and connection between ends of sheets forming tubular structure. Therefore, acid treatment following alkali treatment resulted in the formation of TiO_2 material (Kasuga, et al., 1998).

2.3.6 Solvothermal method

Solvothermal method is similar to hydrothermal method, but non aqueous solvent is used in this method. A choice of different organic solvent with high boiling point can be made in solvothermal method. The size and shape distribution of TiO_2 particles

can be controlled better in solvothermal method when compared to hydrothermal method. A narrow particle size distribution and dispersity seems to be the key feature of this method, hence used as versatile process in producing different TiO_2 particles (Xiao-Lin Li, 2006; J. Xu, Ge, & Li, 2006; Xun, Jing, Qing, & Yadong, 2005). TiO_2 particles and submicron rods are produced by solvothermal method irrespective usage of surfactants (C.-S. Kim, Moon, Park, Choi, & Seo, 2003; B.-M. Wen, C.-Y. Liu, & Y. Liu, 2005; B. Wen, C. Liu, & Y. Liu, 2005a, 2005b; Xiao-Lin Li, 2006; J. Xu, et al., 2006; Xun, et al., 2005).

In one of the procedures toluene with weight ratio of (1—3:10) was mixed with TTIP for 3hrs at 250°C. It was found that the average particle size was directly proportional to TTIP composition of weight ratio (1—3:10) (C.-S. Kim, et al., 2003). However, at 1:20 and 2:5 weight ratios, crystalline phase of TiO_2 was not produced (C.-S. Kim, et al., 2003). Redispersible TiO_2 particles can be obtained by controlled hydrolyzation of Ti $(OC_4H_9)_4$ and linoleic acid (Xiao-Lin Li, 2006). NH_4-HCO_3 was decomposed to provide H_2O for hydrolyzation reaction. In the preparation of TiO_2 particles, linoleic acid plays a vital role of co-ordination surfactant and solvent/reagent. However the catalyst (Triethylamine) for polycondensation had little influence of product morphology. Long chain organic acid greatly influenced the formation of TiO_2 (Xiao-Lin Li, 2006). Solvothermal method also helps in synthesizing TiO_2 material (C.-S. Kim, et al., 2003; Xiao-Lin Li, 2006). In a typical procedure, dissolution of TTIP in an anhydrous toluene with OA as surfactant is processed for 20hrs in an autoclave with no stirring at 250°C (C.-S. Kim, et al., 2003). With a sufficient amount of TTIP surfactant in solution, long dumbbell shaped material were obtained due to the oriented growth of particles along the [001] axis. It was observed that concentration of TiO_2 was directly proportional to the concentration of titanium precursor in the

solution at precursor to surfactant ratio of 1:3. This morphology was greatly influenced by precursor/surfactant weight ratio.

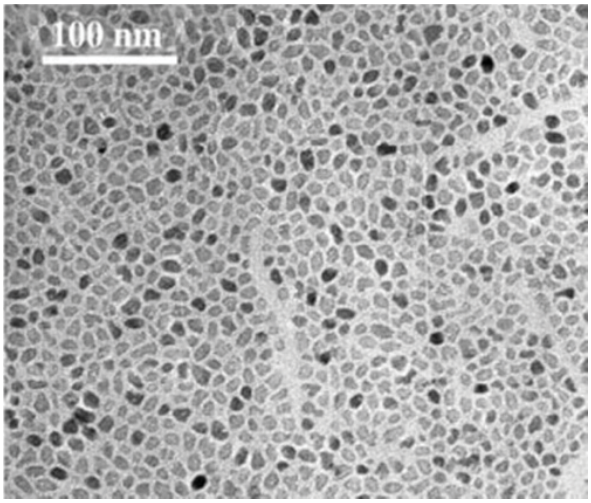

Figure 17: TEM micrographs of TiO2 particles prepared with the solvothermal method (Li, X.L et.al 2006)

For a precursor surfactant weight ratio more than 1:3 anatase were obtained with their diameter and length ranging from 3—5nm and 18—25nm (C.-S. Kim, et al., 2003).

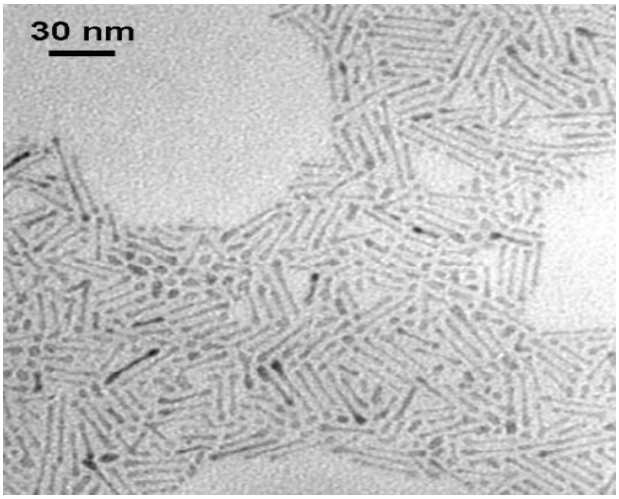

Figure 18: TEM micrographs and electron diffraction patterns of products prepared from solutions at the weight ratio of precursor/solvent/surfactant) 1:5:3 (Kim, C.S et.al 2003)

2.3.7 Direct Oxidation Process

Oxidation of titanium metals yields TiO_2 materials by using oxidants or anodization. Direct oxidation of titanium metal plate with hydrogen peroxide yields in crystalline TiO_2. In this procedure, titanium plate is immersed in 50ml of 30wt% H_2O_2 solutions at 353K for 12hrs, the dissolution precipitate mechanism results in the formation of crystalline TiO_2. Crystalline phase of TiO_2 can be tuned by the addition inorganic salts of NaX (X= F^-, Cl^-, SO_4^{2-}, anatase is obtained by adding F^- and SO_4^{2-} while addition of Cl^- results in rutile). In an experiment conducted by Peng and Chen, acetone was used as an oxygen source at high temperature, which plays a vital role in oxidation. Pure O_2 or argon mixed O_2 results in only crystal grain films or grains with random submicron fibres formation, whereas acetone used as oxygen source yields an array of highly dense and well-arranged TiO_2 submicron material. The morphology of TiO_2 depends on diffusion of titanium and oxygen in titanium oxidation process. The reaction of Ti cations diffused to oxide surface and an adsorbed acetone species result in well aligned TiO_2 material when titanium substrate was oxidized using acetone at 850°C for 90min.

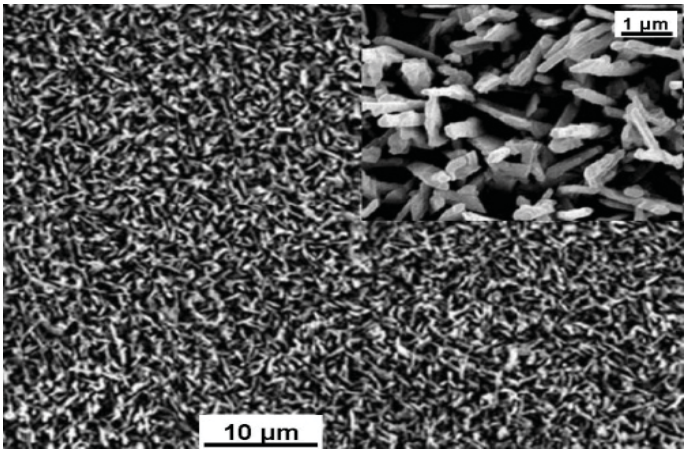

Figure 19: SEM images of large-scale sub-micron rod arrays prepared by oxidizing titanium with acetone at 850 °C for 90 min by direct oxidation method (Peng, X & Chen, A. 2004)

An anodic oxidation of titanium foil resulted in formation of submicron tubes. In this procedure platinum was used as a counter electrode after anodizing Ti plate in 0.5% HF solution for 10—30min under 10—20V, which was followed by annealing for 6hrs at 500°C in an oxygen chamber. An applied potential between 1 and 25V helps in tuning the length and diameter TiO_2 submicron tubes ranging diameter from 15—120 nm and length from 20nm to 10μm (Peng, X., & Chen, A. 2004).

2.3.8 Chemical Vapor Deposition (CVD)

In a vapor deposition, a solid phase material is formed by condensation of vapor state materials. The vapor deposition process involving chemical reaction is called chemical vapor deposition (CVD) and those that don't involve chemical reaction are called physical vapor deposition (PVD). The CVD method is usually implied to alter the mechanical, electrical, thermal and optical properties of various materials. Fabrication of various materials is its recent achievement. There are different CVD methods in producing the material such as electrostatic spray, hydrolysis (Park & Burlitch, 2002), diffusion flame pyrolysis (Gurav, Kodas, Pluym, & Xiong, 1993; Jang & Kim, 2001), thermal plasma pyrolysis (Li & Ishigaki, 2004; Y.-L. Li & Ishigaki, 2002; S.-M. Oh, Kim, Lee, Ishigaki, & Park, 2003), ultrasonic spray pyrolysis (Nedeljkovic, Saponjic, Rakocevic, Jokanovic, & Uskokovic, 1997), laser-induced pyrolysis and ultrasonic assisted hydrolysis. In a typical CVD process which takes place in a vacuum chamber, the deposition reaction are driven by the gases heated by thermal energy in coating chamber (X. Chen & Mao, 2007).

This method helps in producing TiO_2 particles ranging from 10nm—30nm. The method adopted here is pyrolysis of TTIP in a mixed He/O_2 atmosphere using liquid precursor delivery (X. Chen & Mao, 2007; Seifried, Winterer, & Hahn, 2000). In this

method, an amorphous TiO_2 particles can be obtained and crystallized with high surface area after the process of annealing (high temperature) (Ayllón, et al., 1999). This is possible when the vapor are deposited on possible when the vapors are deposited on the cold areas of the reactor below 90°C with plasma enhanced CVD. In the 2nd method, TiO_2 submicron rods are produced on fused silica substrate with a template catalyst free MOCVD (metal organic CVD).

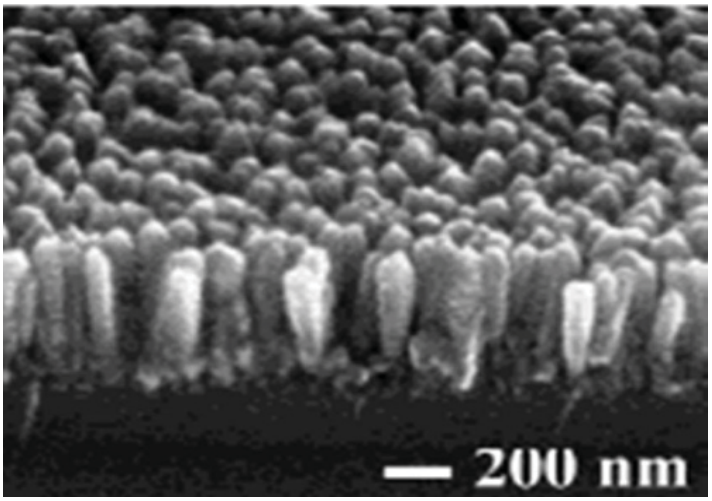

Figure 20: SEM images of TiO_2 sub-micron rods grown at 560 °C by CVD method (Wu, J.J et.al 2004)

In this method, N_2/O_2 flow at high temperature (500—700°C) drives the vaporization of titanium actetylacetonate (Ti ($C_{10}H_{14}O_5$)) in furnace (200—230°C). Hence producing submicron structured TiO_2 on substrate TiO_2 can be controlled by tuning reaction parameters like temperature and pressure (J.-J. Wu & Yu, 2004).

2.3.9 Physical Vapor Deposition

Unlike CVD, the material are first evaporated and then condensed to form solid phase. Primary PVD methods involve thermal deposition, ion plating, ion implantation, sputtering, laser deposition and laser surface alloying. Either thermal deposition or simple PVD method results in an array of TiO_2 submicron wires (J.-M.

Wu, Shih, & Wu, 2005; J.-M. Wu, Shih, Wu, Tseng, & Chen, 2005). A tube furnace containing Ti metal on quartz boat is pumped down to ~300 torr of pressure and increased the temperature to 850°C carried by argon gas flow with rate of 100sccm and held for 3hrs. A layer of TiO_2 material is obtained after the completion of the reaction. Before the growth of TiO_2 submicron wires, a layer of TiO_2 submicron particles can be deposited on the substrate in which Au is used as catalyst (J.-M. Wu, Shih, & Wu, 2005).

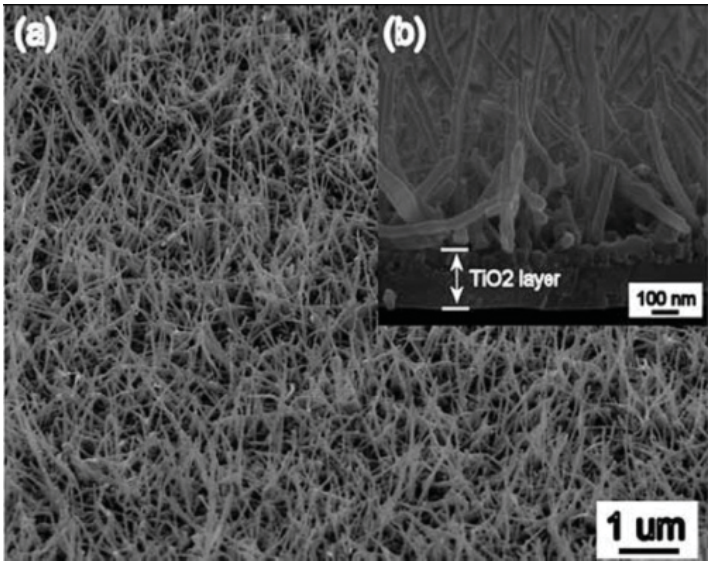

Figure 21: SEM images of the TiO_2 sub-micron wires arrays prepared by the PVD method (Wu, J.M 2005)

2.4 Applications of Titanium di oxide

TiO_2 has a wide range of application worldwide. TiO_2 particles are used in day to day life. Applications of TiO_2 are studied briefed in the following section:

Materials coated with TiO_2 particles have an existing and promising application in fields such as painting, cosmetic formulation, toothpaste, self-cleaning agent, UV protection, catalysis, photocatalysis, photovoltaics, sensing, electrochromics (Bonhôte, Gogniat, Grätzel, & Ashrit, 1999; Akira Fujishima, Rao, & Tryk, 2000; Garzella,

Comini, Tempesti, Frigeri, & Sberveglieri, 2000; Grätzel, 2001; Hwang, et al., 2003; Popov, Priezzhev, Lademann, & Myllyla, 2005; Yongping, Shangang, & Fuan, 2002).

2.4.1 Photocatalytic application

Recently, photocatalysis has drawn loads of attention around the world in the field of scientific research. In the list of photocatalysts being used currently, TiO_2 is probably the only appropriate material for industrial use (K. Hashimoto, Irie, & Fujishima, 2005). One can say TiO_2 as an ideal photocatalyst due its most efficient photoactivity, high stability and low cost (Akira Fujishima, et al., 2000). Brief mechanism of photocatalytic reaction is as follows: Electron hole pairs are formed on photon absorption with energy greater than the band gap of TiO_2, resulting in excited valence band from the conduction band (X. Chen & Mao, 2007).

Photocatalytic applications are classified based on the TiO_2 materials produced. In case of pure TiO_2 particles, as per the previous studies, we know that redox reaction is enhanced by an increase in the band gap energy which is achieved by decreasing the size of the materials (X. Chen & Mao, 2007). It is also evident that enhanced photocatalytic efficiency is observed for an optimal size of TiO_2 particles ranging from 21—11nm in the chloroform decomposition, but reduced activity is observed with particle size <6nm, this is due to quantum confinement effect (C.-C. Wang, Zhang, & Ying, 1997). Contradicting results were obtained on 2 propanol decomposition (Chae, et al., 2003).

In an experiment performed by Peng et al photocatalytic activity of TiO_2 obtained, was inversely proportional to calcination temperature, as a result of which higher photocatalytic activity was observed with TiO_2 particles calcined at 400°C compared to deguessa P25 TiO_2 and the activity was gradually decreased with an increase in

calcination temperature (Peng, Zhao, Dai, Shi, & Hirao, 2005). TiO_2 aerogel is regarded as a potential photocatalyst. In an experiment performed by Dagan et al. TiO_2 aerogels prepared with 90% porosity and 600m^2/g surface areas was subjected to photodegradation of salicyclic acid, in the presence of UV illumination for 1hr resulted in photocatalytic acitivity 10 times faster than deguessa P25 TiO_2 (Dagan & Tomkiewicz, 1993).

Several studies are being performed on metal doped TiO_2 particles, which results in an enhanced photocatalytic activity for degradation of organic pollutants i.e., in the presence of visible light irradiation (Y. Bessekhouad, Robert, Weber, & Chaoui, 2004; Chang, Lai, & He, 2005; X. Chen, et al., 2005; Egerton, Kosa, & Christensen, 2006; Enache, Schoonman, & Krol, 2004; Kemp & McIntyre, 2006; D. H. Kim, et al., 2005; K. D. Kim, et al., 2005; Klosek & Raftery, 2001; W. Li, et al., 2003; Peill, Bourne, & Hoffmann, 1997; Ranjit & Viswanathan, 1997; Sahoo, Gupta, & Pal, 2005; H. Wei, Wu, Lun, & Zhao, 2004; J.-C. Xu, Lu, Guo, & Li, 2005; K. Xu, 2007).

In many cases, doped TiO_2 particles find a wide area of functionalized technical application compared to pure TiO_2 particles. Doping with traces of transition metals increase the quantum yield in photocatalytic degradation process as a result of alter in structure, electronic properties or thermal stability of TiO_2 materials (Batzill, Hebenstreit, Hebenstreit, & Diebold, 2003; Batzill, Katsiev, Gaspar, & Diebold, 2002; Diebold, 2003; D. Morris, et al., 2000; Taverner, Gulino, Egdell, & Tate, 1995). A study based on photocatalytic activity was performed by doping TiO_2 particles with 21 transition metal elements. It was found that photocatalytic activity on metal doped TiO_2 materials was based on electron configuration of dopant ion (W. Choi, Termin, & Hoffmann, 1994).

Dopant like Fe^{3+}, Mo^{5+}, Ru^{3+}, Nd^{3+}, Pd^{2+}, Pt^{4+}, Os^{3+}, Re^{5+}, V^{4+} and Rh^{3+} at 0.1—0.5% increase the photoreactivity for both oxidation and reduction, whereas dopant like Co^{3+}, Al^{3+} decreases the photoreactivity (W. Choi, et al., 1994; Shah, Li, Huang, Jung, & Ni, 2002) as highest quantum yields are usually observed at 0.5%. Enhanced interfacial charge transfer in the presence of effective dopants appears to be the most important factor in enhancement of photoreactivity of doped TiO_2. The dopant functions as an effective trap which depends on the factors such as dopant concentration, the energy level of dopants within the TiO_2 lattice, their d electronic configuration, the distribution of dopants within the particles, the electron donor concentration, and the incident light intensity. Photoreactivities of doped titania increases upto optimal dopant concentration (0.5%) above which the photoreactivity decreases. In an experiment performed by Burda et al, nitrogen was doped on to TiO_2 particles, which resulted in effectiveness of using sub micrometer scale materials in developing efficient visible light activated photocatalyst. This study may also lead to the production of environmentally benign photocatalyst that exceed the efficiency of current catalysts, especially for visible light activation (Burda, et al., 2003). Photocatalytic activity of doped TiO_2 particles varies by the presence of dopant ion in TiO_2 matrix, which drives the charge recombination rates and interfacial electron transfer rates. Parameters such as dopant concentration, energy level of dopant within the TiO_2 lattice, their d-electronic configuration, distribution of dopant, the electron donor concentration and light intensity influence the photocatalytic activity of doped TiO_2 materials (X. Chen & Mao, 2007). Hence metal doped TiO_2 materials need not necessarily have higher photoreactivity, they might as well have lower photoreactivity. For e.g. Sn^{4+} doped TiO_2 materials show higher photoreactivity on phenol photo-degradation compared to pure TiO_2 under both UV and visible light (Cao, Yang, Zhang, Liu, & Yue, 2004). Whereas V^{4+} doped TiO_2 material display lower

photoreactivity on photo-oxidation of 4-chlorophenol compared to pure TiO_2 particles (Martin, Morrison, & Hoffmann, 1994).

2.4.2 White Pigment

The white pigment market is totally dominated by TiO_2, in particular rutile titania. TiO_2 pigment is much safer and is economical to use. Due to their high refractive index, they are most effective scatterers of visible light. Their tendency of providing brightness, non-corrosive nature, stability and non-toxicity compared to other pigment is the pick of the properties. Due to the above properties they have greater demand in the field of paint and oil coating industry. They are used in decorative and architectural paints mainly house buildings, industrial coating and automobile paints. Other than paint industries TiO_2 pigment also has a wide range of uses. TiO_2 is used in the plastic industry. In plastics, TiO_2 pigments are used to optimize PVCs performance for less than 1vol%. Excellent optical properties, brightness and opacity exhibited by TiO_2 pigment finds its use in the paper industry, depending on the quality of the paper pulp (Koleske, 1995).

Pure TiO_2 has found application in our daily life as it is used in cosmetic products like sunscreen/sun block due to its absorption and scattering characteristics of UV radiation (Turkoglu & Yener, 1997). TiO_2 is used as a food additive e.g. TiO_2 is used in skimming of milk or food coloring agent (Phillips & Barbano, 1997). Factors such as ink rheology, abrasiveness, gloss, redispersibilty are affected by the grade of TiO_2 in the ink industry. Some of ink application with TiO_2 are inks for wood molding, marking pen, decorative sheets, ink correction fluid, inks for lottery ticket scratch offs (F. Lin, 2006). TiO_2 pigment are used in anti-reflective coatings, dielectric mirrors for lasers and many more thin film optical devices, due to its optical transmittance property in visible and IR region (Selhofer & Muller, 1999).

2.4.3 Catalyst Support/Promoter

TiO_2 is employed as a catalyst promoter in many of hydrogenation reactions and electronic devices like sensors with film technology (Henrich, 1983; Stashans, Lunell, & Grimes, 1996). TiO_2 is also used as a textural promoter/Ni support in reaction of methane decomposition (Lazaro, et al., 2008). TiO_2 coated with carbon acts as a high performance electrocatalyst support (Shanmugam & Gedanken, 2007). In diesel engines, sulfated titania was used as a catalyst support to make V_2O_5/TiO_2 catalyst (I. Y. Lee, Lee, Park, & Hong, 2009). TiO_2 is also used as a support to catalyst for catalytic combustion of methane or sewage disposal (Garcia, Solsona, Amoros, Solano, & Taylor, 2006). In Pt-TiO_2/C composite, TiO_2 acts as a catalyst support improving the cathode stability and cathode performance for proton exchange membrane fuel cell (Von Kraemer, Wikander, Lindbergh, Lundblad, & Palmqvist, 2008). Compared to Al_2O_3 and SiO_2, TiO_2 is not suitable as a structural support material, but a small amount of TiO_2 can tune metal based catalyst to an extent (Pan & Madey, 1993; Pesty, Steinruck, & Madey, 1995).

2.4.4 Gas Sensors

Gas sensors are commonly used for oxygen detection at medium or high temperature and detection of low gas concentrations at medium temperature and constant oxygen pressure (Sberveglieri, 1995). Gas sensing technology is adopted on the mechanism of surface interaction between a metal ion semiconductor and gas molecule. Assuming that submicron particles imply higher surface area and porosity, the behavior of surface interaction can be tentatively rationalized. The response and recovery times for ethanol is very high, hence can be used in control food analyser, wine identifications, electronic noses and medical devices. Maintaining a good semiconductor surface properties at temperature >400°C is of particular interest for

gas sensor applications (Garzella, Comini, Tempesti, Frigeri, & Sberveglieri, 2000). Anatase titania (TiO_2) exhibits sensitivity towards oxygen and reducing gases such as ethanol and hydrogen (H. Tang, Prasad, Sanjines, & Levy, 1995). Hence TiO_2 is commonly used as oxygen gas sensor. TiO_2 is used evaluating combustion process of fuel in car engines to control pollution (Francioso, Presicce, Epifani, Siciliano, & Ficarella, 2005). It is observed that UV radiation can significantly increase the conductivity and sensitivity of TiO_2 gas sensor at high temperature (T. Y. Yang, Lin, Wei, Wu, & Lin, 2003). TiO_2 doped with other metal oxide makes them sensitive to different gases TiO_2 doped with Cr showed promising performance in detection of dilute NO_2 in the air at 500°C (Ruiz, et al., 2003). Nb-TiO_2 is used in carbon monoxide sensing studies at high temperature (Anukunprasert, Saiwan, & Traversa, 2005). Hydrogen sulfide detected using Pt doped TiO_2 (H. M. Lin, Hsu, Tung, & Hsu, 1995).

2.4.5 Photoinduced Hydrophilicity

When the surface of TiO_2 is exposed to UV light, electrons and holes are produced. These electron tend to reduce the Ti(IV) cations to Ti(III) state, and the holes oxidize the O^{2-} anions. Hence the oxygen atoms are ejected, creating oxygen vacancies, producing adsorbed OH groups, which tend to make the surface hydrophilic. The longer the surface is illuminated with UV light, the smaller the contact angle for water becomes; after some time the contact angle approached zero, making the water layer to spread flat across the surface. TiO_2 coated materials exhibit a unique property of self-cleaning and anti-fogging characteristics. Self-cleaning works on the following mechanism, when TiO_2 coated material is exposed to stain and rainfall, water from rain soaks and adsorbs stain on highly hydrophilic TiO_2 surface, this decomposes the stain by conventional photocatalytic reaction and is washed away by rainwater as shown in figure 4. Usually TiO_2 coated glass exterior are used as building material. A

uniform thin film of water is formed on hydrophilic surface instead of droplets during fogging; this uniform layer of water prevents fogging. Hence this mechanism is applied in glass products, mirrors and eyeglasses. It is also used in side view mirrors of cars (T. Hashimoto, et al., 1994).

2.4.6 Other applications

A dye sensitized film coated with TiO_2 is used in a solar cell due to high surface area of the semiconductor and ideal spectral characteristic of the dye. The mechanism of dye sensitized TiO_2 submicron particles generally involves the excitation of the dye and the charge transfer from dye to TiO_2 particles. TiO_2 is also used in removal of foul odor from acetaldehyde, anemone, trimethyalmin, hydrogen sulfides, and methyl-melcaptan. TiO_2 is used in removal of dissolved organic compounds like chlorine and other pollutants in water purification process. The bacterial disinfectant property of TiO_2 makes it suitable for applications such as medical devices, food preparation surface, air conditioning filters and sanitary ware surfaces (H. A. Lim, 2003). In addition, TiO_2 is used in removal of ethylene from air in fruits; vegetables and cut flower storage areas to increase products shelf life and prevent spoilage (Guarino, Costa, & Porro, 2008).

3 Experimental Design

In this project, chloride process is employed in producing TiO_2 fine particles. This method is advantageous compared to sulfate process, considering waste disposal, operation cost and availability of raw materials. This process has been divided into 3 sections (Figure 5) namely:-

1. Dissolution
2. Hydrolysis
3. Calcination

Dissolution is the first step which helps us obtain TiO_2 and FeO concentrated liquor, by digesting ground ilmenite using concentrated hydrochloric acid at < 90°C for 3hrs. This step is very important as weak dissolution may result in undesirable product. In this step, the metal oxides are separated from its ore using concentrated acid followed by the reduction of Fe^{3+} to Fe^{2+} and Ti^{4+} to Ti^{3+} using iron fillings.

Hydrolysis is the second step which controls the crystal size and structure of TiO_2, depending on the additives (SDA) used. This step is equally important as dissolution and calcination steps, as uncontrolled hydrolysis may lead to poor quality of the product. The additives used in hydrolysis step are phosphoric acid, tri sodium citrate, citric acid. The hydrolyzed mixture of water, digested liquor and additives is filtered, thoroughly washed with 10% HCl and dried to form dry hydrate, which is further subjected to XRD to identify the phase of TiO_2 obtained. The waste filtrate obtained from hydrolysis can be recycled for hematite byproducts and HCl recovery (which can be used for dissolution again), thus resulting in effluent free disposal.

Calcination is the third and final step which helps us understand the TiO_2 behavior on thermal treatment. As a result of elevated temperature, change in phase and crystallite size of TiO_2 is observed. In this step, potassium additive is mixed with hydrate sample from hydrolysis and then calcined at higher temperature ranging from 925°C—1000°C. The calcined sample is subjected to XRD and SEM to study their structural characteristics. Each section of this process is described in details in the following chapters.

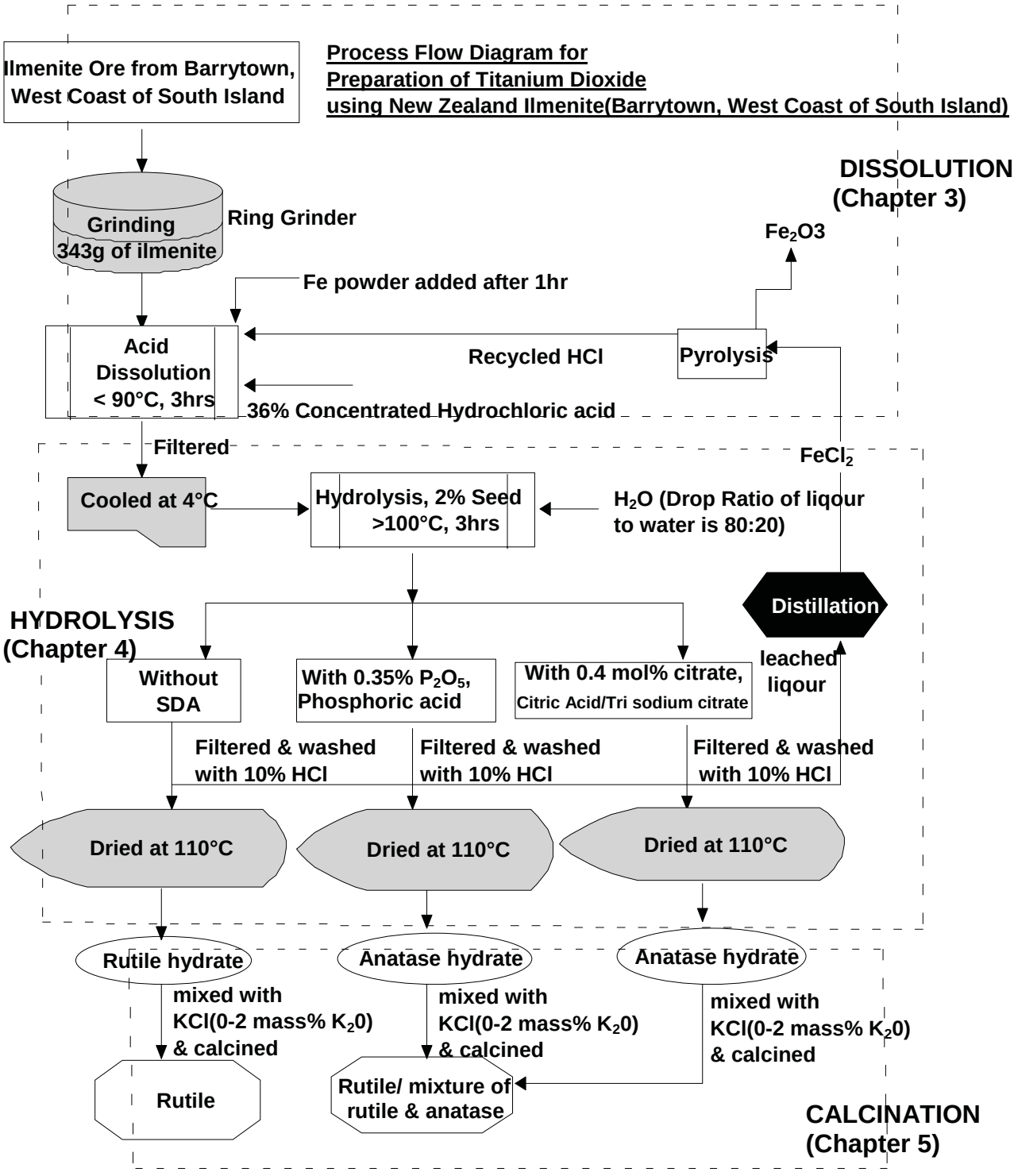

Figure 22: Process flow diagram for preparation of titanium dioxide by using New Zealand Ilmenite (Barrytown, West Coast of South Island)

4 Ilmenite Dissolution

In this chapter, we discuss the ilmenite dissolution mechanism, the parameters influencing the rate of ilmenite dissolution and experimental results.

4.1 Introduction

Ilmenite is a common mineral found in metamorphic and igneous rocks. It is named after the locality where it was first found, Ilmen Lake in the Ilmen Mountains, Russia. It is either black or iron black in color (Amethyst, 2009; Valentine, 2006). Ilmenite is a weak magnetic mineral (Mindat.org, 2009). Its chemical formula is $FeTiO_3$, which represent that ilmenite is a source of both iron and titanium dioxide. Iron can be present in the form of ferrous and ferric oxides. Ilmenite is used as a raw material in manufacturing TiO_2 pigments (Duncan & Metson, 1982). Commercial utilization of ilmenite is based on the dissolution rate of ilmenite by acid attack.

Table 1 : Major constituents of New Zealand ilmenite (Barrytown)(Christie, Douch, Winfield, & Thompson, 2000; Judd, 1986).

Constituents	Content (wt %)
TiO_2	47
FeO	38.4
Fe_2O_3	4.6

Source

On the west coast of South Island ilmenite black sand (commonly known as iron sand) is abundantly available, hence the Barrytown in Westland is the largest resources of ilmenite(6.9 Mt of Ilmenite). However, titanium dioxide content of New

Zealand ilmenite (45—47 % TiO_2) is low compared to the world standards (52—57 % TiO_2 for Western Australian ilmenite). Along with TiO_2, large proportion of iron is also present in the ferrous state as shown in table1 (Christie, et al., 2000; Judd, 1986) and traces of silicates has also been found. Ilmenite belongs to the class of oxide-hydroxide and hematite group. It's a black to brownish red and an opaque mineral.

4.2 Mechanism of Ilmenite dissolution

The mechanism of dissolution of ilmenite takes place in 3 steps (Duncan & Metson, 1982; van Dyk, Vegter, & Pistorius, 2002).

i. Approach of reactants towards the mineral surface

ii. Surface Interaction (adsorption of reactants + reaction + desorption of products)

iii. Drifting away of product from the surface.

Step i and iii can be tuned by controlling mass transfer in the system, which can also be increased by bringing agitation into light while interaction with mineral surface, which is the rate determining step (van Dyk, et al., 2002; Welham & Llewellyn, 1998); In other words ilmenite dissolution could be chemically controlled. Both iron and titanium go into the leach solution leaving unstable Ti (IV) in the form of titanyl ion TiO^{2+} (Duncan & Metson, 1982), which in turn polymerizes in concentrated HCl solution (van Dyk, et al., 2002). Hence showing titanium concentration in dissolving solution is also a rate controlling step in ilmenite dissolution (Duncan & Metson, 1982). However, an occurrence of polymerization of titanium was to be determined (Nabivanets & Kudritskaya, 1967). Cservenya'k calculated that polymerization of titanium would occur when Ti (IV) $>10^{-3}$M and (H [I]) >0.5M as the figure 6 shown

below. Hence showing that Ti (IV) and Cl (-I) concentrations are directly proportional to the Ti (IV) dependence in the solution. Initial acid strength normally concludes Cl (-I) concentration with leach solution (Cservenyák, Kelsall, & Wang, 1996). TiO^{2+} ions have been reported as predominating in acidic Ti^{IV} solutions in the absence of TiO_2. However, complexation occurs in chloride electrolytes

$$TiO^{2+} + nCl^- \longleftrightarrow [TiOCl_n]^{(2-n)+} \qquad \text{where } n = 1,2,3,4$$

$TiOCl^+$ and $TiOCl_2$ species were predicted to predominate at pH < 0 and chloride concentrations of l-5 $kmolm^{-3}$, though there are equilibria between TiO^{2+} ions and dihydroxo species, protonated monomers and oligomeric species. Then again promotion of solid species of iron and titanium precipitates resulting in formation of product layer on the surfaces of particles. The ilmenite dissolution reaction can be described by the following chemical reaction:

$$FeTiO_3 + 2HCl \longrightarrow Fe^{2+} + TiO^{2+} + 2Cl^- + 2OH^-$$

Once the Ti (IV) concentration goes beyond 10^{-3}M value, diffusion of polymer chain becomes the rate limiting step in the reaction, which in turn depends on the acid to ilmenite ratio. As per Jackson and Wadsworth, critical concentration requisite for polymerization may never be reached because of high acid to ilmenite concentration used (Duncan & Metson, 1982). However as per Sinha polymerization is observed at an early stage of leaching with low acid to ilmenite concentration (Sinha, 1984). The subsequent event that controls the rate of reaction is $TiOCl_2$ precipitate formation, which is the result of polymerization of titanium using high dissolution temperature and low initial acid to ilmenite mole ratio (van Dyk, et al., 2002). Diffusion of reacting species thus becomes the rate determining step. Additives can control the titanium concentration in the solution, hence the rate determining step. Lastly, the dissolution

reaction can be controlled by considerable reduction in hydrogen ion concentration (van Dyk, et al., 2002). Hence the rate limiting step is now the diffusion of hydrogen ions to reaction boundary.

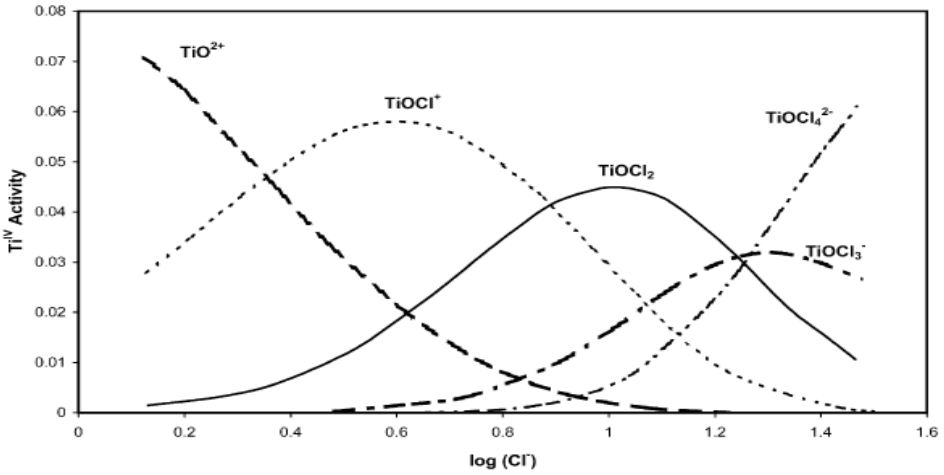

Figure 23: Ti (IV) – chloride speciation diagram for 0.1 Ti (IV) activities at 298 K as calculated by Cservenya´k et al. (1996).

4.2.1 Factors affecting dissolution rate of Ilmenite

There are numerous factors that affect the dissolution rate of ilmenite. As per the experiments performed, the dissolution depends on parameters such as particle size (Collins, 1997; El-Hazek, Lasheen, El-Sheikh, & Zaki, 2007; Kroger, 1964; Mahmoud, Afifi, & Ibrahim, 2004; Olanipekun, 1999; van Dyk, et al., 2002), acid concentration (Duncan & Metson, 1982; El-Hazek, et al., 2007; Hussein MK , Kolta GA , & El, 1976; Imahashi & Takamatsu, 1976; Lasheen, 2005; Mahmoud, et al., 2004; Olanipekun, 1999; van Dyk, et al., 2002), temperature (Duncan & Metson, 1982; El-Hazek, et al., 2007; Imahashi & Takamatsu, 1976; Mahmoud, et al., 2004; Olanipekun, 1999; Sinha, 1984; van Dyk, et al., 2002), pulp density (El-Hazek, et al., 2007; Lasheen, 2005), stirring (Duncan & Metson, 1982; Olanipekun, 1999; Sinha, 1984; Tsuchida, Narita, Takeuchi, Adachi, & Okabe, 1982; van Dyk, et al., 2002), time (El-Hazek, et al., 2007;

Lasheen, 2005), addition of iron powder (El-Hazek, et al., 2007; Lasheen, 2005; Mahmoud, et al., 2004) and additives (Duncan & Metson, 1982; Ismail Girgin, 1990; van Dyk, et al., 2002).

4.2.1.1 Particle Size

Particle size affects the chemical surface reaction. In dissolution, amorphous material is preferred over crystalline materials as the amorphous materials tend to dissolve more rapidly due to higher surface energy per unit volume compared to larger particles (Kroger, 1964). It is observed that the rate of dissolution increases by exposing large surface area of the soluble crystal face when subjected to milling or grinding (Collins, 1997). In a typical experiment conducted by Olenipuken, the sample with the smallest size fraction (20—73μm) were leached in 7.2M HCl at 70°C at an acid to ilmenite mole ration of 8:1, thus resulting in 62% dissolution of iron and 58% dissolution of titanium (Olanipekun, 1999). Therefore, the average diameter of particle size is inversely proportional to the rate of dissolution of ilmenite (El-Hazek, et al., 2007; Mahmoud, et al., 2004; van Dyk, et al., 2002).

4.2.1.2 Acid Concentration

In many cases, the acids used for dissolution of ilmenite are concentrated sulfuric acid or hydrochloric acid. In an experiment conducted by Imahashi and co workers, showed that the dissolution rate of ilmenite in H_2SO_4 solution is better than the dissolution rate of ilmenite in HCl solution (Imahashi & Takamatsu, 1976). Focusing on the environmental impacts caused by acid wastes, usage of HCl in dissolution helps in recovering free acid easily from its waste solution. Usually alcoholic hydrochloric acid is preferred over aqueous hydrochloric acid for better dissolution rates (Olanipekun, 1999). Acid concentration plays an important role in dissolution of

ilmenite (El-Hazek, et al., 2007; Lasheen, 2005; Olanipekun, 1999; van Dyk, et al., 2002). In a typical experiment, about 35% of iron was extracted in 6.8M HCl solution after 160min at an initial acid to ilmenite mole ratio ranging from 6:1 to 17:1, where as 7% of iron was removed with 2.16 M HCl solution after same duration and temperature (90°C) (Hussein MK , et al., 1976). In another experiment,about 100% of iron and titanium were extracted in 6M HCl solution after 400min by leaching at 90°C at an initial acid to ilmenite mole ratio ranging from 188:1 to 353:1, whereas 10% of iron and titanium were extracted in 4M solution for the same duration (Duncan & Metson, 1982). On the other hand high acid concentration has a definite impeding effect on hydrolysis reaction resulting in high titanium losses in solution (Mahmoud, et al., 2004).

4.2.1.3 Temperature

In a typical experiment, ilmenite ore of size fraction 53—74μm was subjected to dissolution using 7.2M HCl solution at different temperatures (70°C, 80°C and 90°C) and from the results obtained it was found that both iron and titanium were largely dissolved at 90°C further test were carried out at higher temperatures but found that it would increase the rate of corrosion and HCl vapor loss (Olanipekun, 1999). In an experiment performed by Jackson and Wadsworth, an acid concentration of 6M HCl with 692:1 initial acid to ilmenite ratio is subjected to dissolution for 100min at 90°C, as a result of which 100% titanium and iron was dissolved, where as 90% titanium and iron was dissolved at 70°C. Hence proving that the rate of ilmenite dissolution increases with an increase in dissolution temperature (Duncan & Metson, 1982). The reaction of ilmenite is best studied at temperatures from 50°C-80°C. In an experiment conducted by Sinha, iron was largely dissolved at higher temperature (Sinha, 1984; van Dyk, et al., 2002). In an experiment performed by Hazek and coworker, several

trails of dissolution were performed at different temperature ranging from room temperature to 100°C. From these experimental results, it was found that 25% titanium and 38% iron were dissolved at room temperature. This is due to low reactivity of ilmenite at room temperature. About 98% of titanium was dissolved at 80°C. At higher temperature (100°C) titanium dissolution is affected due to polymerization and hydrolysis. Hence 80°C is considered as an optimum temperature for 98% of titanium and iron dissolution (El-Hazek, et al., 2007).

4.2.1.4 Pulp density

In an experiment performed by Lasheen, the effect of pulp density on ilmenite dissolution was studied using concentrated HCl solution (12M). It was concluded that at high temperature and low initial acid/solid mole ratio rapid polymerization reaction is observed in the product layer (Lasheen, 2005). Hazek also came up with similar results stating that relatively low pulp density results in high leaching rate of titanium. It was observed that decrease in pulp density from the ratio of 9/1 to 1/20 increased the dissolution of titanium and iron from 11% to 92% with negligible effect thereafter (El-Hazek, et al., 2007).

4.2.1.5 Stirring

Stirring did not draw any special attention or any significant importance in an increase in titanium and iron extraction as per Jackson and Wadsworth (Duncan & Metson, 1982; Olanipekun, 1999). Sinha and Tsuchida found that surplus quantities of <10μm TiO_2 particles are produced by increasing the stirring speed in their respective experiments (Sinha, 1984; Tsuchida, et al., 1982; van Dyk, et al., 2002).

4.2.1.6 Additives

Addition of an additive might either increase or decrease the rate the ilmenite dissolution (van Dyk, et al., 2002). In an experiment performed by Duncan and Metson, an increased dissolution rate of ilmenite was observed using bisulfate and fluoride as additives to the leach solution, whereas a decreased ilmenite dissolution rate was reported with phosphoric acid as an additive (Duncan & Metson, 1982). In another experiment performed by Girgin, the dissolution rate increased with the addition of methanol as an additive when compared to 3M normal HCl solution (I Girgin, 1990).

4.2.1.7 Time

As a result of extending digestion time it was observed that the dissolution efficiency of titanium and iron increases (Lasheen, 2005). An optimum time for increasing the leaching of iron and titanium would be 2.5 hrs, if anything more than the above optimum time would result in some unfavorable effects on titanium and iron dissolution due to hydrolysis effect (El-Hazek, et al., 2007).

4.2.1.8 Addition of Fe Powder:

The quality of product obtained also depends on the addition of iron powder (El-Hazek, et al., 2007; Lasheen, 2005; Mahmoud, et al., 2004). In a typical experiment performed by Mahmoud, digestion was carried out by incorporating Fe powder at various interval of time (from 0 to 90min). It was observed that addition of Fe powder after 15min from the start of the experiment not only resulted in improved quality of rutile with 0.6% Fe as Fe_2O_3 and 87.5% Ti as TiO_2, but also increased the rutile recovery to 97% (Mahmoud, et al., 2004). Optimum time for addition of Fe is 30min above which negligible effect is observed, this is because of the amount of Ti^{4+} leached

increased with time. Hence large amount of Ti^{3+} are formed when Fe powder is added after longer times of leaching. Presence of Ti^{3+} enhances the dissolution rate by maintaining the dissolved iron in divalent state and the reducing conditions for a longer time (El-Hazek, et al., 2007; Mahmoud, et al., 2004).

In another experiment conducted by Hazek, the dissolution (time ranging from 1—2.5hrs) was carried out at 80°C with 1/10 as the solid/liquid ratio using 0.1kg of Fe powder for every kg of ilmenite. From this experiment it is concluded that, addition of Fe powder increases the titanium dissolution to 94% despite low acid concentration (S/L-1/10)(El-Hazek, et al., 2007). Increase in reductant (Fe powder) content results in an increase in acid consumption as a part of iron dissolution. Hence Optimum addition of Fe powder is in the ratio of 0.1kg/kg ilmenite.

4.3 Experimental

4.3.1 Materials

In this experiment ilmenite ore extracted from beach sand of Barrytown, West Coast of South Island, New Zealand, is used as the raw material, 37% hydrochloric acid, and Iron powder

4.3.2 Equipments

Straight sided reaction vessel, reflux condenser, thermometer, hotplate, funnel, glass fiber filter paper, mechanical agitator with teflon coated stirring rod, 4 necked lid and power supply

4.3.3 Procedure

Firstly 70g of ilmenite ore is ground finely in large TEMA mill (or ring grinder) for about 3 minutes, resulting in particle size fraction ranging from 50−100μm. In this

case, a straight sided reaction vessel with 4 necked lid with a reflux condenser, thermometer and a mechanical agitator with Teflon coated stirring rod is used on a hotplate. The dissolution conditions are fixed at 12M HCl solutions, 90°C, 3hrs total reaction time, a solid/liquid weight/volume ratio of 1:3 at 200rpm mixing rate. Dissolution of powdered ilmenite ore was carried out using 37% concentrated hydrochloric acid. About 1136ml(S:L-1:3) of 37% HCl was taken in a reaction vessel and heated up to 48—50°C (as HCl would vaporize above its boiling point, > 50°C). About 343g(S:L – 1:3) of ground ilmenite is now added to hot concentrated HCl solution with continuous stirring (stirring speed ~ 200rpm). Time and temperature is recorded at regular time interval. The above slurry is heated to about 80°C with continuous stirring (if not the ilmenite ore clusters up at the bottom of the reaction vessel resulting in poor ilmenite dissolution). 3g of Fe powder is added after 1 hr from time ilmenite was added to the acid. The digestion is allowed to take place for 2hrs from the time ilmenite is added. A sample of digested liquor is analyzed using cerium sulfate ($Ce(SO_4)_2$) titration almost during the end of the digestion process. The digested slurry is then filtered through a glass fiber filter paper. The filtered liquor was then divided equally in 500ml duran bottle and stored at 4°C.

4.4 Analysis of Ti, Fe and Ti^{3+}

Dissolved liquor is used for analyzing total Ti, Fe and Free Ti^{3+} present in the solution, following procedure was employed.

A sample of about 2g of filtered liquor was transferred to Erlenmeyer flask using a hot pipette. This was followed by the addition of 50ml of 10% HCl, 12ml conc. H_2SO_4 and 2g of aluminum foil, which results in a vigorous reaction. In order to arrest the reaction and get the reaction completed, a bung is put on the flask with a tube connecting to sodium bicarbonate solution. Once the reaction is complete, the

reaction mixture is titrated against cerium sulfate solution (0.1215 mol/dm^3). Methyl blue is used as an indicator for the first end point (for total Ti) and n-phenylanthranilic acid as an indicator for second end point (for total Fe). For analysis of Free Ti^{3+} present in the dissolved liquor, 2g of filtered liquor was treated with 50ml of 10% HCl and 12ml conc. H_2SO_4, which was then titrated against $Ce(SO_4)_2$ of 0.1215 mol/dm^3. In this case, Methyl blue is used as an indicator for the end point.

Concentration of total Ti & Fe in Solution

2g of sample, concentration of $Ce(SO_4)_2$ ⟶ 0.1215 mol dm^{-3}

Titration values:

Amount of $Ce(SO_4)_2$ used for 1st End Point ⟶ 'x' ml

Amount of $Ce(SO_4)_2$ used for 2nd End Point ⟶ 'y' ml

$x(0.1215) / (1000) = (1.215)\,xe^{-4}$, $y(0.1215) / (1000) = (1.215)y\,e^{-4}$

$1.215x\ x\ e^{-4} / (2e^{-3}) = (0.06)x$ mol kg^{-1} ⟶ Ti Eqn (1)

$1.215y\ e^{-4} / (2e^{-3}) = (0.06)y$ mol kg^{-1} ⟶ Fe Eqn (2)

Molecular weight of TiO_2 = 79.9, Molecular weight of FeO = 71.85

Hence, TiO_2 = 79.9Eqn (1) gkg^{-1} TiO_2

FeO = 71.85Eqn (2) gkg^{-1} FeO

Ce(SO4)2 used / *Sample*	*x (ml)*	*y (ml)*	*z (ml)*
R1	*19.5*	*20*	*17*

R2	*21.2*	*20*	*18*
R3	*21.2*	*20*	*18*
A1	*21.2*	*23*	*17.5*
A2	*17*	*14.5*	*13*
A3	*17*	*14.5*	*13*
A4	*19.5*	*18.7*	*17.2*
A5	*20*	*18*	*18*

Concentration of Free Ti^{3+} in the solution

2g of sample, concentration of $Ce(SO_4)_2$ ⟶ 0.1215 mol dm^{-3}

Titration values:

Amount of $Ce(SO_4)_2$ used for 1st End Point ⟶ 'z' ml

$x(0.1215) / (1000) = (1.215)\ xe^{-4}$,

$1.215x\ x\ e^{-4} / (2e^{-3}) = (0.06)x$ mol kg^{-1} ⟶ Ti Eqn (3)

Molecular weight of TiO_2 = 79.9, TiO_2 = 79.9Eqn (3) gkg^{-1} TiO_2

4.5 Results and Discussion

There are few factors that draw our interest in the ilmenite dissolution process using HCl such as particle size, acid to ilmenite ratio, iron content in the mixed slurry, optimum dissolution temperature. Dissolution is the first step that helps us obtain the dissolved liquor containing titanium which is further subjected to hydrolysis. This

process separates iron and titanium dioxide from ilmenite ore using concentrated HCl.

Chemical reactions:

$$FeTiO_{3\,(s)} \xrightarrow{36\%\ HCl} Ti^{4+}{}_{(aq)} + Fe^{2+}{}_{(aq)}$$

$$FeTiO_{3\,(s)} + 4HCl_{(aq)} \longrightarrow TiOCl_{2\,(aq)} + FeCl_{2\,(aq)} + 2H_2O_{(l)} \quad (Digestion)$$

The extraction of titanium species is inversely proportional to the particle size of the ground ore. Particle size fraction of ground ilmenite ore ranging from 50–100μm was used in this case. It is observed that particle size of the ilmenite ore plays an important role in dissolution reaction. By increasing the ore fineness, the surface area of each fines exposed to the acid (conc. HCl) also increases, which results in better dissolution rate under optimum dissolution conditions. Acid concentration had an impeding effect on ilmenite dissolution rate. Though acid like H_2SO_4 is preferred for dissolution, HCl aids in controlled dissolution rate with the help of iron powder and by using HCl it easy to recover free acid in waste acid solution. An acid to ilmenite ratio of 3:1(Liquid:Solid) resulted in extraction of 84.1–97.7g/kg of titanium and 78.6–87.2g/kg of iron with 12M HCl solution. Titanium species [Ti (IV)] that are formed are polymerised in hydrochloric acid solutions. The rate determining step in this experiment is the formation of Ti species, which is dependent on Cl (-I) and Ti (IV) concentration in the solution. The Ti (IV) concentration increases as the dissolution reaction progresses. Once the Ti (IV) concentration surpasses 10^{-3} M, polymerization of Ti(IV) would occur resulting in the formation of $TiOCl_2$ fines. With high dissolution temperature, the titanium polymerization reaction proceeds very rapidly,

resulting in the precipitation of $TiOCl_2$. The predominant species of titanium at the used HCl concentration is $TiOCl_2$.

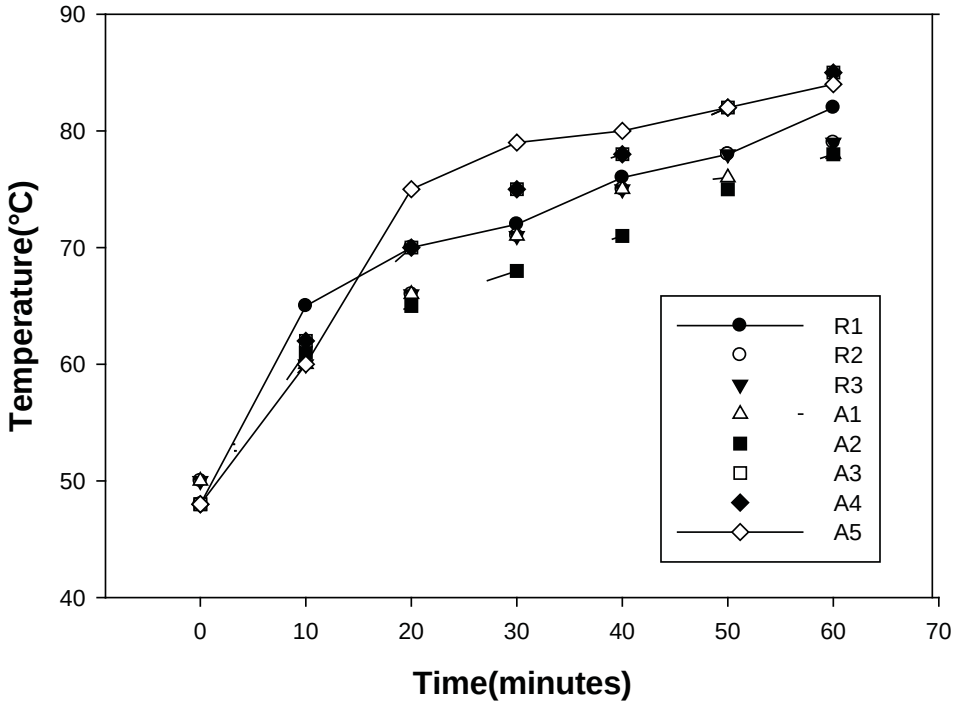

Graph 1 : Behavior of temperature with time during the 1st hour of the digestion process at 12M HCl solution, 200rpm and S/L ratio - 1:3; by plotting temperature versus time. The temperature and time readings of these samples are shown in table 9.

In the graph 1, it is observed that dissolution temperature increases with time. When ilmenite was added to HCl solution, a rapid increase in temperature is observed as a result of exothermic reaction. Higher dissolution temperature above 40°C increased the quantity of dissolved titanium. It is observed that, at a dissolution temperature above 90°C, there is titanium loss. From the table 2, it is evident that sample leached at higher temperature yields in higher TiO_2 concentration as a result of enhanced dissolution rate. For e.g. From Table 2, R1 leached at 85°C has TiO_2 concentration of

94.28g/kg and FeO concentration of 87.29g/kg whereas R2 leached at 78°C has TiO_2 concentration of 84.1g/kg and FeO concentration of 63.23g/kg. The particle size of ilmenite also helps in better dissolution rate, as the particles with larger surface area increased the dissolution rate. It is observed that ilmenite has better reactivity for dissolution at optimum temperature of 85°C—90°C above which affects the titanium dissolution.

From table 2, it is observed that the amount of TiO_2 dissolved has increased with increase in temperature. At 77°C, the amount of TiO_2 dissolved is 82.3g/kg (sample A2). At 88°C, better titanium recovery of 97.7g/kg (sample A5) is observed. From this it is observed that at higher temperature, the ilmenite reactivity with acid is high, hence resulting in higher titanium dissolution. At 88°C, amount of titanium dissolved was high but increasing dissolution temperature to 100°C seriously decreases and affects titanium dissolution due to polymerization and hydrolysis, without affecting iron, also higher dissolution temperatures would be less suitable due to increase loss of HCl vapour. Titanium solution at higher temperature (>100°C) hydrolyse readily in hydrochloric acid, so the temperature must be carefully regulated to delay hydrorysis until the digestion is at or near completion so that the gangue minerals are removed from the liqour. Continuous stirring has resulted in higher quantity of titanium and FeO. It is observed that poor stirring results in a weak dissolution rate, thus resulting in formation of clusters in mixture.

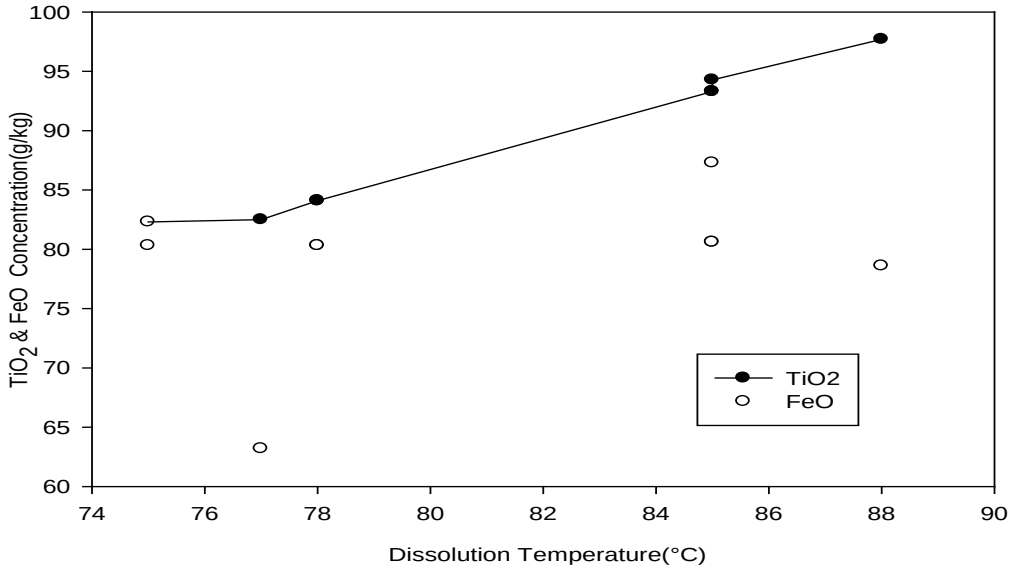

Graph 2: Relation between TiO_2 and FeO concentration with optimum dissolution temperature

Addition of iron powder after 1hr from the start of the dissolution process resulted in improved quality of titanium. Reduction in solution promotes the leaching of ilmenite ore in hydrochloric acid. Iron metal is considered as the most suitable reductant, since no foreign ions are introduced in the reaction medium. Ti^{3+} started to appear in the solution as a result of consequent reduction of Ti^{4+} once the Fe powder was added and suddenly increased with time. The total extracted Ti rapidly increased after addition of the Fe powder.

Table 2 : TiO_2 and FeO concentration at different optimum dissolution temperature

Sample Name	TiO_2 Conc (g/kg)	FeO Conc (g/kg)	Temperature (°C)
R1	94.2	87.2	85
R 2	84.1	79.6	78
R 3	84.1	79.6	78

A1	82.3	80.3	75
A 2	82.5	63.2	77
A 3	93.3	80.6	85
A4	93.3	80.6	85
A5	97.7	78.6	88

Addition of iron results in Ti^{3+} formation, presence of which increased the dissolution rate of titanium. Iron-ilmenite ratio of 0.1g of Fe/g of ilmenite increased titanium dissolution to 94%.

Chemical Reactions:

$$Fe_{(s)} + Fe^{3+}_{(aq)} \longrightarrow 2Fe^{2+}_{(aq)} \quad (Reduction)$$

$$Fe_{(s)} + 2Ti^{4+}_{(aq)} \longrightarrow 2Ti^{3+}_{(aq)} + Fe^{2+} \quad (Reduction)$$

Formation of Fe^{3+} is prevented by adding iron powder. The Fe^{3+} present in the solution absorbs onto titania, as a result of which discoloration is observed. Iron powder also prevents co-precipitation of iron (III) ions during hydrolysis. It is observed that dissolution reaction carried for more than 2—2.5hrs leads to the formation of unfavorable product. From graph 2, it is evident that with the increase in optimum dissolution temperature, the concentration of titanium increases and the iron concentration level stays well below titanium concentration, which helps us understand that this process was carried out at a good dissolution rate.

5 Hydrolysis

In this chapter, we discuss the hydrolysis of dissolved liquor ($TiOCl_2$); parameters influencing hydrolysis, structure determining agents (SDA), experimental setup and results.

5.1 Introduction

Hydrolysis is a chemical reaction, in which parent molecules are cleaved into 2 parts by the addition of the water molecule, where one group of the parent molecule gains hydrogen (H^+) from additional water molecule and other group of the parent molecule accumulates the hydroxyl group (OH^-). Hydrolysis is the critical step in titanium pigment production. Like Dissolution, hydrolysis also depends on few parameters like acid concentration, hydrolysis temperature and presence of Fe^{2+} and Fe^{3+} species. If hydrolysis is slow then TiO_2 loss in the solution increases (Mahmoud, et al., 2004). High acid concentration has definite hindering effect on hydrolysis reaction, whereas high hydrolysis temperature helps in Fe removal from the product, also helps in rutile recovery. At higher temperature, hydrolysis reaction of $TiOCl_2$ is known to be enhanced. Hence the optimum temperature for hydrolysis is 110°C.

5.1.1 Hydrothermal Hydrolysis

In this method, titanium dioxide is obtained by $TiOSO_4$ (an intermediate product of ilmenite and sulfuric acid dissolution) hydrolysis (Blumenfeld method) (Barbara Grzmil, Grela, & Kic, 2008). Here, water was heated up to 96°C and titanium liquor was introduced drop wise for 20 minutes, when desired temperature was attained. This was followed by an increase in temperature till the reaction mixture started

boiling. Boiling point of the reaction mixture was considered as the starting step of hydrolysis. Hydrolysis was influenced by initial concentration of $TiOSO_4$. Free Sulfuric acid also influences the degree of hydrolysis. Initial concentration of $TiOSO_4$ is inversely proportional to degree of hydrolysis (Barbara Grzmil, et al., 2008). This method was implied for many years on a large scale, but the complication involved in this process made it less familiar.

5.1.2 Hydrolysis in Micro emulsion

In this method, TiO_2 particles were obtained in micro emulsions using titanium tetraisopropoxide as surfactant, water and toluene as oil phase in controlled hydrolysis of TTIP in DBS and DS micelle resulted in TiO_2 particles. The factor that influence the degree of hydrolysis in this method was the water to surfactant ratio (R. Zhang, Gao, & Zhang, 2004).

5.1.3 THyCA method

In another experiment, TiO_2 powder were produced by THyCA method (transfer hydrolytic crystallization in alcohols) in which titanium alkoxide was dissolved in a portion of an alcohol and was set to autoclave at (250°C—300°C) with nitrogen purging. The resultant powder was then washed with acetone, dried and calcined at respective temperature to obtain a desired product (Kominami, et al., 1999).

Zhu and coworkers conducted an experiment, in which titanium butoxide was subjected to hydrolysis at room temperature resulting in submicron sized TiO_2. In this method, anhydrous titanium butoxide with alcohol is vigorously mixed with de-ionized water with anhydrous ethanol and acetic acid, aq. ammonia was added as a catalyst (Y. C. Zhu & Ding, 1999).

In this method, TiO_2 was prepared by subjecting $TiCl_4$ to hydrolysis. $TiCl_4$ is used as the raw material and is dissolved in distilled water. Titanium concentration is controlled around 3M. The above aqueous solution is treated with $(NH_4)_2SO_4$ (SDA) solution or distilled water. This is subjected to stirring and drop wise addition $TiCl_4$ at 70°C (hydrolysis temperature) for an hour. To obtain a pH 7, the above solution was treated with 2.5M dil. NH_4OH resulting anatase formation. Rutile crystals are formed by diluting $TiCl_4$ solution with 0.5M HCl solution (0°C), without using NH_4OH. The reaction mixture was kept in a constant temperature bath (70°C) for 5hrs. Titanium dioxide hydrate was separated by centrifugation and continuous washing with distilled water. The hydrate was then dried at 110°C and finely ground and subjected to calcinations (400°C, 600°C or 700°C for 2hrs) resulting in synthetic rutile. Xie et al investigated that the temperature of hydrolysis and presence of sulfate ions influences the crystalline morphology. Sulfate ions hinder the formation of rutile phase during hydrolysis of $TiCl_4$ at 70°C. The sulfated titania consisted of pure anatase phase with predominant particle size of 3.5nm which is much smaller than powders prepared from titanium alkoxides. Addition of small amount of SO_4^{2-} promotes the formation of anatase phase as SO_4^{2-} ions induce the growth of TiO_2 clusters to antase phase thus inhibiting rutile formation. When sulfate ions were introduced into the TiO_2, an increase in specific surface and pole volume was observed.

In this method, crystalline anatase titanium dioxide is produced by $TiCl_4$ hydrolysis. Here, 98% $TiCl_4$ was used as starting material without any further purification. In this method, $TiCl_4$ is digested with hydrochloric acid and then diluted using water. $TiCl_4$ concentration was set to 3M in water. To obtain desired pH, hydrazine hydrate (H_6N_2O – Ranbaxy) solution was added drop wise to the above solution. Hydrolysis

and condensation started immediately as mixing of the above mixture was initiated, which resulted in large cloudy floc which settled at the bottom of the reaction vessel. The reaction mixture was subjected to high speed constant stirring on a magnetic stirrer for 1hr at room temperature. The slurry was then subjected to filtration. The obtained hydrate was dried and calcined yielding crystalline titanium dioxide (Madhusudan Reddy, et al., 2001).

In this method, $TiCl_4$ was used as the starting material. It is observed that the hydrolysis of $TiCl_4$ in water and air are quicker, resulting in amorphous titania. So in this experiment Chu and worker made an attempt to hydrous $TiCl_4$ using concentration HCl (0.1M, 1.5M, and 5M). Degree of hydrolysis slows down with acid concentration in aqueous solution, which results in the crystalline phase formation (R. Chu, et al., 2004). However, this experiment clearly shows different size and shaped product was obtained at different concentration of HCl. Similarly, concentration of $TiCl_4$ plays a vital role in product size and shape showing that with same acidity and by increasing TiCl4 concentration severe agglomeration is observed (Cheng, Ma, Zhao, & Qi, 2002). The precipitate was then centrifuged washed with 0.1M HCl, dissolved water to eliminate unreacted reactants and absolute ethanol to dissolve soft template. The hydrate was then dried and calcined. HCl with 0.1 concentration yields a mixture of anatase and rutile, whereas with 1.5M HCl pure rutile was produced. Similar results were obtained by Wu and coworkers hence supporting the above methodology (M. Wu, et al., 1999).

In another experiment conducted by Yu and coworkers, TTIP was chosen as the source for producing TiO_2. TTIP was first treated with anhydrous ethyl alcohol to bring its high reactivity to normal. Here, HNO_3 and NH_4OH were used as hydrolysis catalyst. Hydrolysis was initiated by treating various aq. catalyst concentrated

solutions with ethanol solution. This mixture was subjected for stirring for 1hr at room temperature. The resultant slurry was then irradiated in an ultrasonic cleaning bath for 2hrs, which then was aged for 24hrs for further hydrolysis of TTIP. The hydrate was further dried at 100°C and calcined at respective temperature for an hour, resulting in xerogel powders (J. Yu, et al., 2003).

In another experiment conducted by Barringer and coworker, TiO_2 powder was prepared by hydrolysis of dilute ethonolic titanium tetra ethoxide solution ($Ti(OC_2H_5)_4$) using de-ionized water. To reduce the amount of insoluble impurities and to achieve homogenous nucleation of particles, water and ethanol was ultra-filtered using 0.22μm pore size millipore fibers. In this experiment, ethoxide was mixed with ethanol and water in a separate part of ethanol (one-half of the total volume) ethoxide solution was mixed with ethanol and water using a magnetic stirrer. The molar ratio of water to ethoxide was more than 2.5. The stirring rate was gradually reduced to a minimal level in order to minimize coagulation of titanium particles at the start of the reaction. This was later observed with precipitate (time between mixing and first turbidity observation). The intermediate products (TiO_2 alcohol powder) were then washed with water by continuous centrifugation and ultra-sonic dispersion cycle, which was effective in removing alcohol and unreacted alkoxide. Since the obtained product (powder) from this method could not be completely redispersed, they were only used for physical property characterization studies (Barringer & Bowen, 1985).

5.2 Structure Determining Agents

We know that TiO_6 octahedron binds the formation of rutile and anatase in Ti (IV) complexes. An interaction of 2 octahedral complexes by their vertices results in anatase formation, while interaction of 2 octahedral complexes by their edges results in rutile formation (Fahmi, Minot, Silvi, & Causá, 1993). In hydrolysis, anatase

structure is produced when Ti (IV) composites with the formation of 1 reaction active centre, whereas rutile is produced when Ti (IV) composites with the formation of 2 reaction active centre. Anatase is produced in a solution containing sulfuric acid as only one reaction active centre is possible for Ti (IV) complexes (Karvinen, 2003).

Crystal structure of TiO_2 can also be varied by using structure determining agents (SDA) at the beginning of hydrolysis process. The concentration and type of SDA used determines the morphology of particles. Usually structure determining agents have the function of self assembly of 2 hydrophilic ends in the synthesis of ordered arrays of structures (Xia, Liu, & Zhang, 2008). SDA is reckoned as a crucial template for preparation of materials with novel properties and morphologies. Many studies on non hydrolytic synthesis with different SDAs have been reported earlier (Trentler, et al., 1999; Vioux, 1997). SDA, which are amphillic poly block co-polymers are commonly used in non aqueous synthesis of TiO_2 (Ao, Xu, & Fu, 2009; Kavan, Rathouský, Grätzel, Shklover, & Zukal, 2001; Vukicevic, Ziemian, Bismarck, & Shaffer, 2008; P. Yang, Zhao, Margolese, Chmelka, & Stucky, 1999; Yu-de, Chun-lai, Xiao-dan, & Heng-de, 2003; Yue & Gao, 2000). Some of the other structure determining agents used in hydrolytic synthesis are phosphoric acid, nitric acid, citric acid, hydrofluoric acid and hydrochloric acid (Andersson, Osterlund, Ljungstrom, & Palmqvist, 2002; D. Huang, Luo, & Wang, 2005; M. Wu, et al., 1999; Yin, et al., 2001; J. C. Yu, Zhang, Zheng, & Zhao, 2003; Zaban, Aruna, Tirosh, Gregg, & Mastai, 2000). By using HCl as a template, rutile phase TiO_2 was obtained at higher acid concentration (Andersson, et al., 2002; M. Wu, et al., 1999). Whereas with higher concentration of phosphoric acid and nitric acid catalysts, the resultant TiO_2 phase is mainly anatase (Andersson, et al., 2002; D. Huang, et al., 2005; Samantaray & Parida, 2001; M. Wu, et

al., 1999). In the following section effects of SDA (phosphoric acid and citric acid) is briefly discussed.

5.2.1 Phosphoric acid

Unlike sulfated (SO_4^{3-}) titanium dioxide, not much literature or report is available for phosphated (PO_4^{3-}) titanium dioxide. Phosphoric acid is said to enhance the thermal stability and acidity of mesoporous materials (H.-R. Chen, Shi, Hua, Ruan, & Yan, 2001; Ciesla, Schacht, Stucky, Unger, & Schüth, 1996). There is also a debate whether it is a chemical promoter or a support stabilizer (Fitz & Rose, 1983; Gishti, Iannibello, Marengo, MorelliLi, & Tittarelli, 1984). However, earlier reports show that metal phosphate or phosphoric acid was used as a dopant in many catalysts like silica, zirconia, alumina, alumina-supported Niw, CoMo HDS and HDN catalysts (Busca, et al., 2002; Lewis & Kydd, 1991; Parida & Pattnayak, 1996; Pattnayak & Parida, 2000; Ramis, et al., 2002). The network structure of polymerized phosphoric acid is firmly attached to the surface of mesoporous material making them shrinkage resistant during thermal and hydrothermal treatment. Phosphorous can stabilize the structure of the resultant phosphated product with high surface area and high photocatalytic activity compared to the product obtained without phosphorous (J. C. Yu, et al., 2003).

Using Phosphoric acid as an SDA, anatase phase of titanium dioxide is obtained exhibiting high photocatalytic activity (D. Huang, et al., 2005). Concentration of phosphoric acid plays a vital role in pore size and its distribution. At high phosphoric acid concentration, poly-phosphoric acid is formed as a result of unequal bonding between metal complex and surplus molecules of phosphoric acid. The resultant poly-phosphoric acid cannot be removed at the later stage either by washing or calcination resulting in an asymmetrical pore size (D. Huang, et al., 2005). Hence

maintaining an optimum concentration of phosphoric acid as an SDA is very important.

In an experiment performed by Samantaray et.al, it was found that the phosphate ion concentration increased with an increase in activation temperature (i.e. @ higher calcination temperature) from 110°C to 500°C due to loss of water by dehydration, after which the phosphate ion concentration remains constant till 900°C. From the results obtained from XRD pattern, it was concluded that phosphate ion stabilizes the anatase phase of TiO_2, whereas a mixture of rutile and anatase was obtained with a sample without phosphate ion and only rutile was produced at higher calcination temperature (900°C). It was evident that phosphate ion percentage and the source have nothing to do with crystallinity of TiO_2(Samantaray & Parida, 2001).

In addition to the above phosphate treatment efficiently inhibits the growth of TiO_2 crystal grain, indicative of the vital role played by the P species on titania particles. This mainly due to the defect sites on the surface of titania particle. These defect sites on the surface of titania particles are either occupied or deactivated by P species of phosphate ions. This results in steric effect, which is exhibited by the phosphate ions on the surface of TiO_2 averting the direct contact of particles, hence inhibiting the crystal growth. The growth rate is large at higher temperatures because the activation energy is small; the growth rate is small at lower temperatures because the activation energy is big. Therefore, the grain size increases slowly at lower calcination temperatures while the grain size increases rapidly at higher calcination temperatures. It is also observed that P content decreases to some extent with the increase in calcination temperature resulting in slow growth of P-TiO_2 grain size at higher calcination temperatures (Feng, Liu, Li, Zhang, & Wei, 2009; Samantaray & Parida, 2001; J. C. Yu, et al., 2003).

5.2.2 Citric acid

Citric acid is a weak organic acid and a carboxylic acid. This weak organic acid is preferred over nitric acid because of hazardous effect on disposal of nitric acid (Wikipedia, 2009a). Citric acid is said to be a complexing agent (Dhage, Pasricha, & Ravi, 2003). Not much literature is available about the interaction of citric acid and colloidal TiO_2 particles.

In an experiment performed by Jiang et al, carboxylic acid (e.g. citric acid, oxalic acid etc) and nitric acid were used as modifiers in tuning the morphology and particle size distribution of TiO_2 (Jiang, et al., 2005). However, metatitanic acid (H_2TiO_3) was used as the starting material. Metatitanic acid contains 2 wt% of anatase crystal with particle size ranging from 2—5nm, as an intermediate product in the manufacture of TiO_2 pigment. This small amount of anatase crystal seeds can yield anatase phase from amorphous using modifiers such as citric acid and other carboxylic acids. Using citric acid as a modifier resulted in smaller and narrower particle size distribution and average particle size of TiO_2. This is because of the interaction between the carboxylic group and TiO_2 particle surface (Jiang, et al., 2005).

Dhage et al showed that addition of citric acid to $TiOCl_2$ solution leads to anatase phase formation on calcining at 350°C, as a result of arrangement TiO_6 octahedra by sharing faces. The XRD pattern obtained from the experiment matched the reported values for anatase phase with a surface area 60 m^2g. However, further increase in calcination temperature results in an initiation of phase transition from anatase to rutile, as a result of rearrangement of TiO_6 octahedra by sharing the edges. Hence subsequent protonation and face sharing TiO_6 octahedra results in anatase phase, in the presence of citric acid at ≤ 350°C (Dhage, et al., 2003).

In an experiment performed by Liu et al, it was evident that pure anatase phase was obtained in the presence of citric acid. In this method, $TiCl_4$ was used as a starting material. The coordination effects of carboxylic acids with titanium ions and their adsorption on titanium particles surfaces affects the crystal size and change of phase composition. Apparently anatase titania prepared in the presence of citric acid confirmed high photocatalytic activity for degradation of methyl orange and rhodamine B (Liu, Liu, & Zhang, 2008).

In another experiment performed by Yin et al, phase pure anatase TiO_2 crystals were obtained by using citric acid as an additive. $TiCl_4$ was used as a starting material in this method. The mixture was subjected to autoclave at 220°C for 2—4hrs indicating the degree of crystallization of anatase TiO_2 increases with calcination time. The same procedure was repeated in the absence of citric acid, which resulted in rutile crystals, as a result of quick hydrolysis of aq. solution of $TiCl_4$ to form small particles with size distribution ranging from 38 to 66 nm, whereas no particle formation could be detected in the presence of citric acid and $TiCl_4$ to prevent rapid hydrolysis of $TiCl_4$. Moreover, using HCl in the above process results in faster nucleation of the anatase TiO_2 rather than crystal growth (Yin, et al., 2002). In an earlier experiment performed by Yin et al, it was shown that addition of citric acid to $TiCl_4$ leads to rutile formation, this is due to chelation of citrate ion to the TiO_6 octahedra resulting in edge sharing polycondensation between TiO_6 octahedra by spatial effect benefit. As a result of high degree of protonation, TiO_6 octahedra enhanced their diffusion supporting chelation of citrate to TiO_6 resulting in rutile formation (Yin, et al., 2001).

5.3 Experimental Procedure

In this experiment, the liquor prepared from the earlier dissolution process is subjected to controlled hydrolysis using water and the hydrate is filtered and dried at

110°C. Rutile is produced without using structure determining agents. Anatase is produced using phosphoric acid, tri sodium citrate and citric acid as the structure determining agents. Hence, there are 3 procedure stated below

5.3.1 Materials

In this experiment, the materials used are dissolved liquor, water, 10% hydrochloric acid, 0.1M phosphoric acid and citric acid.

5.3.2 Equipments

Apparatus used in this experiment are 5 litre round bottom flask, reflux condenser, thermometer, heating mantle, dropping funnel, glass fiber filter paper, mechanical agitator with teflon coated stirring rod, 4 necked lid and power supply

5.3.3 Procedure (Rutile formation without SDA)

Firstly, the cold liquor stored in duran bottle at 4°C, prepared from dissolution of ilmenite is subjected to water bath at 80°C till all the $FeCl_2.4H_2O$ crystals are dissolved. In this experiment, the 5lts round bottom flask with 4 necked lid with a reflux condenser, thermometer and a mechanical agitator with teflon coated stirring rod is used on a heating mantle. Drop ratio of liquor to water used by volume is 80:20 i.e. 80 parts of liquor and 20 parts of water (for e.g. 20ml of water is added for 80ml of filtered liquor). So 20 parts of water is now added in a RBF on a heating mantle. The seed is prepared in RBF flask. The reaction mixture is brought to boiling temperature of ≥100°C. The remaining bulk liquor is then slowly added through a dropping funnel for about 30 minutes. It is important to keep the reaction mixture boiling and stirring throughout the process. Extra care has to be taken while adding bulk liquor as it should drop right into the solution and not onto the sides of the reaction vessel, which might result in an uncontrolled hydrolysis and cracks on the sides of the

reaction vessel. After the addition of the entire liquor, the reaction mixture is boiled for 3hrs under reflux. The resultant liquor is filtered using a glass fiber filter paper and then thoroughly washed with 10% HCl (if not the product would possess yellow color which represent the presence of iron content). The hydrate is then dried in an oven at about 100°C. The resultant hydrate is then ground and subjected to X-Ray powder diffraction (XRD) to investigate the structural properties of product obtained before calcination. The filtered liquor washed with 10 % HCl is subjected to evaporation and pyrolysis for HCl recovery, which is again used in dissolution process. Also, Fe_2O_3 is obtained as a byproduct, extracted from $FeCl_2$ crystals from filtered liquor.

Seeding or Seed preparation

About 100ml of water is added to the flask and heated to 96°C. About 8ml(2% of bulk liquor(400ml) obtained from digestion) of filtered liquor is added through a pipette (preheated) in a drop-wise manner for 30—40 seconds with continuous stirring. The reaction mixture is aged for 5 minutes at 96°C. This mixture is called the 'Seed'.

5.3.4 Procedure (Anatase formation using SDA)

For anatase phase TiO_2, the SDA used are phosphoric acid, tri-sodium citrate and citric acid. The apparatus used in this case is similar to the one used for rutile production. The procedure remains the same but this time the hydrolysis is initiated in the presence of phosphoric acid, sodium citrate or citric acid. The amount of SDA to be used also plays a vital role.

5.3.4.1 Phosphoric acid

The experimental procedure for producing anatase using phosphoric acid is same as the procedure followed for rutile production (5.2.3.1) except one step. In this

procedure phosphate ion is introduced in the form of phosphoric acid. About 'X'g (amount of phosphoric acid to be added depends on the volume of filtered liquor obtained from dissolution, which is shown in table 3) of phosphoric acid is mixed with 20 parts (for e.g. 20ml of water is added for 80ml of filtered liquor) of water and the mixture is heated to 96°C with continuous stirring. This step is followed by the addition of 2% seed to boiling water in RBF. In this procedure, the remaining bulk liquor is added much slower (40 minutes in dropping funnel) than the procedure followed in rutile production. The mixture is then boiled for 3hrs under reflux condenser, filtered, thoroughly washed with 10% HCl (if not the product would posses yellow color which represent the presence of iron content) and dried. The dry hydrate sample is subjected for XRD to identify its phase and crystallite size.

5.3.4.2 Citric acid and Tri-Sodium citrate

The procedure followed in this method is same the procedure followed for obtaining anatase using phosphoric acid except one step. In this procedure, citrate ion is introduced in the form of citric acid/tri-sodium citrate. About 'X'g (amount of citric acid/ tri-sodium citrate to be added depends on the volume of filtered liquor obtained from dissolution which is shown in table 3) of citric acid/tri-sodium citrate is mixed with 20 parts (for e.g. 20ml of water is added for 80ml of filtered liquor) of water and the mixture is heated to 96°C with continuous stirring. This step is followed by the addition of 2% seed to boiling water in RBF. In this procedure, the remaining bulk liquor is added much slower (40 minutes in dropping funnel) than the procedure followed in rutile production. The mixture is then boiled for 3hrs under reflux condenser, filtered, thoroughly washed with 10% HCl (if not the product would posses yellow color which represent the presence of iron content) and dried. The dry

hydrate sample is subjected for XRD to identify the phase and crystallite size of TiO_2 obtained.

5.3.4.3 Amount of SDA (Phosphoric acid, Citric acid and Tri-Sodium citrate) to be used

Since SDA plays a vital role in building the product phase and its properties. It is important to add an appropriate amount of SDA in hydrolysis step to obtain the desired product. Excess or less usage of SDA may result in undesired reaction phase. SDA to be used is directly proportional to the volume of liquor obtained by dissolution process. In this project, SDA such as phosphoric acid, citric acid and tri-sodium citrate are used to obtain anatase phase of TiO_2. The pH of the SDA also plays a vital role in obtaining a product. SDA with high concentration reduces the hydrolysis rate thus resulting in high TiO_2 loss in the solution. Hence SDA with appropriate pH value which favors hydrolysis is chosen.

5.4 Sample Characterization by X-Ray Diffraction (XRD) and Scanning Electron Microscopy (SEM)

Crystal phase identification and crystallite size were analyzed using XRD patterns. XRD measurements were performed at room temperature on hydrated sample of TiO_2 using Philips PW1729 (PW1840 v2.4) and visual XRD computer programs. XRD on hydrate and calcined samples were carried out using CoKα radiation at 2θ ranging from 20°—90°, step size of 0.05°, scan speed of 0.02°/sec, slit width of 0.05mm and time constant of 2s, which is run at a power of 40kv—40mA. Rutile percentage or rutile anatase ratio was determined from integrated XRD peak intensities. The weight fraction of rutile was determined using the following equation (Barbara Grzmil, Rabe, Kic, & Lubkowski, 2007; Spurr & Myers, 2002).

$$W_R = \left(1+I_A/(kI_R)\right)^{-1}$$

Where W_R is the weight fraction of rutile in sample, I_A and I_R are the intensities of anatase and rutile obtained from the areas of the peak relative to 101 and 110 reflections respectively and k is the coefficient ratio of peak intensity of anatase to rutile. The k value varies from 0.8—1.25. The average crystallite size of the product was determined by using Scherrer's equation (Zhao, Li, Zhang, Evans, & Duan, 2002).

$$L = k\lambda/(\beta(\theta)\cos(\theta))$$

Where L is the crystallite size, λ is the wavelength of X-ray radiation (CoKα – 1.790 A°), K is usually 0.89, β (FWHM) is the peak width at the half-maximum height after subtraction of the apparatus broadening, is the bragg's diffraction angle. $2\theta_A$ = 29.3° and $2\theta_R$ = 32.2° for TiO_2 (anatase) and TiO_2 (rutile) respectively. Scanning electron microscopy (SEM) was performed on FEI Quanta 200 Environmental Scanning Electron microscope (ESEM) to determine the structural characterization of the material. The dried powder samples of TiO_2 are sputter coated with gold on an aluminum stub which is mounted on a double sided tape and studied on FEI Quanta 200 Environmental Scanning Electron microscope.

5.5 Results and Discussion

From table 3, it is shown that hydrolysis is a very important step in developing the TiO_2 phase. Factors such as SDA, seed ratio, hydrolysis temperature and concentration of solution influence the TiO_2 phase. In this experiment, it is observed that hydrolysis temperature plays a vital role in controlling Fe content in the product. Higher hydrolysis temperature aids in the removal of Fe content in the product. It is

also observed that the initial concentration of $TiOCl_2$ liquor solution is inversely proportional to the degree of hydrolysis, as hydrolysis slows down with the increase in pH of the solution. About 93%—96% TiO_2 yield is obtained by using TiO_2 seed at the start of the hydrolysis reaction.

Chemical Reactions:

$$TiOCl_{2\,(aq)} + 2H_2O_{\,(aq)} \longrightarrow TiO(OH)_2 + 2HCl \longrightarrow TiO_2.xH_2O + 2HCl \quad (Hydrolysis)$$

$$Fe^{2+}{}_{(aq)} + 2HCl_{\,(aq)} + 4H_2O_{\,(l)} \xrightarrow{Distillation} FeCl_2.4H_2O_{\,(s)} + H_2 \ (Crystallization)$$

$$2FeCl_2.4H_2O_{\,(s)} \xrightarrow{Pyrolysis} Fe_2O_{3\,(s)} + 4HCl_{\,(g)} + H_2O_{\,(g)} + H_{2\,(g)} \uparrow (Recycling)$$

It is observed in table 3 that digested liquor subjected to hydrolysis without using SDA or additive results in formation of rutile, whereas the liquor subjected to hydrolysis with 0.35% P_2O_5 and 0.4% citrate as additive results in anatase or mixed phase (anatase and rutile). The sample without SDA uses HCl as a template and results in the formation on rutile. It is observed that rutile is formed when 2 octahedral composite interact by their edges increasing the Ti-O distance. Thus, the use of SDA results in modifying the crystal phase and particle size distribution of TiO_2.

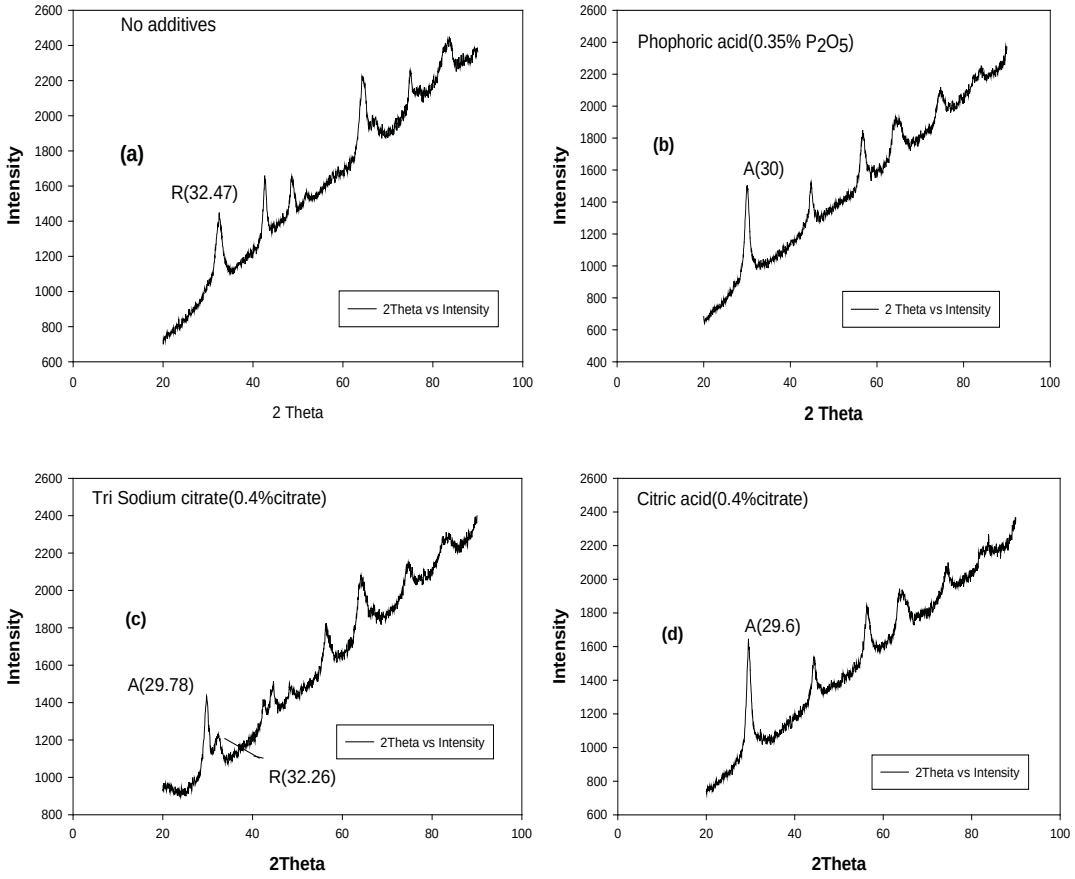

Graph 3 : Illustration of peak intensity of anatase and rutile by plotting 2theta versus intensity for hydrate samples produced using different SDA additives.

In this experiment, phosphoric acid plays a role of stabilizing agent. The use of phosphoric acid helps in maintaining high surface area and photocatalytic activity of the product, thus exhibiting the prime features of anatase. Due to higher activation energy possessed by TiO_2 particles containing phosphate ion, the crystallite size of anatase phase is smaller. The phosphate ion targets the deficient location on the TiO_2 surface and neutralizes its contact with TiO_2 particles thus hindering the crystal growth. In this experiment, we also use carboxylic acids such as citric acid and Tri-sodium citrate. The interaction between carboxylic acids and TiO_2 particles surface

resulted in pure anatase phase of TiO_2. Also, due to chelating of citrate ions with TiO_6 octahedra, with few samples mixed phase (anatase and rutile) of TiO_2 was observed.

Seed must be added before the heating of the solution is commenced. The precise time and the mode of addition of seed to the solution will affect the hydrolysis and precipitation. Hence the seed is added 5 minutes before the bulk liquor. In this method, the aging of 2% seed for 5 minutes results in better hydrolysis rate. It is observed that hydrolysis reaction is accelerated in presence of seed. The seeding technique is quite useful for the systematic control of the final particle size and for reducing the size distribution of the final product by the growth of a large number of seeds. The seed acts as nuclei to accelerate hydrolysis. The nuclei usually will be small particles of TiO_2, which can be formed from part of the solution of $TiOCl_2$, which is to be hydrolyzed.

Percentage recovery of dissolved TiO_2 from the hydrate is shown in table 3. The recovered amount of TiO_2 depends on the yield of the hydrate and the concentration of TiO_2. In case of rutile1, the yield is 35g and the percentage of TiO_2 recovered from the hydrate is 73.56%.

Table 3: Percentage of rutile and anatase obtained using different SDA in hydrolysis

Sample No.	**Additive**	**Amount of Additive , 'X'(gm)**	**Rutile percentage (%)**	**Anatase percentage (%)**	**Yield (gm)**	**Dissolved TiO_2 recovered as hydrate (%)**
Rutile 1	------	------	99.94	----	35	73.56
Rutile 2	------	------	99.94	----	37	87.11
Rutile 3	------	------	99.94	----	41	96.52
Anatase	0.35% P_2O_5					

phosphate 1	(Phosphoric acid)	0.252	0.084	99.91	24.9	74.90
Anatase phosphate 2	0.35% P_2O_5 (Phosphoric acid)	0.252	58.56	41.43	35.3	84.47
Anatase citrate 1	0.4% citrate (Tri-Sodium citrate)	1.4	51.41	48.58	39.7	84.25
Anatase citrate 2	0.4% citrate (Tri-Sodium citrate)	1.4	0.091	99.90	34.6	73.42
Anatase citrate 3	0.4%citrate (Citric acid)	1.1	0.075	99.92	40	81.01

For rutile3 with yield of 41g, the percentage of TiO_2 recovered from the hydrate increased to 96.52%. Amount of yield produced is dependent on the volume of bulk liquor added during the hydrolysis process. In case of anatase phophate1, the volume of bulk liquor added was 320ml which resulted in lesser yield of 24.9g.

XRD patterns obtained from the samples (a), (b), (c) and (d) prepared from hydrolysis of $TiOCl_2$ with phosphoric acid, citric acid and tri-sodium citrate as modifiers is shown in graph 3. The sloping background in the XRD patterns of the hydrate samples appears exaggerated due to the low intensity of the hydrate peaks. This is because these poorly crystalline materials weakly scatter X-rays and therefore have low peak intensities so that the displayed intensity scale is expanded. This makes the

background appear to be more steeply inclined than for the crystalline samples, whereas it is similar but the scale is expanded. From graph 3 (a), it is observed that pure rutile peaks were observed without using SDA. From graph 3 (b) and (d), pure anatase peaks were observed with the use of phosphoric acid and citric acid. From graph 3 (c), a mixture of anatase and rutile peaks was observed with the use of tri sodium citrate as SDA. The so obtained TiO_2 were either rutile or anatase and in a couple of case a mixture of both rutile and anatase. About 99.9% rutile was obtained without using any modifiers. About 99.9% anatase was obtained using modifiers such as phosphoric acid, citric acid and tri-sodium citrate at hydrolysis temperature of 110°C. A mixed phase of TiO_2 was obtained using SDA due to chelation. Maintaining the optimum pH for modifiers is also important as excess concentration of modifiers may result in uneven metal complex bonding and excess of phosphate and citrate ion, which cannot be eliminated at the later stage either by washing or by calcination. Crystallite size of the different hydrate sample was also analyzed from XRD results obtained which is shown in table 4.

Table 3 : Crystallite size of rutile and anatase obtained using different SDA in hydrolysis

Sample No.	**$2\theta_{Rutile}$**	**$2\theta_{Anatase}$**	**$FWHM_{Rutile}$**	**$FWHM_{Anatase}$**	**Crystallite size, d_{Rutile} (nm)**	**Crystallite size, $d_{Anatase}$ (nm)**
Rutile 1	32.44	---	1.55	---	29.24	---
Rutile 2	32.23	---	1.97	---	23	---
Rutile 3	32.47	---	1.73	---	26.20	---
Anatase phosphate 1 (Phosphoric acid)	---	30.06	---	1.3	---	34.6
Anatase						

phosphate 2 (Phosphoric acid)	32.23	29.78	2.22	0.921	20.4	48.9
Anatase citrate 1 (Tri-Sodium citrate)	32.27	29.78	1.41	1.11	32.13	40.5
Anatase citrate 2 (Tri-Sodium citrate)	---	30.08	---	1.32	---	34.14
Anatase citrate 3 (Citric acid)	---	29.6	---	1.11	---	40.20

6 Calcination

6.1 Introduction

Calcination is a process in which materials are subjected to heat treatment at a temperature below the melting point of the resultant material, as a result of which change in physical and chemical composition of material is observed (Gesenhues, 2001). The purpose of calcination is:

1. To remove moisture vapor and volatile substances present in material.
2. To measure the crystallite size of the material.
3. To study the changes that occurs on the crystalline phase of the material.

6.1.1 Heating medium

There are different kinds of Industrial furnace used worldwide for calcination e.g. blast furnace, cement kiln, electric arc furnace, induction furnace, kiln, muffle furnace, reverberatory furnace, Solar furnace, vacuum furnace. In this experiment an electric muffle furnace with thermocouple is used for accurate temperature readings.

6.2 Effect of Calcination

Calcination is a common heat treatment method employed in changing the crystallinity and photocatalytic activity of TiO_2 powder depending on calcination temperature (Q. Zhang, Gao, & Guo, 2000b). To obtain crystallization of TiO_2 particles before using them as photocatalyst for reactions, calcination of hydrated sample was

necessary (Addamo, et al., 2004). The quality of TiO_2 not only depends of the preparation method but also on calcination. The crystal phase of TiO_2 material is controlled by calcination temperature, hence high crystallinity of TiO_2 is stimulated by calcination (X. Chen & Mao, 2007). On calcinations, a significant change in the physical property of product is observed (J. Chen & Poon, 2009). Calcination at low temperature results in an increase in surface area, which exhibits better UV absorption and photoreactivity of TiO_2 photocatalyst (L. Zhang, et al., 2003), but calcination at higher temperature results in a decrease in specific surface area, due to increase in particle size and pore size (S. W. Oh, Park, & Sun, 2006).

Effect of calcination on micro structural behavior and photo activity of degussa p-25(~70% Anatase and 30% Rutile) was studied by Porter et al. It is evident that anatase rutile transition is slow at 600°C due to no change in relative intensity of peaks. However, at a temperature of 700°C and above, the intensity of rutile peak gradually increased while that of anatase decreased (Porter, Li, & Chan, 1999). The kinetics of anatase to rutile transition is observed as a result of shrinkage of O_2 structure and a cooperative movement of ions. This process requires high activation energy (>400KJ/mol) which is supplied by means of high temperature (Shannon & Pask, 1965). Phase transition from anatase to rutile occurs at higher temperature. As anatase is a metastable state of titania with high surface area. Higher calcination temperature not only increases the rutile percentage in TiO_2 but also increases crystallite size and particle size of the product (Porter, et al., 1999; Yan, He, G. Evans, Duan, & Zhu, 2005; J. G. Yu, et al., 2003). Its best explained in 3 key steps.

- Intra-agglomerate densification
- Anatase to rutile transformation

- Intra-agglomerate densification

Samples calcined at higher temperature results in lesser surface area, thus decreasing the photocatalytic activity. However, photo-activity of rutile and anatase is significantly increased with calcination temperature ranging from 400°C—600°C (Q. Zhang, et al., 2000b). At a temperature ranging from 350°C—450°C amorphous–anatase transformation is observed (D. J. Kim, Hahn, Oh, & Kim, 2002; S. J. Kim, Park, Jeong, & Park, 1999; Xiao, Liao, Zhang, & Chen, 2007; J. Yu, Wang, Cheng, & Zhou, 2007). Anatase-rutile transformation is observed at ranging from 600°C—1000°C (Ovenstone & Yanagisawa, 1999). In an experiment performed by Zhang et al, it is observed that photocatalytic activity of sample calcined at 400°C is higher than the photocatalytic activity of uncalcined sample. As a result of higher calcination temperature (>600°C), increase in size of semiconductor is observed which leads to rearrangement of photo generated holes and electrons. Thus, reducing the photo-activities of the product catalyst (Q. Zhang, et al., 2000b). Calcination reduces the photocatalytic activity due to (Gun'ko, et al., 2009):

i. Anatase to rutile transformation

ii. Sintering of particles, since the d_{XRD} value grows for all calcined titania.

In an experiment performed by Kim et al, the phase transformation of anatase-rutile occurred at 1000°C. At this point, the intensity of anatase peaks decreased rapidly while that of rutile increased. A similar result was obtained from an experiment performed by Xiao et al., where a small amount of anatase peak was observed with an increase in calcination temperature, whereas distinctive diffraction peak of rutile was observed at higher calcination temperature (Xiao, et al., 2007). Further calcination at 1100°C, anatase peaks almost disappeared. It was also observed that the

catalyst used in sol preparation controls the phase transition temperature (D. J. Kim, et al., 2002). In evidence to this statement, Hashimoto et al reported similar conclusion, where rutile peaks were observed at 650°C using di-ethalnolamine as a catalyst. Whereas rutile peaks failed to appear even at 800°C using HNO_3 as a catalyst (T. Hashimoto, et al., 1994). It is observed that the crystalline size of anatase at 1000°C increase 4 times compared to the crystallite size of anatase at 400°C (D. J. Kim, et al., 2002). Adherence of crystalline TiO_2 particles is enhanced at higher calcination temperature resulting in higher amplitude of interference spectra, thus decreasing the transmittance of TiO_2 film. The refractive index of TiO_2 thin film increased with an increase in calcination temperature, while the porosity was inversely proportional to calcination temperature. Hence, rutile phase of TiO_2 exhibit higher refractive index compared to anatase phase.

In an experiment performed by Gennari et al., commercial TiO_2 powder with 95% anatase and 5% rutile was subjected to calcination at 875°C, which also resulted in anatase to rutile transformation. However, Fe_2O_3 was used to boost anatase to rutile transition (Gennari & Pasquevich, 1999; Q. Zhang, Gao, & Guo, 2000a). Zhang et al. confirmed that small amount of SO_4^{2-} ions not only promotes anatase formation but also slows down anatase to rutile transformation, so that the sample remains completely in anatase phase even when calcined for 2hrs at 650°C and transformation to rutile occurs at temperature $\geq$700° C. In the absence of SO_4^{2-} ions, the phase transition occurs at 600°C (Q. Zhang, et al., 2000a). Unstable thermal behavior of anatase phase results in rutile phase transformation with diminutive photoactive property. In an experiment performed by Vishwanath and Ramasamy, titania-silica composites were prepared by sol-gel method. In this method, pure anatase phase was retained even at calcination temperature of 900°C, which is by introducing secondary

metaloxide into titania matrix. Thus, enhancing the thermal stability of titania (Viswanath & Ramasamy, 1998).

In an experiment performed by Jung et al., titania, silica/titania, zirconia/titania and alumina/titania mixed oxide were prepared by sol-gel method. In this method, it is concluded that crystallite size of anatase phase is linearly related to photoactivity of titania. Whereas with silica embedded titania composite, the photoactivity increased with higher calcination temperature without forming rutile phase even at 700°C. This is due to improvement in thermal stability of anatase phase. It concludes that increase in surface area and crystallinity of anatase phase greatly improved the photoactivity of the composite (Jung & Park, 2001). It is observed that when TiO_2 is heated to a temperature above 400°C an irreversible change and yellowing of the product occurs mainly due to expansion in a crystal lattice, particle size and rutile formation accompanied by recrystallization (B. Grzmil, Kic, & Rabe, 2004).

6.3 Additives used during calcination

Even though, phase transformation is greatly influenced by preparation method of TiO_2, additives can promote or inhibit the phase transformation and grain growth of TiO_2 to some extent. Additives like MoO_3, Cr_2O_3, Li_2O, ZnO, MgO, Sb_2O_3, NiO, CoO, CuO, MnO_2, and Fe_2O_3 are considered as promoters of anatase to rutile transformation and grain growth of TiO_2. While additives like Na_2O, WO_3, CeO_2, Al_2O_3 are considered as inhibitors of phase transition and has little or no effect on grain growth (Francisco & Mastelaro, 2002; B. Grzmil, et al., 2004; Iida & Ozaki, 1961). In an experiment performed by Ratajska, additives with compounds such as potassium, phosphorous, zinc, magnesium and aluminum added to hydrated TiO_2 before calcination has a significant effect on the product obtained (B. Grzmil, et al., 2004; Ratajska, 1992).

It is observed that particles of additives present on the titanium dioxide surface (phosphates and alkali ions with the exception of Li+) limit the growth of grains during calcination and increase the temperature of anatase-rutile transformation, whereas the ones dissolved in TiO2 bulk accelerate it. Atoms of additives, introduced into the regularly occupied lattice, may bring about the formation of atomic or electronic defects. There are two ways of building-in of foreign atom into the lattice. An atom of an additive locates in the lattice site instead of a regular atom or it takes place in the interstitial of the lattice. If the foreign (irregular) atom has a valence different from the regular atom, then the substitution is followed by the formation of vacancies in anion or cation sublattices or by the formation of interstitial atoms. An effect that is known as valence control by doping occurs when the regular atoms may take different oxidation states. It was suggested that additives increasing the number of vacancies in the titanium dioxide anion sublattice (Li+, K+, Cu2+, Al3+) act as promoters of the anatase-rutile transformation, whereas additives (Nb2O5, PO43-, SO42-) reducing the number of vacancies are responsible for the transformation inhibition. Addition of additives which promotes rutilization not only increases the rutile stability but also increases the calcination temperature required for transformation, which significantly weakens the optical properties of TiO_2 (Barbara Grzmil, et al., 2007). It is also evident that additives increase the reaction rate constants at comparable temperature (MacKenzie, 1975). In an experiment performed by Grzml et al., additives such as phosphates and lithium were introduced in the form of $NH_4H_2PO_4$, K_2SO_4 and Li_2SO_4. The hydrated samples were doped with the above additives and were then subjected to calcination (Barbara Grzmil, et al., 2007).

6.3.1 Phosphate content

It was observed that with an increase in phosphate percentage in hydrated sample, the rutilization ratio faded away. However, the above process depends on calcination time and temperature, as rutilization process is rapid at higher calcination temperature and time even with high percentage of phosphate content. Hence at respective calcination temperature phosphate additives helps in inhibiting unwanted growth of crystallites (anatase and rutile). The calcined samples with phosphate content had lower crystallite size compared to the samples without phosphate content (Barbara Grzmil, et al., 2007).

6.3.2 Potassium/Lithium content

The hydrated samples containing higher potassium/lithium tend to enhance the transformation ratio to maximum not only at higher calcination temperature but also at lower calcination temperature. Not much of a difference in crystallite size was observed. Hence potassium/lithium additives help in promoting rutilization compared to the sample without potassium/lithium content. As far as the pigment stability is concerned additives such as Si, Al, Zn act as the prime promoters used (Barbara Grzmil, et al., 2007).

Additives (Li^+, K^+, Cu^{2+}, Al^{3+}) that increase the vacancy number in TiO_2 anion sublattice act as rutilization promotes while additives responsible for decreasing the vacancy number act as transformation inhibitors for e.g. Nb_2O_5, PO_4^{3-}, SO_4^{2-} (MacKenzie, 1975 ; Mills & Le Hunte, 1997; Ruiz, Dezanneau, Arbiol, Cornet, & Morante, 2004). In an experiment performed by Grzmil et al., potassium and phosphate weight ratios were varied and were introduced to hydrated TiO_2 suspension, as a result of which the anatase to rutile transformation decreased with an increase in potassium content in hydrated TiO_2 irrespective of process temperature

and phosphate content. Influence of potassium was higher calcination temperature and higher phosphate content. The average size of rutile crystals was reduced by 60nm at lower calcination temperature. Hence the influence of increase in potassium content on anatase and rutile crystallite size was weak compared to the one obtained by transformation degree. It is evident that potassium/phosphate additives in TiO_2 hydrate causing larger surface area affect the elevation temperature of rutilization, thus limiting the crystallite growth compared to non-modified TiO_2 (Barbara Grzmil, et al., 2007). Alkali compunds, such as potassium salts are introduced to improve the tinting strength and hiding power and to resist the sintering of TiO_2 during calcination.

6.4 Experimental procedure

In this experiment, electric muffle furnace with thermal couple is used to record accurate temperature readings. After hydrolysis, step the hydrate is dried in an oven at 110°C. Potassium (K_2O) additive is used in the form of KCl solution. Different concentrations of KCl solution ranging from 0—2 K_2O% are prepared. About 0.5ml of KCl solution with different concentration is added and mixed well with 1g of hydrated TiO_2 samples. The mixture is dried further at 110°C and ground for better mixing process. Hydrated TiO_2 sample with potassium content is now subjected to different calcination temperature ranging from 925°C—1000°C maintaining the calcination time as constant (1hr). The calcined sample is then ground and subjected to XRD and SEM to study the structural, optical and photocatalytic properties of the calcined sample. In this process, all hydrate samples from hydrolysis are calcined but 4 different calcined samples are studied namely rutile3, anatase phosphate1, anatase citrate1 and anatase citrate3. The data for other calcined samples (rutile1, rutile2,

anatase phosphate2 and anatase citrate2) are listed in appendices (Tables 11, 12, 15 17 and Graphs 8, 9, 10, 11).

6.5 Results and Discussion

The purpose of performing calcination is to investigate the TiO_2 behavior at higher calcination temperature, the effect potassium additive on hydrated sample of TiO_2 and the effect of calcination temperature on crystallite size. The XRD patterns of calcined samples are illustrated in graph 4 [(a), (b), (c) and (d)]. Where (a) represents XRD reading of rutile(no SDA) with 1.5% K_2O calcined at 975°C, (b) represents anatase phosphate(phosphoric acid) with 1.5% K_2O calcined at 975°C, (c) represents anatase citrate(tri sodium citrate) with 1.5% K_2O calcined at 975°C and (d) represents anatase citrate(citric acid) with 1.5% K_2O calcined at 975°C. From the previous chapter, we know that the peaks of anatase (101) and rutile (110) at 2θ= 29.3° and 2θ= 32.3° respectively. Comparing the graph 3 and graph 4, a relative shift in peak is observed with calcined samples from graph 4[(a), (b), (c) and (d)]. This indicates that the peak at the Bragg's angle (2θ) has shifted from 29.3 to 32.23 as a result of calcination at higher temperature.

Chemical Reaction:

$$TiO_2.\ xH_2O\ (s) \xrightarrow{\Delta\ K_2O} TiO_2\ (s) + xH_2O\ (g) \uparrow$$

From tables 5, 6, 7, and 8, it is observed with an increase in calcination temperature, the peak intensity of rutile increases and that of anatase decreases thus increasing the degree of rutile transformation. The intensity of anatase almost disappeared while that of rutile increased at a temperature higher than 950°C. This helps us understand that the degree of rutilization is higher at higher calcination temperature, indicating the increase of rutile content in the sample with the increase in calcination

temperature. The rutile hydrate sample when calcined at 975°C, results in higher rutile percentage as illustrated in graph 5 (a), whereas anatase hydrates when calcined at 975°C rutile phase transformation was rapid and higher rutile percentage was observed as shown in graph 5 (b), (c) and (d). Hence higher activation energy is required for anatase-rutile transition, which is sourced by elevated temperatures.

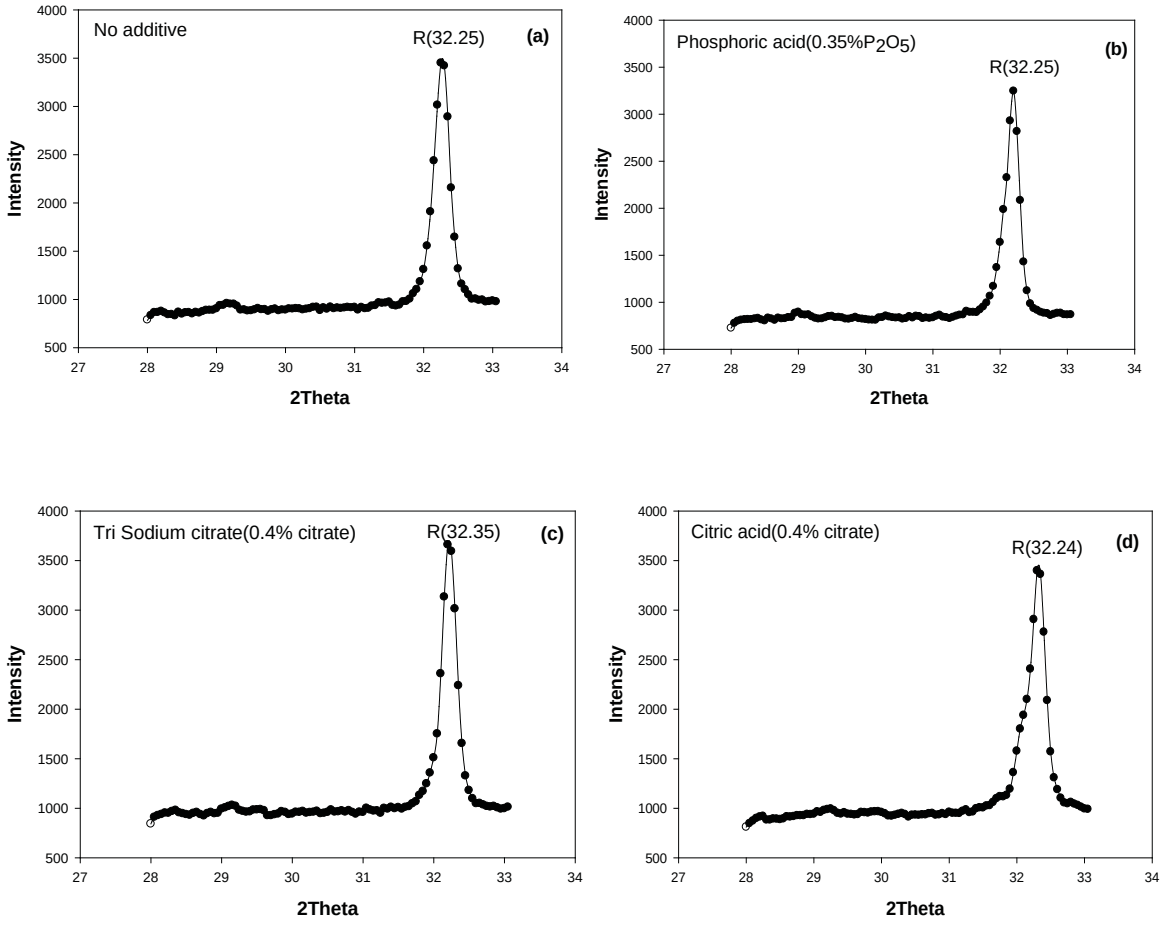

Graph 4 : Illustration of different sample [(a), (b), (c) and (d)] showing peak intensity after calcination of hydrate samples with 1.5% K_2O calcined at 975°C by plotting intensity versus 2Theta. (a) – Rutile3 (no SDA); (b) - Anatase phosphate1 (phosphoric acid); (c) - anatase citrate1 (tri sodium citrate); d - anatase citrate3 (citric acid)

However, slight variation in rutile percentage is negligible, as the different scale considered in graph 5 (a), was not of a big margin. The percentage rutile in graph 5 (a) was not less than 99.96%, hence a different scale was used.

The behavior of hydrate samples with potassium additives is studied under calcination. In this experiment, a distinct phase transition rate with potassium additives in hydrated TiO_2 is explained. With an increase in potassium content on hydrated TiO_2 (0—2 mass% K_2O w.r.t TiO_2), degree of rutile formation increased with calcination. At higher calcination temperature the effect of potassium content on hydrated TiO_2 has negligible effect on rutile percentage. Since noticeable difference was observed with samples having 0% K_2O and sample with 1.5% K_2O at different calcination temperature, the tables below (table 5, 6, 7 and 8) shows the samples with potassium content of 0% K_2O and 1.5% K_2O at different calcination temperature. Appendices (table 13, 14, 16 and 18) are referred for samples with 0.5%, 1% and 2% K_2O. However, the graphs plotted consists of potassium content ranging from 0—2%.

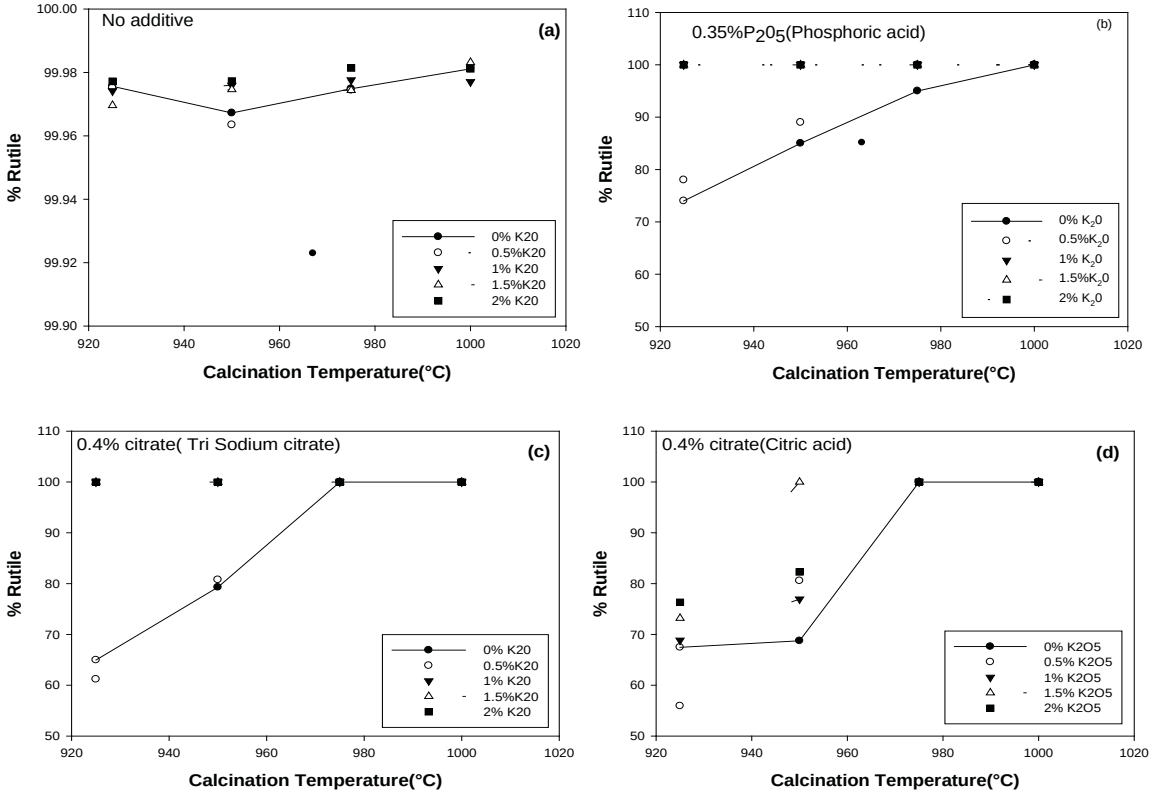

Graph 5 : Different samples [(a), (b), (c) and (d)] illustrating the degree of rutilization at different calcination temperature and potassium content (a) – Rutile3 (no SDA); (b) - Anatase phosphate1 (phosphoric acid); (c) - anatase citrate1 (tri sodium citrate); (d) - anatase citrate3 (citric acid). Note: different scale is chosen for TiO_2 without SDA (a).

Table 5, 6, 7 and 8 helps us understand that potassium acts as a promoter for rutilization. From graph 5 [(a), (b), (c) and (d)], comparing the samples with no potassium content (0% K_2O) and samples with potassium content(0.5—2% K_2O) at elevated temperatures, the rutile transformation is increased with an increase in potassium content and calcination temperature ranging from 925°C—1000°C. Where (a) represents a sample of rutile(no SDA) with 0—2% K_2O calcined at a temperature from 925°C—1000°C, (b) represents anatase phosphate(phosphoric acid) with 0—2% K_2O calcined at a temperature from 925°C—1000°C, (c) represents anatase citrate(tri sodium citrate) with 0—2% K_2O calcined at a temperature from 925°C—1000°C and

(d) represents anatase citrate(citric acid) with 0—2% K_2O calcined at a temperature from 925°C—1000°C.

Table 4 : Rutile3 (no SDA) after calcination showing Rutile percentage (%) and crystallite size at different potassium content (0%K_2O and 1.5%K_2O)

Calcination temperature (°C)	**Rutile percentage (%)**	**$2\theta_R$**	**β_R**	**Crystallite size,d_R (nm)**
0% K_2O				
925	99.9756	32.28	0.37	12.24
950	99.9672	32.14	0.26	17.26
975	99.9748	32.39	0.25	17.71
1000	99.9811	32.47	0.19	23.61
1.5%K_2O				
925	99.9790	32.22	0.30	18.05
950	99.9749	32.35	0.29	19.70
975	99.9807	32.25	0.29	20.50
1000	99.9839	32.19	0.21	22.94

Hence potassium content and calcination temperature go together with rutilization. The potassium content exceeding the optimum range may either result in decreasing effect or no effect on rutilization during calcination for e.g. samples with 2% K_2O has negligible effect on the degree of rutile formation(table 11—18).

The potassium adsorbs on the surface of hydrated TiO_2, thus filling the vacancy in TiO_2 crystal lattice resulting in rutile formation. From table 5, it is observed the rutile

sample has little or no effect on potassium additive while in the case of anatase phosphate (phosphoric acid) increase in potassium content with 0%K_2O at 925°C has 22% anatase and 78% rutile, while 1%K_2O at 925°C has 99.97% rutile as shown in table 6. Anatase phosphate with 0% K_2O at 950°C and 975°C still results in anatase peaks.

Table 5 : Anatase phosphate1 (phosphoric acid) after calcination showing percentage and crystallite size of rutile and anatase at different potassium content (0%K_2O and 1.5%K_2O)

Calcination temperature (°C)	**Rutile percentage (%)**	**Anatase percentage (%)**	**$2\theta_R$**	**β_R**	**$2\theta_A$**	**β_A**	**Crystallite size,d_R (nm)**	**Crystallite size,d_A (nm)**
%0 K_2O								
925	74.2451	25.7552	32.26	0.26	29.77	0.37	16.96	12.17
950	83.3056	16.6944	32.33	0.23	29.86	0.30	19.79	15.01
975	95.9304	04.0696	32.24	0.23	29.18	0.19	21.57	22.60
1000	99.9840	00.0159	32.29	0.19	---	---	22.54	---
1.5% K_2O								
925	99.9790	00.0209	32.22	0.30	---	---	18.05	---
950	99.9749	00.0250	32.35	0.29	---	---	19.70	---
975	99.9807	00.0192	32.25	0.29	---	---	20.50	---
1000	99.9839	00.0160	32.19	0.21	---	---	22.94	---

Pure rutile peak was observed at 1000°C without potassium content but with increase in potassium content 1.5% K_2O at 950°C and 975°C resulted in the disappearance of anatase peak and increase in rutile peak. From this, we can say that the phosphate ion attached to TiO_2 at a given calcination temperature inhibits rutilization, while potassium additive promotes rutilization at same calcination temperature.

Table 6 : Anatase citrate1 (tri sodium citrate) after calcination showing percentage and crystallite size of rutile and anatase at different potassium content (0%K_2O and 1.5%K_2O)

Calcination temperature (°C)	**Rutile percentage (%)**	**Anatase percentage (%)**	**$2\theta_R$**	**β_R**	**$2\theta_A$**	**β_A**	**Crystallite size,d_R (nm)**	**Crystallite size,d_A (nm)**
%0 K_2O								
925	64.9558	35.0441	32.21	0.30	29.71	0.30	15.10	15.01
950	79.2954	20.7045	32.49	0.28	29.97	0.30	15.75	15.02
975	99.9782	00.0217	32.28	0.26	---	---	16.91	---
1000	99.9836	00.0163	32.28`	0.21	---	---	21.57	---
1.5% K_2O								
925	99.9781	00.0218	32.23	0.24	---	---	18.87	---
950	99.9777	00.0222	32.26	0.24	---	---	18.88	---
975	99.9815	00.0184	32.35	0.22	---	---	20.60	---
1000	99.9841	00.0158	32.30	0.17	---	---	25.60	---

A maximum amount of rutile is observed at with the sample containing 2% K_2O at 1000°C (table 13, 14, 16 and 18). Similar observations were made with anatase citrate (tri-sodium citrate) shown in table 7, In case of anatase citrate (tri sodium citrate/citric acid), it is observed that rapid rutilization occurs with calcination temperature above

950°C irrespective of potassium content as shown in table 8 and 9. Hence potassium additive promotes rutile transformation on samples of anatase phosphate (phosphoric acid) and anatase citrate (tri sodium citrate/citric acid) at given calcination temperature. The citrate ions present in TiO_2 inhibits the rutile transformation at given calcination temperature in the absence of potassium additive, while anatase to rutile transformation is enhanced rapidly at the same calcination temperature in the presence of potassium content. It may be due to the pH level of carboxylic acids that hinders the rutile formation in the absence of potassium content in the sample. At higher calcination temperature ranging from 975°C—1000°C, the citrate ions hardly influences the degree of rutilization regardless of presence of potassium content. At higher calcination temperature, the citrate will burn off leaving little or no effect on anatase/rutile content. Hence it is concluded that citrate ions attached to TiO_2 hinders rutilization at a given calcination temperature due to protonation followed by the possible face-sharing TiO_6 octahedra which will slow down the formation of rutile phase, whereas potassium additive promotes rutile transformation on samples of anatase citrate (citric acid/tri sodium citrate) at the same calcination temperature (925°C–950°C).

Table 7 : Anatase citrate3 (Citric acid) after calcination showing percentage and crystallite size of rutile and anatase at different potassium content (0%K_2O and 1.5%K_2O)

Calcination temperature (°C)	**Rutile percentage (%)**	**Anatase percentage (%)**	**$2\theta_R$**	**β_R**	**$2\theta_A$**	**β_A**	**Crystallite size,d_R (nm)**	**Crystallite size,d_A (nm)**
%0 K_2O								

925	55.9291	44.0708	32.25	0.41	29.75	0.37	11.05	11.99
950	80.5604	19.4395	32.25	0.25	29.71	0.30	18.05	15.01
975	99.9774	00.0225	32.35	0.24	---	---	18.13	---
1000	99.9818	00.0181	32.18	0.23	---	---	19.61	---
1.5% K_2O								
925	73.1773	26.8226	32.16	0.30	29.80	0.27	15.10	16.19
950	99.9770	0.02297	32.23	0.30	29.77	0.30	15.10	15.01
975	99.9751	0.02480	32.24	0.28	---	---	15.79	---
1000	99.9781	0.02185	32.24	0.26	---	---	16.88	---

Degree of rutilization usually goes along with growth in crystallite size. From graph 7 [(i), (ii), (iii) and (iv)], where (i) represents the sample of rutile(no SDA) with 0—2% K_2O calcined at a temperature from 925°C—1000°C, (ii) represents anatase phosphate(phosphoric acid) with 0—2% K_2O calcined at a temperature from 925°C—1000°C, (iii) represents anatase citrate(tri sodium citrate) with 0—2% K_2O calcined at a temperature from 925°C—1000°C and (iv) represents anatase citrate(citric acid) with 0—2% K_2O calcined at a temperature from 925°C—1000°C, it is evident that the crystallite size of hydrated TiO_2 increases with an increase in calcination temperature. However, potassium content in hydrated sample has no effect on crystallite size of the product samples. From table 5, we can see that the crystallite size of rutile increases above 925°C, a significant increase in crystallite size are observed at 1000°C. Table 6 shows that crystallite size of both anatase and rutile increases and above 975°C the anatase phase disappears, thus showing maximum crystallite size for rutile at 1000°C. Similar observations were made with table 7 and 8. The peak width

(FWHM, β) is inversely proportional to the crystallite size. From graph 6[(1), (2), (3) and (4)], (1) represents the sample of rutile(no SDA) with 0—2% K_2O calcined at a temperature from 925°C—1000°C, (2) represents anatase phosphate(phosphoric acid) with 0—2% K_2O calcined at a temperature from 925°C—1000°C, (3) represents anatase citrate(tri sodium citrate) with 0—2% K_2O calcined at a temperature from 925°C—1000°C and (4) represents anatase citrate(citric acid) with 0—2% K_2O calcined at a temperature from 925°C—1000°C. It is observed that, with an increase in calcination temperature, FWHM of rutile peak (β_R) decreases (graph 6).

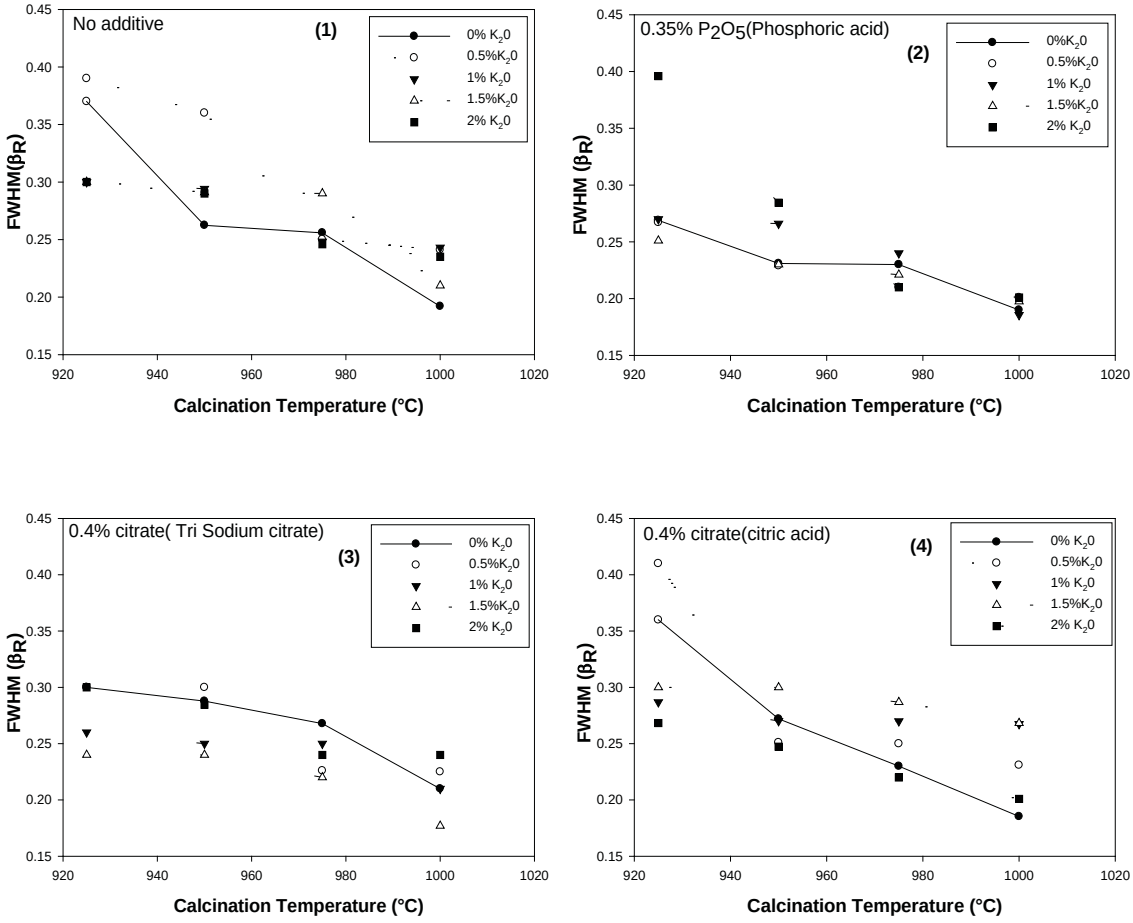

Graph 6 : Illustrates the relation between FWHM and calcination temperature of different samples [(1), (2), (3) and (4)]. (1) – Rutile3 (no SDA); (2) - Anatase phosphate1 (phosphoric acid); (3) - anatase citrate1 (tri sodium citrate); (4) - anatase citrate3 (citric acid), β_R –FWHM of rutile peak

Similar observations were made with anatase samples, the calcination temperature is linearly proportional to FWHM of anatase peak (β_A). As a result of increase in calcination temperature the β_A decreases, thus increasing the crystallite size of anatase phase. At one point of calcination, crystallite size of anatase keep decreasing and anatase phase is almost disappeared with an increase in calcination temperature as a result of rutilization.

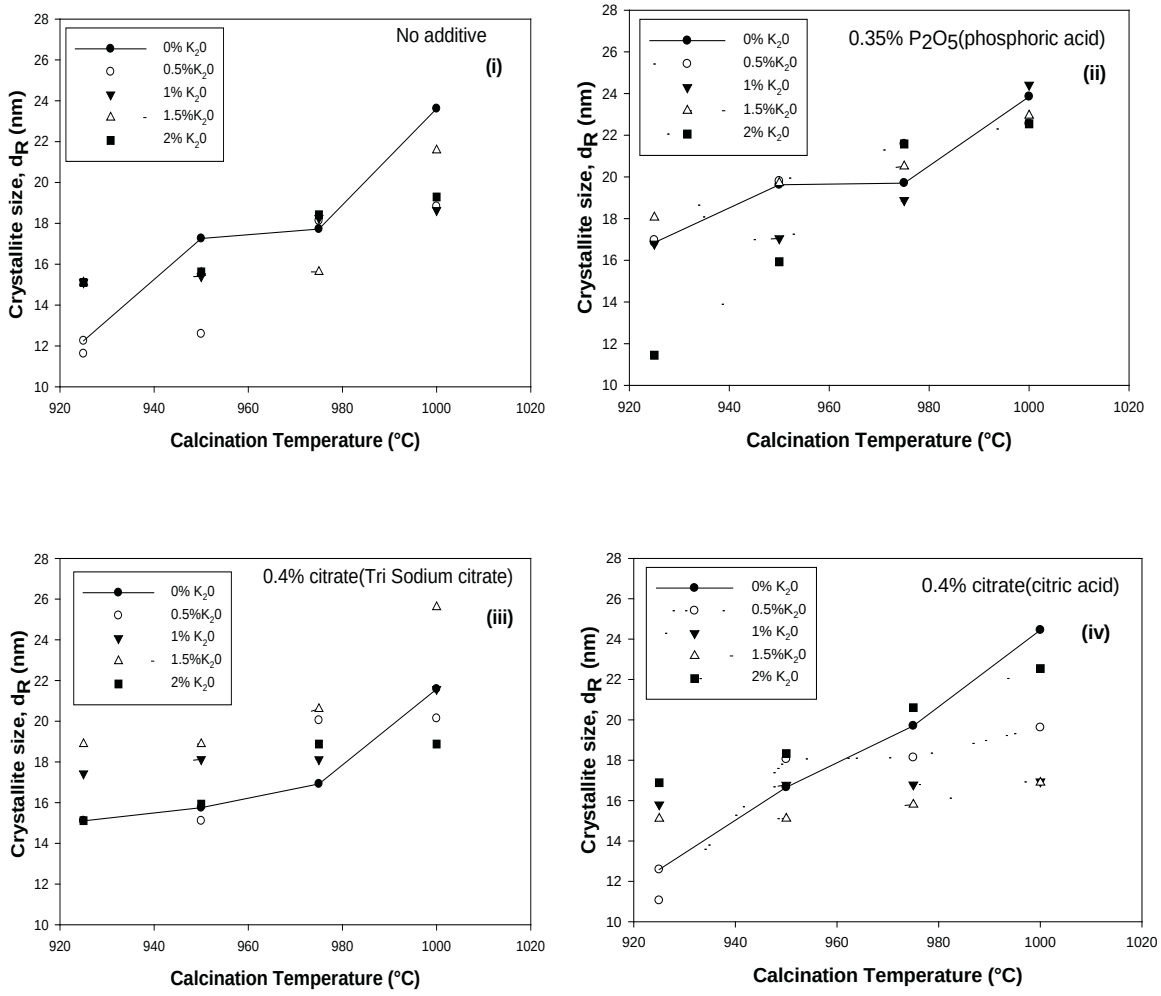

Graph 7 : Illustrates the influence of calcination temperature on crystallite size of TiO_2 particles on different samples [(i), (ii), (iii) and (iv)]. (i) – Rutile3 (no SDA); (ii) - Anatase phosphate1 (phosphoric acid); (iii) - anatase citrate1 (tri sodium citrate); (iv) - anatase citrate3 (citric acid), d_R – crystallite size of rutile phase

High calcination temperature weakens the course of anatase crystals and helps the rutile nuclei to bind and grow along through anatase matrix, thus rutilization simultaneously increases the crystallite size of TiO_2.

SEM performed on calcined samples was mainly to examine the structural characteristics of TiO_2 fine particles as shown in figure 7[(i), (ii), (iii) and (iv) with 1.5% K_2O calcined at 975°C], where (i) represents the sample of rutile (no SDA), (ii) represents anatase phosphate (phosphoric acid), (iii) represents anatase citrate (tri sodium citrate) and (iv) represents anatase citrate (citric acid). The micrographs obtained from ESEM revealed physical appearance of TiO_2 agglomerates with 1.5% K_20 calcined at 975°C.

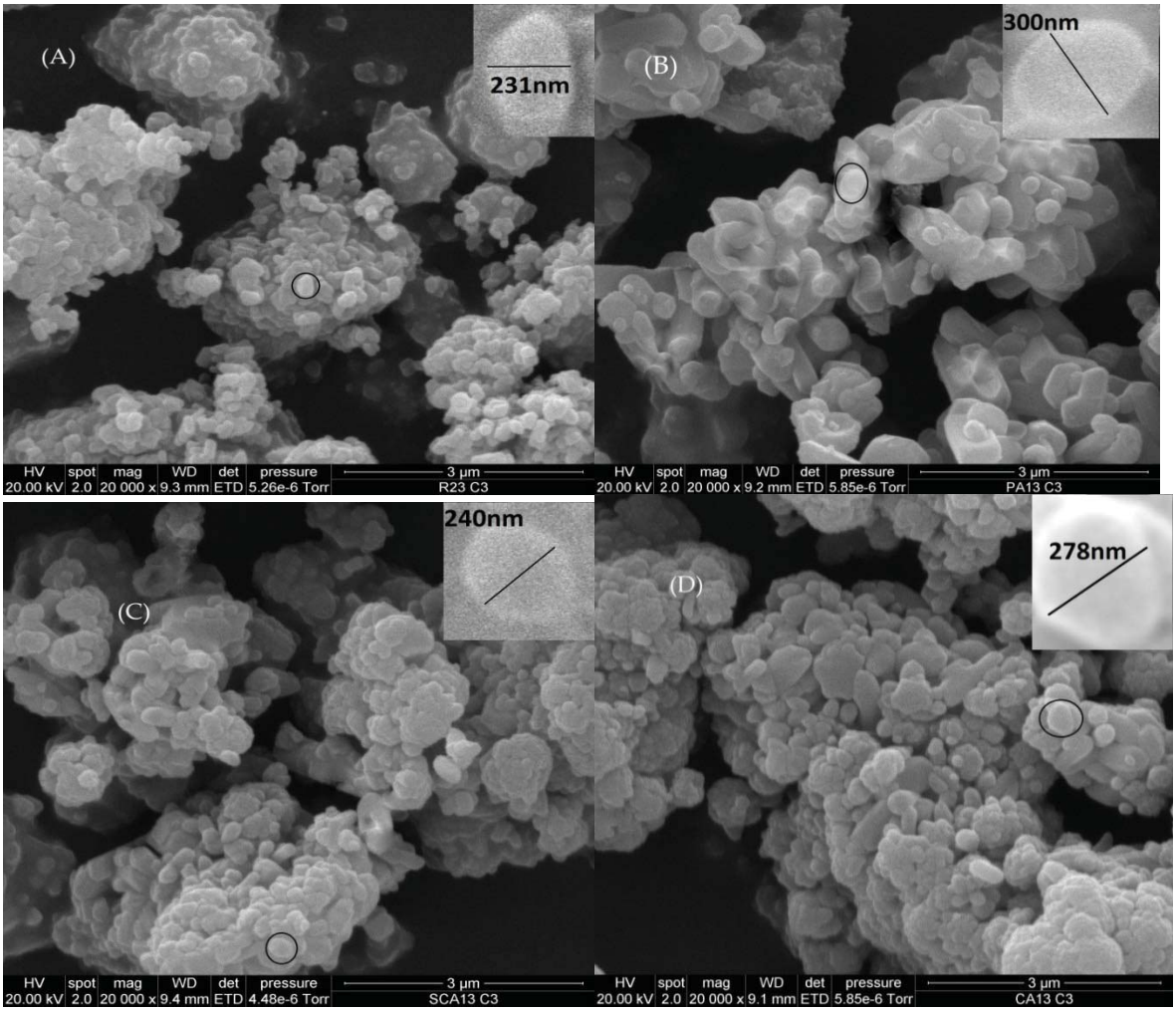

Figure 24: ESEM micrograph of TiO_2 fine particles showing the size and shape of different samples [(A), (B), (C) and (D)] with 1.5% K2O calcined at 975°C. (A) – Rutile3 (no SDA); (B) - Anatase phosphate1 (phosphoric acid); (C) - anatase citrate1 (tri sodium citrate); (D) - anatase citrate3 (citric acid).

Samples with same potassium content (1.5% K_2O) and calcination temperature (975°C) were chosen to determine the effect of phosphate ion and citrate ion on the particle size and shape of TiO_2 particles. The calcined sample with no SDA showed spherical shaped TiO_2 agglomerates, with average maximum particle size of 300nm±10nm (Figure 7(A)). The calcined sample with phosphoric acid as SDA showed rod shaped TiO_2 agglomerates with few spherical shaped TiO_2 agglomerates,

with average maximum particle size of 440nm±10nm(Figure 7(B)). The calcined sample with tri sodium citrate as SDA showed spherical shaped TiO_2 agglomerates, with average maximum particle size of 230±10nm(Figure 7(C)). Lastly the calcined samples with citric acid as SDA showed spherical shaped TiO_2 agglomerates, with average maximum particle size of 300±10nm(Figure 7(D)).

From the XRD line-broadening of the diffraction peak, crystallite size of the samples ranging from 15 – 20nm was obtained. SEM observation reveals that the samples consisted of the agglomerates of primary particles of an average diameter ranging from 200–300nm, which is not in a good agreement with the crystallite size estimated from the XRD pattern. The average particle size is found to be 15 times larger than the average crystallite size. The particle size is not as same the crystallite size. The particles produced are polycrystalline that are composed of many crystallites of varying size and orientation. Therefore, each particle observed in SEM should be poly TiO_2 crystals. In this case, the crystal lattices of the sample are not continuous and are broken at the edges with grain boundaries. With the increase calcination temperature and potassium content, rapid growth in grain size of TiO_2 is observed.

Addition of potassium does not only enhance the catalytic performance but also increase the chemical reactivity. The potassium reacts with TiO_2 surface by transferring an electron charge to its surface, which leads to formation of K_2O multilayers that grow, extracting more oxygen atoms from the surface. An alternative product of such a reaction can simply be a potassium titanate, known to have lower melting point than TiO_2. Such a compound can easily desorb from the surface, leaving it highly disrupted. A surface "patch" of K_2TiO_3 on the TiO_2 would therefore be very mobile under the evacuation conditions (400°C) and still show some mobility under reduction (200°C). Thus, the presence of potassium in the TiO_2 samples would

greatly assist any tendency to form a covering layer of Ti oxide. The particles of K_2O deposit onto the surface of the TiO_2, then melt and flow along the surface to cover the entire particle. K_2O heterogeneously condenses on the surface of TiO_2. The particles of K_2O deposit uniformly onto the surface of titanium oxide, and then fuse into a smooth coating layer, thus increasing the porous size. It is observed that the particle size is increased and grain boundary becomes clear as catalyst concentration increases. The agglomerates at 900°C are densified resulting from the elimination of intercrystallite pores. The size of particles increases considerably to 150–300 nm at a temperature of 975°C as shown in figure 28. The ESEM results show that the rutile phase with additive (phosphate and citrate ions) is denser compared to the rutile phase without additive. Therefore, the growth of crystalline TiO_2 particles is accelerated at higher calcination temperatures and potassium content. The reason being, the anatase to rutile transformation can effectively enhance densification process of titania during calcination. Particle growth in crystalline TiO_2 can be regarded as the coalescence of some smaller neighboring grains, during which the movement of grain boundaries and the atomic diffusion or the cooperative rearrangements of atoms (high mobility of atoms due bond breakage during rutile transformation) are inevitably involved. Thus the potassium oxide not only promotes the anatase to rutile transformation but also facilitates the particle growth.

7 Environmental Consideration of TiO_2 Plant on Industrial Scale

In this section, an overview of environmental impact is discussed.

7.1 Environmental impact

Environmental effects of TiO_2 production on a large scale can be studied based on the means of discharge, mainly air, land and water discharge. The main air effluent in this method is possible release of HCl gas during start up and shut down of the plant, when HCl stores are replenished and from TiO_2 while calcination. An HCl management plan should be implemented to minimize HCl gas contamination of the environment.

Hazard effects of HCl with different classes are shown below.

6.1B – substance which is highly toxic by inhalation

6.1D – substance which is harmful if swallowed

6.7B – Limited evidence of a carcinogenic effect

8.1A – substance which is highly corrosive to metals

8.2B – substances that are moderately corrosive to dermal tissue

8.3A – substance that are corrosive to eyes

9.3C – substance that are eco-toxic affects the terrestrial vertebrates.

The solid waste stream discharged requires a trade waste agreement with local district council. The components of solid waste stream mainly comprise impurities

from locally sourced ilmenite. The solid waste also contains 3% HCl solution which is subjected to neutralisation prior to discharge by using sodium carbonate. The solid waste from dissolution process can be recycled.

The waste liquid discharge in TiO_2 production is mainly from hydrolysis. This liquid discharge mainly consists of HCl and iron oxides which is toxic to aquatic life on disposal, hence the waste liquid stream is recycled to make disposable liquid stream and make beneficial byproducts.

7.2 Recycling

The recyclable impurities have a wide range of advantage over the product compared to the one obtained with non-recyclable impurities. In this experiment, every process has recyclable wastes. For e.g. in dissolution step the impurities removed from ilmenite dissolution mainly consist of alumina and silica in the form of aluminosilicates, depending on the quality and quantity of the aluminosilicates there might be a potential market for this byproduct. Whereas in hydrolysis step the waste filtrate obtained after washing with 10% HCl was subjected to distillation and pyrolysis. It was interesting to find the result obtained. Not only HCl was recovered from the waste solution but also a profitable byproduct was obtained in the form of hematite (Fe_2O_3).

Chemical Reaction:

$$12FeCl_{2\,(aq)} + 3H_2O_{\,(g,aq)} + 3O_{2\,(g)} \longrightarrow 3Fe_2O_{3\,(s)} + 6FeCl_{3\,(aq)} + 6HCl_{\,(g,aq)}$$

This is mainly because the ilmenite ore is a large source of iron. The HCl recovered from the waste solution was reused for dissolution and titanium dioxide washing. Lastly in calcination step, the gas emitted during calcination contains HCl which can

be recycled and reviewed for its usage. Since a major part (hematite and ferric chloride) of the wastes obtained by this process can be recycled. The post recycle discharged wastes (wastes after recycling process) are not hazardous to the environment unlike sulfate process and are easily disposable. Hence this method is highly recommended as it is economically and environmentally feasible.

7.3 Operating cost

A brief discussion on operating cost and equipment costing is listed. Equipment cost was tuned based on factors such as,

- Increase in plant cost index from 2004-2009
- Material of construction (glass lined steel, polypropylene and titanium)
- Pressure factors for some equipments.

Operating cost includes raw materials, labour, utility, maintenence and repair, waste disposal, overhead, taxes and administration tool. Working capital consists of capital invested in raw material and supplies, stocks, finished and semi-finished products in stock, startup capital, accounts receivable, accounts payable, taxes payable and cash on hand of operating expenses. It assumed to be 20% of fixed capital. This process runs 300 days a year and 24hrs a day producing 3 tonnes batches of titanium dioxide per day. Increasing the batch size may make the plant more economical as more revenue could be generated per batch.

The total capital cost of TiO_2 plant was ≅ $21.9 million per annum. This includes full installation of process equipment and cost of the land. The operating costs were ≅ 5.4 million per annum with revenue of 8.1 million. Additional investigation may be performed on design aspects to result in more profitable and economical product.

8 Conclusion

High quality TiO_2 fine particles extracted from naturally occurring ilmenite ore using HCl has both economic and environmental advantages over any sulfate process used. HCl recovery and hematite (Fe_2O_3) byproduct obtained from the waste slurry makes this method more promising and reliable. The use of Structure determining agents (SDA) in hydrolysis helps us obtain the desired TiO_2 phase. By tuning calcination temperature, behavior of TiO_2 phase and crystallite size of the product was examined. Rutile and anatase composite greatly depend on the SDA used in hydrolysis and calcination temperature. In the liquor obtained from dissolution, the concentration of TiO_2 increased with an increase in optimum dissolution temperature. The particle size of the TiO_2 agglomerates was ranging from 200nm—300nm.

Additives in this method play a vital role in controlling the quality of the product. The use of iron powder in dissolution process not only helps in good dissolution rate as a result of which higher concentration of titanium is dissolved but also eliminates Fe^{3+} in the solution which could otherwise absorb onto the TiO_2 resulting in discoloration. Phosphoric acid/Tri-sodium citrate/Citric acid stabilize the anatase phase of TiO_2 during hydrolysis. While potassium additive used during calcination acts as a rutilizing agent at higher calcination temperature. However, the effect of potassium additive over crystallite size is negligible as little or no difference is noticed with the presence of potassium in TiO_2. The presence of phosphate/citrate ions in TiO_2 has an interesting effect on the degree of rutile formation. Both phosphate and citrate ion have a tendency to inhibit rutile formation at a given calcination temperature in the absence of potassium additives. At higher calcination

temperature the effect of phosphate and citrate ions on TiO_2 are neutralized resulting in pure rutile phase TiO_2.

Rutile is thermo chemically stable at higher calcination temperature, as the calcined samples at 1000°C show rutile phase of TiO_2. Anatase transforms to rutile at higher calcination temperature, thus indicating the activation energy of anatase to rutile transformation is higher at higher calcination temperature. Crystallite size and the Rutile percentage of TiO_2 increase exponentially with an increase in calcination temperature. The crystallite size of the samples produced varies from 11nm—26nm. However, behavior of anatase phosphate and anatase citrates produced by this method can be studied at lower calcination temperature (400°C—600°C), which might result in the production of highly active TiO_2 photocatalyst. The final product obtained by this method is mainly used as a pigment as the resultant product is rutile.

Appendices

Table 8 : shows the behavior of temperature with time during the 1st hour of digestion process for different sample liquor

Sample → / Time ↓	R1 Temp (°C)	R2 Temp (°C)	R3 Temp (°C)	A1 Temp (°C)	A2 Temp (°C)	A3 Temp (°C)	A4 Temp (°C)	A5 Temp (°C)
0	48	50	50	50	48	48	48	48
10	65	60	60	60	61	62	62	60
20	70	66	66	66	65	70	70	75
30	72	71	71	71	68	75	75	79
40	76	75	75	75	71	78	78	80
50	78	78	78	76	75	82	82	82
60	82	79	79	78	78	85	85	84

Table 9 : shows the amount of K_2O to be added in the form of KCl

K_2O, %	KCl, %w/w in TiO_2	KCl solution concentration, %w/g	KCl to make 50ml solution, g
0	0	0	0
0.5	0.79	1.58	0.79
1	1.58	3.17	1.58
1.5	2.38	4.75	2.38
2	3.17	6.33	3.17

Table 10: Rutile1 (no SDA) after calcination showing Rutile percentage (%) and crystallite size at different potassium content (0-2%K_2O) and at different calcination temperature

Calcination temperature (°C)	**Rutile percentage (%)**	**$2\theta_R$**	**β_R**	**Crystallite size,d_R (nm)**
0% K_2O				
925	99.9688	32.22	0.37	12.179
950	99.9758	32.21	0.28	15.841
975	99.9791	32.24	0.23	19.633
1000	99.9691	32.26	0.19	23.849
0.5% K_2O				
925	99.9746	32.22	0.35	12.746
950	99.9757	32.18	0.26	17.424
975	99.9809	32.29	0.23	19.571
1000	99.9800	32.23	0.22	19.741
1% K_2O				
99.9781	99.9726	32.09	0.35	12.941
99.9777	99.9766	32.52	0.27	16.617
99.9815	99.9742	32.38	0.23	19.040
99.9841	99.9813	32.23	0.21	20.635
1.5% K_2O				
925	99.9766	32.21	0.30	15.102
950	99.979	32.27	0.27	16.355
975	99.9775	32.27	0.23	19.702
1000	99.9770	32.27	0.22	20.597
2% K_2O				

925	99.9797	32.51	0.29	15.381
950	99.9744	32.17	0.27	16.706
975	99.9803	32.27	0.26	17.055
1000	99.9841	32.25	0.18	24.890

Table 11: Rutile2 (no SDA) after calcination showing Rutile percentage (%) and crystallite size at different potassium content (0-2%K_2O) and at different calcination temperature

Calcination temperature (°C)	**Rutile percentage (%)**	**$2\theta_R$**	**β_R**	**Crystallite size,d_R (nm)**
0% K_2O				
925	99.9737	32.18	0.30	15.101
950	99.9745	32.21	0.30	15.102
975	99.9796	32.26	0.25	17.496
1000	99.9763	32.31	0.25	17.772
0.5% K_2O				
925	99.9694	32.72	0.51	08.842
950	99.9778	32.23	0.28	15.746
975	99.9749	32.20	0.23	18.956
1000	99.9751	32.31	0.221	20.506
1% K_2O				
99.9781	99.9694	32.23	0.3	15.103
99.9777	99.9778	32.22	0.27	16.287
99.9815	99.9749	32.26	0.26	16.973

99.9841	99.9751	32.17	0.25	17.809
1.5% K_2O				
925	99.9771	32.15	0.31	14.613
950	99.9798	32.32	0.26	16.977
975	99.9800	32.24	0.24	18.879
1000	99.9791	32.31	0.24	18.883
2% K_2O				
925	99.9712	32.03	0.38	11.658
950	99.9764	32.33	0.26	16.792
975	99.9719	32.24	0.26	17.427
1000	99.9820	32.33	0.21	21.581

Table 12: Rutile1 (no SDA) after calcination showing Rutile percentage (%) and crystallite size at different potassium content (0.5%K2O, 1%K2O and 2%K2O) and at different calcination temperature

Calcination temperature (°C)	**Rutile percentage (%)**	**$2\theta_R$**	**β_R**	**Crystallite size,d_R (nm)**
0.5% K_2O				
925	99.9751	32.21	0.39	11.617
950	99.9634	32.26	0.36	12.587
975	99.9743	32.2	0.25	18.122
1000	99.9813	32.75	0.24	18.825

1% K_2O				
925	99.9741	32.36	0.30	15.108
950	99.9758	32.26	0.29	15.408
975	99.9775	32.32	0.24	18.258
1000	99.9770	32.10	0.243	18.640
2% K_2O				
99.9781	99.9771	32.26	0.30	15.104
99.9777	99.9772	32.23	0.29	15.624
99.9815	99.9814	32.14	0.24	18.420
99.9841	99.9811	32.44	0.23	19.291

Table 13: Anatase phosphate1 (phosphoric acid) after calcination showing Rutile percentage (%) and crystallite size at different potassium content (0.5%K2O, 1%K2O and 2%K2O) and at different calcination temperature

Calcination temperature (°C)	**Rutile percentage (%)**	**Anatase percentage (%)**	**$2\theta_R$**	**β_R**	**$2\theta_A$**	**β_A**	**Crystallite size,d_R (nm)**	**Crystallite size,d_A (nm)**
0.5% K_2O								
925	78.3451	0.02075	32.20	0.26	---	---	16.962	15.01
950	89.5644	20.6863	32.38	0.22	29.86	0.30	19.793	15.02
975	99.9805	0.01943	32.28	0.21	---	---	21.578	---
1000	99.9839	0.01608	32.28	0.20	---	---	22.545	---
1% K_2O								

925	99.9754	0.02452	32.32	0.27	---	---	16.785	---
950	99.9741	0.02587	32.42	0.26	---	---	17.042	---
975	99.9752	0.02476	32.19	0.24	---	---	18.877	---
1000	99.9837	0.01628	32.27	0.18	---	---	24.412	---
2% K_2O								
99.9781	99.9726	0.02737	32.28	0.39	---		11.444	---
99.9777	99.9744	0.02557	32.19	0.28	---		15.929	---
99.9815	99.9790	0.02099	32.30	0.21	---		21.580	---
99.9841	99.9788	0.02118	32.30	0.20	---		22.546	---

Table 14: Anatase phosphate2 (phosphoric acid) after calcination showing Rutile percentage (%) and crystallite size at different potassium content (0—2%K_2O) and at different calcination temperature

Calcination temperature (°C)	**Rutile percentage (%)**	**Anatase percentage (%)**	**$2\theta_R$**	**β_R**	**$2\theta_A$**	**β_A**	**Crystallite size,d_R (nm)**	**Crystallite size,d_A (nm)**
0% K_2O								
925	81.7932	18.2056	32.0	0.37	29.67	0.21	11.935	21.44
950	99.9490	0.05096	32.11	0.32	---	---	14.155	---
975	99.9703	0.02964	32.18	0.30	---	---	15.101	---
1000	99.9767	0.02322	32.30`	0.30	---	---	15.106	---
0.5% K_2O								
925	89.9709	10.0291	32.22	0.36	29.34	0.19	12.585	23.68
950	99.9477	0.05226	32.16	0.30	---	---	15.101	---
975	99.97475	0.02528	32.27	0.30	---	---	15.104	---

1000	99.9737	0.02622	32.23	0.26	---	---	17.002	---
1% K_2O								
99.9781	99.9751	0.02485	32.22	0.31	---	---	14.615	---
99.9777	99.9762	0.02378	32.19	0.28	---	---	15.996	---
99.9815	99.9749	0.02500	32.24	0.27	---	---	16.252	---
99.9841	99.9781	0.02187	32.29	0.27	---	---	16.704	---
1.5% K_2O								
925	99.9723	0.02760	31.91	0.36	---	---	12.576	---
950	99.9736	0.02632	32.39	0.39	---	---	11.502	---
975	99.9726	0.02738	32.24	0.28	---	---	15.714	---
1000	99.9751	0.02480	32.13	0.28	---	---	16.089	---
2% K_2O								
99.9781	99.97811	0.02186	32.14	0.30	---	---	15.099	---
99.9777	99.9766	0.02337	32.23	0.26	---	---	17.335	---
99.9815	99.9724	0.02755	32.24	0.25	---	---	18.124	---
99.9841	99.9790	0.02097	32.16	0.24	---	---	18.875	---

Table 15: Anatase citrate1 (tri sodium citrate) after calcination showing Rutile percentage (%) and crystallite size at different potassium content (0.5%K2O, 1%K2O and 2%K2O) and at different calcination temperature

Calcination temperature (°C)	**Rutile percentage (%)**	**Anatase percentage (%)**	**$2\theta_R$**	**β_R**	**$2\theta_A$**	**β_A**	**Crystallite size,d_R (nm)**	**Crystallite size,d_A (nm)**

0.5% K_2O								
925	61.1874	38.8125	32.22	0.30	29.9304	0.28	15.103	16.092
950	80.7681	19.2318	32.25	0.30	---	---	15.104	---
975	99.9809	0.01907	32.17	0.22	---	---	20.045	---
1000	99.9831	0.01687	32.23	0.22	---	---	20.137	---
1% K_2O								
925	99.9797	0.02023	32.31	0.26	---	---	17.430	---
950	99.9822	0.01775	32.30	0.25	---	---	18.127	---
975	99.9782	0.02175	32.22	0.25	---	---	18.123	---
1000	99.9806	0.01939	32.30	0.21	---	---	21.580	---
2% K_2O								
99.9781	99.9786	0.02133	32.49	0.30	---		15.113	---
99.9777	99.9804	0.01957	32.40	0.28	---		15.929	---
99.9815	99.9767	0.02321	32.21	0.24	---		18.878	---
99.9841	99.9778	0.02219	32.25	0.24	---		18.880	---

Table 16: Anatase citrate2 (tri sodium citrate) after calcination showing Rutile percentage (%) and crystallite size at different potassium content (0—2%K2O) and at different calcination temperature

Calcination temperature (°C)	**Rutile percentage (%)**	**Anatase percentage (%)**	**$2\theta_R$**	**β_R**	**$2\theta_A$**	**β_A**	**Crystallite size,d_R (nm)**	**Crystallite size,d_A (nm)**
0% K_2O								

925	69.0867	30.9133	32.31	0.26	29.79	0.26	16.830	16.716
950	86.3745	13.6255	32.34	0.21	29.83	0.25	21.582	18.019
975	99.9759	0.02401	32.30	0.22	---	---	20.599	---
1000	99.9817	0.01821	32.25	0.18	---	---	23.992	---
0.5% K_2O								
925	79.5037	20.4963	32.76	0.44	30.16	0.46	10.247	9.6461
950	93.6666	6.3333	32.26	0.26	29.74	0.30	16.849	15.013
975	99.9794	0.02050	32.34	0.22	---	---	20.601	---
1000	99.9762	0.02374	32.29	0.21	---	---	21.356	---
1% K_2O								
925	99.9692	0.03071	32.33	0.39	---		11.620	---
950	99.9749	0.02501	32.15	0.26	---		16.911	---
975	99.9758	0.02414	32.28	0.21	---		21.077	---
1000	99.9821	0.01789	32.35	0.19	---		23.124	---
1.5% K_2O								
925	99.9748	0.02519	32.20	0.26	---	---	16.963	---
950	99.9744	0.02551	32.13	0.23	---	---	19.695	---
975	99.9794	0.02056	32.18	0.21	---	---	21.573	---
1000	99.9840	0.01594	32.13	0.20	---	---	22.536	---
2% K_2O								
925	99.9768	0.02315	32.09	0.28	---	---	16.081	---
950	99.9799	0.02005	32.29	0.25	---	---	18.127	---
975	99.9796	0.02036	32.29	0.24	---	---	18.199	---

1000	99.9792	0.02077	32.26	0.23	---	---	19.119	---

Table 17: Anatase citrate3 (citric acid) after calcination showing Rutile percentage (%) and crystallite size at different potassium content (0.5%K_2O, 1%K2O and 2%K2O) and at different calcination temperature

Calcination temperature (°C)	**Rutile percentage (%)**	**Anatase percentage (%)**	**$2\theta_R$**	**β_R**	**$2\theta_A$**	**B_A**	**Crystallite size,d_R (nm)**	**Crystallite size,d_A (nm)**
0.5% K_2O								
925	55.9291	44.0708	32.25	0.41	29.75	0.37	11.051	11.99018307
950	80.5604	19.4395	32.25	0.25	29.71	0.30	18.052	15.01221337
975	99.9774	0.02255	32.35	0.24	---	---	18.132	---
1000	99.9818	0.01814	32.18	0.23	---	---	19.612	---
1% K_2O								
925	68.8467	31.1532	32.34	0.28	29.84	0.25	15.799	18.020
950	76.9460	23.0539	32.21	0.27	29.69	0.28	16.774	15.661
975	99.9766	0.02331	32.31	0.27	---	---	16.784	---
1000	99.9772	0.02275	32.18	0.26	---	---	16.939	---
2% K_2O								
99.9781	76.3285	23.6714	32.24	0.26	29.73	0.249	16.884	18.087
99.9777	82.2942	17.7057	32.38	0.24	29.20	0.3	18.329	14.994
99.9815	99.9745	0.02544	32.31	0.22	---	---	20.599	---
99.9841	99.9773	0.02266	32.23	0.20	---	---	22.542	---

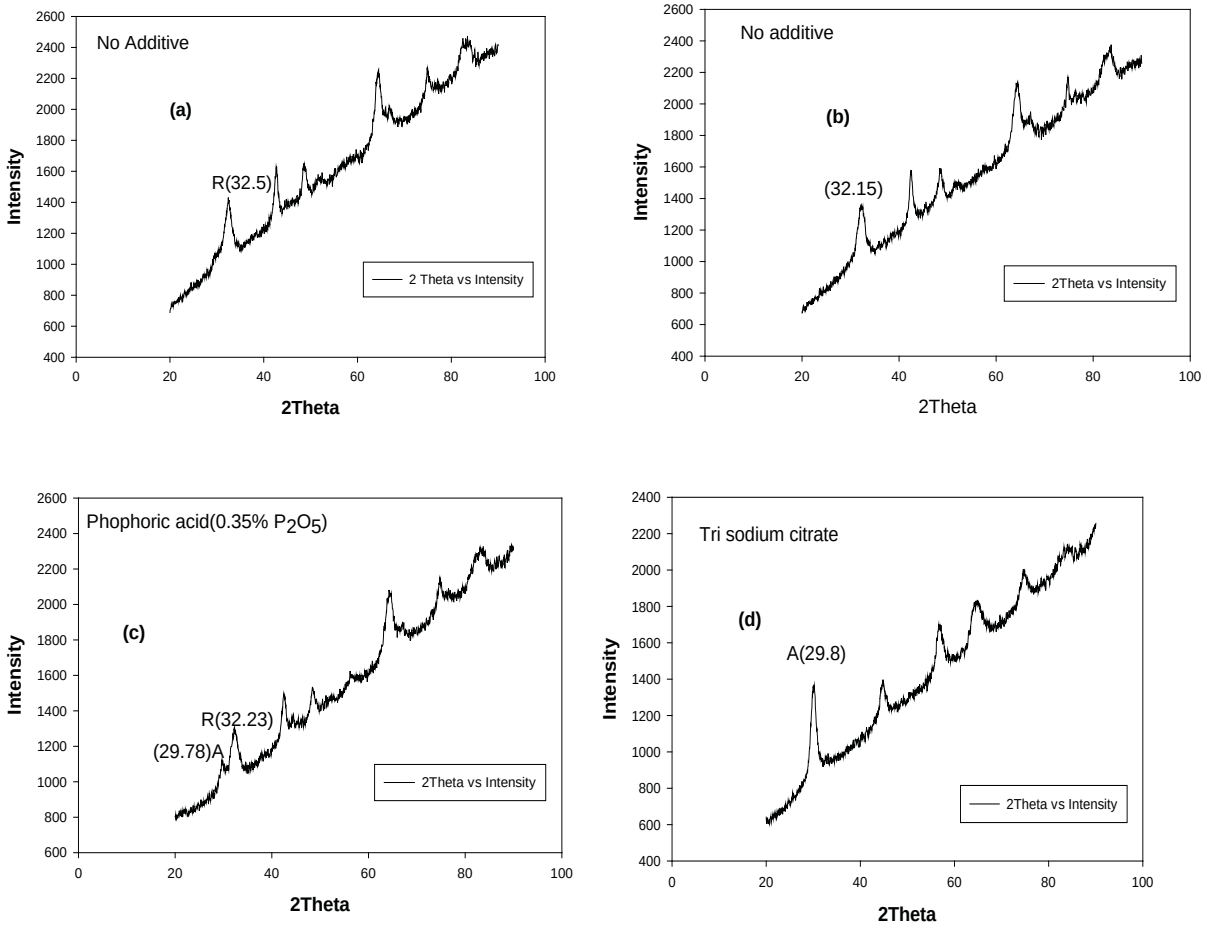

Graph 8: Illustration of peak intensity of anatase and rutile of different samples [(a), (b), (c) and (d)] by plotting 2theta versus intensity for hydrate samples produced using different SDA additives. (a) – Rutile1 (no SDA); (b) – Rutile2 (no SDA); (c) - Anatase phosphate2 (phosphoric acid)); (d) - anatase citrate2 (tri sodium citrate)

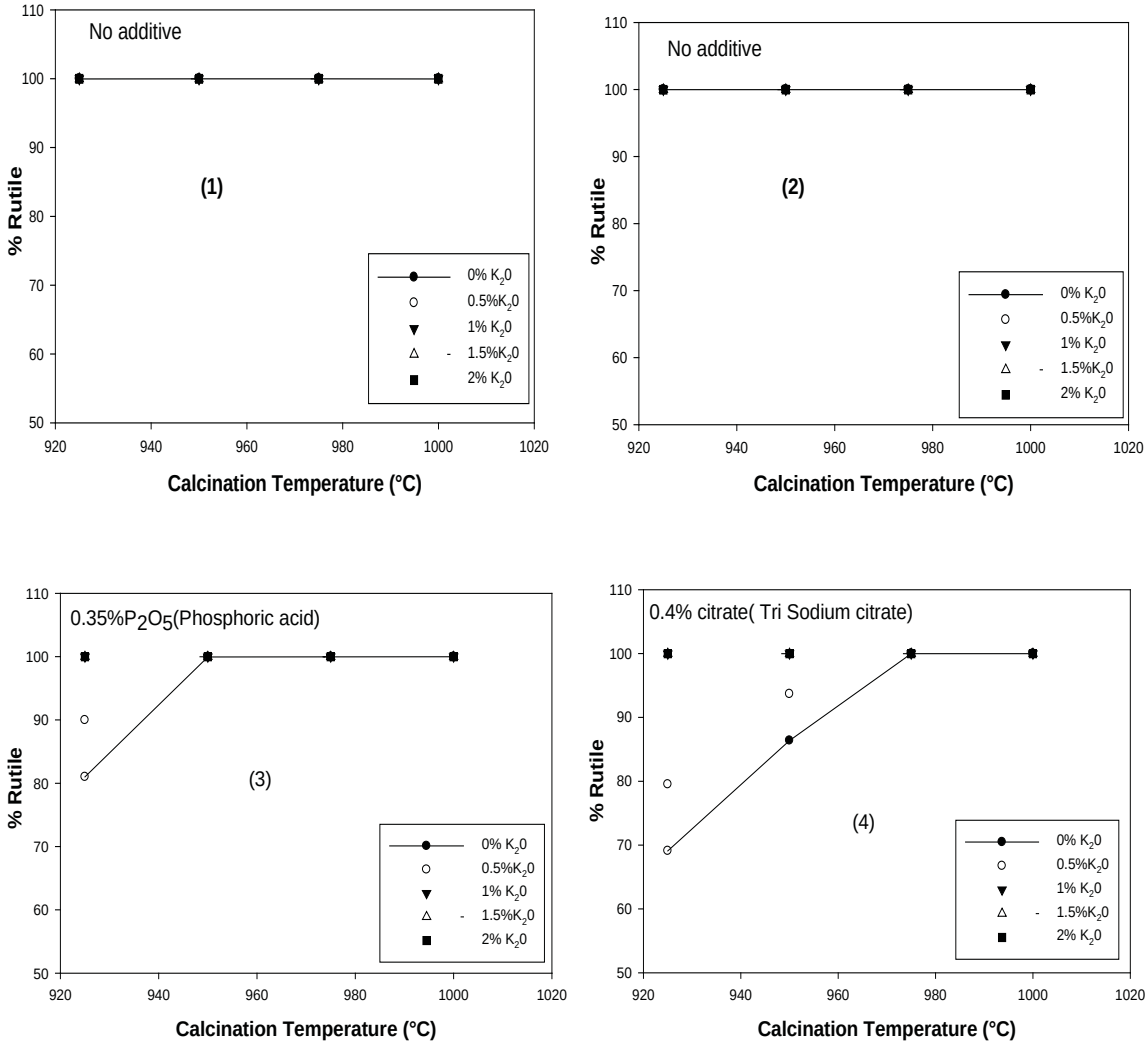

Graph 9: Different samples [(1), (2), (3) and (4)] illustrating the degree of rutilization at different calcination temperature and potassium content. (1) – Rutile1 (no SDA); (2) – Rutile2 (no SDA); (3) - Anatase phosphate (phosphoric acid)); (4) - anatase citrate (tri sodium citrate

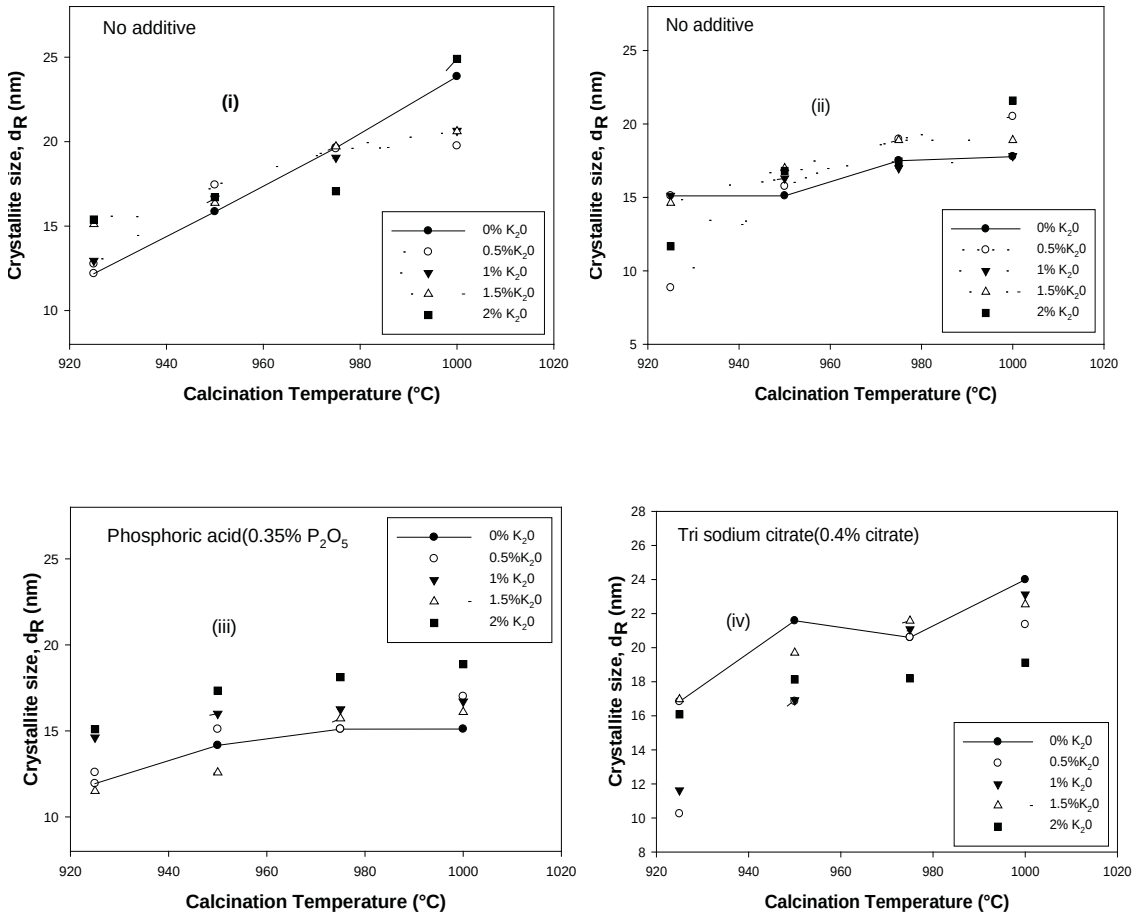

Graph 10: Influence of calcination temperature on crystallite size of TiO_2 fine particles on different samples [(i), (ii), (iii) and (iv)] (i) – Rutile1 (no SDA); (ii) – Rutile2 (no SDA); (iii) - Anatase phosphate2 (phosphoric acid)); (iv) - anatase citrate2 (tri sodium citrate), d_R – crystallite size of rutile

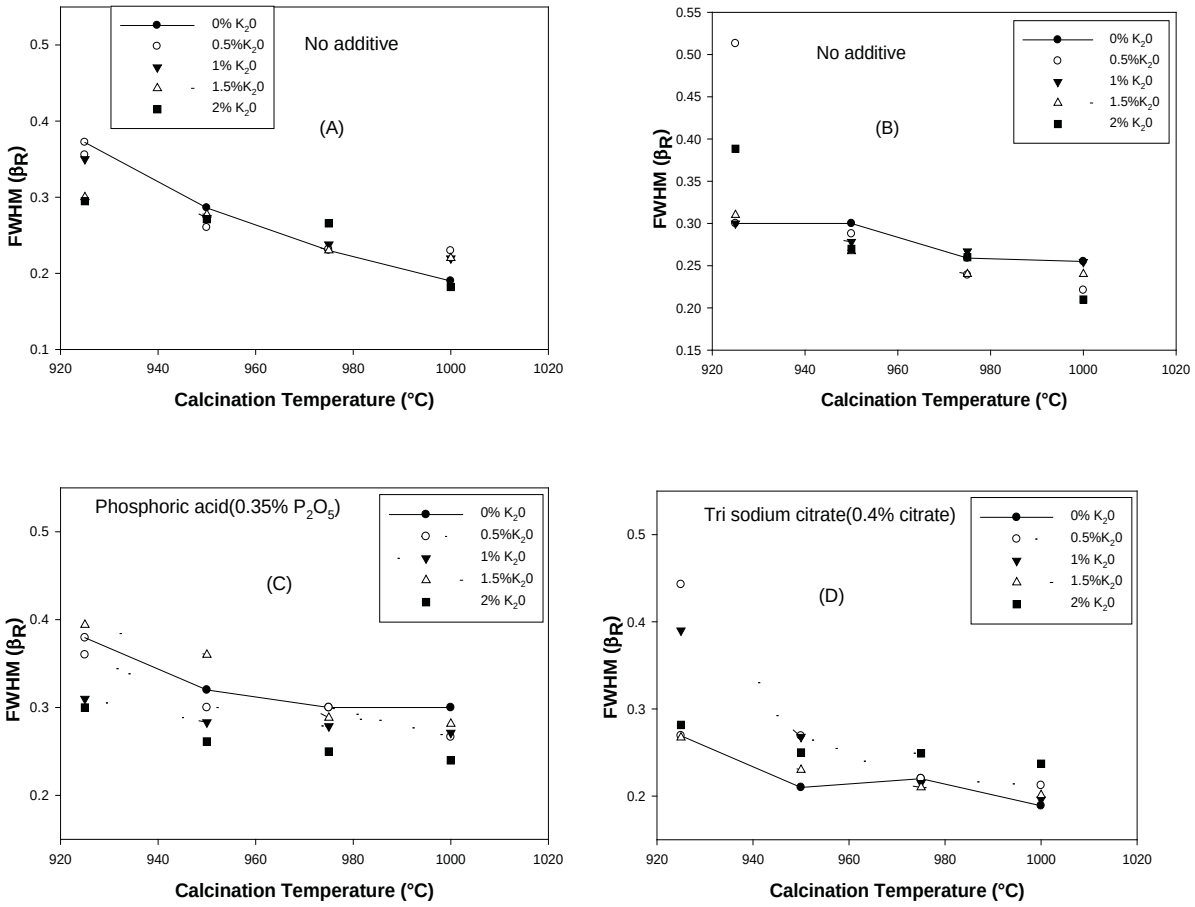

Graph 11: Relation between FWHM and calcination temperature of different samples [(A), (B), (C) and (D)] (A) – Rutile1 (no SDA); (B) – Rutile2 (no SDA); (C) - Anatase phosphate2 (phosphoric acid)); (D) - anatase citrate2 (tri sodium citrate, β_R–FWHM of rutile peak

References

A. Robert Armstrong, G. A., Jesús Canales, Peter G. Bruce, (2004). TiO_{<FONT SIZE='-1'>2</FONT>}-B Nanowires13. *Angewandte Chemie, 116*(17), 2336-2338.

Aarik, J., Aidla, A., Kiisler, A.-A., Uustare, T., & Sammelselg, V. (1997). Effect of crystal structure on optical properties of TiO2 films grown by atomic layer deposition. *Thin Solid Films, 305*(1-2), 270-273.

Abdelkrim Chemseddine, T. M. (1999). Nanostructuring Titania: Control over Nanocrystal Structure, Size, Shape, and Organization. *European Journal of Inorganic Chemistry, 1999*(2), 235-245.

Addamo, M., Augugliaro, V., Di Paola, A., Lopez, E. G., Loddo, V., Marci, G., et al. (2004). Preparation, Characterization, and Photoactivity of Polycrystalline Nanostructured TiO2 Catalysts. *The Journal of Physical Chemistry B, 108*(10), 3303-3310.

Amethyst, G. (2009). THE MINERAL ILMENITE, from http://www.galleries.com/Minerals/OXIDES/ilmenite/ilmenite.htm

Anal K. Jha, K. Prasad, & Kulkarni, A. R. (2009). Synthesis of TiO2 nanoparticles using microorganisms. *Colloid & Surfaces*.

Andersson, M., Osterlund, L., Ljungstrom, S., & Palmqvist, A. (2002). Preparation of Nanosize Anatase and Rutile TiO2 by Hydrothermal Treatment of

Microemulsions and Their Activity for Photocatalytic Wet Oxidation of Phenol. *The Journal of Physical Chemistry B, 106*(41), 10674-10679.

Anpo, M. (2000). Utilization of TiO2 photocatalysts in green chemistry. *Pure And Applied Chemistry Chimie Pure Et Applique Iupac, 72*(7), 1265.

Anukunprasert, T., Saiwan, C., & Traversa, E. (2005). The development of gas sensor for carbon monoxide monitoring using nanostructure of Nb-TiO2. *Science and Technology of Advanced Materials, 6*(3-4), 359-363.

Ao, Y., Xu, J., & Fu, D. (2009). Study on the effect of different acids on the structure and photocatalytic activity of mesoporous titania. *Applied Surface Science, 256*(1), 239-245.

Arnal, P., Corriu, R. J. P., Leclercq, D., Mutin, P. H., & Vioux, A. (1997). A Solution Chemistry Study of Nonhydrolytic Sol−Gel Routes to Titania. *Chemistry of Materials, 9*(3), 694-698.

Asahi, R., Taga, Y., Mannstadt, W., & Freeman, A. J. (2000). Electronic and optical properties of anatase TiO2. *Physical Review B, 61*(11), 7459.

Ayllón, J. A., Figueras, A., Garelik, S., Spirkova, L., Durand, J., & Cot, L. (1999). Preparation of TiO2 powder using titanium tetraisopropoxide decomposition in a plasma enhanced chemical vapor deposition (PECVD) reactor. *Journal of Materials Science Letters, 18*(16), 1319-1321.

Barringer, E. A., & Bowen, H. K. (1985). High-purity, monodisperse TiO2 powders by hydrolysis of titanium tetraethoxide. 1. Synthesis and physical properties. *Langmuir, 1*(4), 414-420.

Batzill, M., Hebenstreit, E. L. D., Hebenstreit, W., & Diebold, U. (2003). Influence of subsurface, charged impurities on the adsorption of chlorine at TiO2(1 1 0). *Chemical Physics Letters, 367*(3-4), 319-323.

Batzill, M., Katsiev, K., Gaspar, D. J., & Diebold, U. (2002). Variations of the local electronic surface properties of TiO2(110) induced by intrinsic and extrinsic defects. *Physical Review B, 66*(23), 235401.

Bavykin, D. V., Gordeev, S. N., Moskalenko, A. V., Lapkin, A. A., & Walsh, F. C. (2005). Apparent Two-Dimensional Behavior of TiO2 Nanotubes Revealed by Light Absorption and Luminescence. *The Journal of Physical Chemistry B, 109*(18), 8565-8569.

Bavykin, D. V., Lapkin, A. A., Plucinski, P. K., Friedrich, J. M., & Walsh, F. C. (2005a). Reversible Storage of Molecular Hydrogen by Sorption into Multilayered TiO2 Nanotubes. *The Journal of Physical Chemistry B, 109*(41), 19422-19427.

Bavykin, D. V., Lapkin, A. A., Plucinski, P. K., Friedrich, J. M., & Walsh, F. C. (2005b). TiO2 nanotube-supported ruthenium(III) hydrated oxide: A highly active catalyst for selective oxidation of alcohols by oxygen. *Journal of Catalysis, 235*(1), 10-17.

Bavykin, D. V., Milsom, E. V., Marken, F., Kim, D. H., Marsh, D. H., Riley, D. J., et al. (2005). A novel cation-binding TiO2 nanotube substrate for electro- and bioelectro-catalysis. *Electrochemistry Communications, 7*(10), 1050-1058.

Bavykin, D. V., Parmon, V. N., Lapkin, A. A., & Walsh, F. C. (2004). The effect of hydrothermal conditions on the mesoporous structure of TiO2 nanotubes. *Journal of Materials Chemistry, 14*(22), 3370-3377.

Benedict, L. X., & Shirley, E. L. (1999). Ab initio calculation of epsilon 2(omega) including the electron-hole interaction: Application to GaN and CaF2. *Physical Review B, 59*(8), 5441.

Bessekhouad, Y., Robert, D., & Weber, J. V. (2003). Synthesis of photocatalytic TiO2 nanoparticles: optimization of the preparation conditions. *Journal of Photochemistry and Photobiology A: Chemistry, 157*(1), 47-53.

Bessekhouad, Y., Robert, D., Weber, J. V., & Chaoui, N. (2004). Effect of alkaline-doped TiO2 on photocatalytic efficiency. *Journal of Photochemistry and Photobiology A: Chemistry, 167*(1), 49-57.

BIN XIA, WEIBIN LI, BIN, Z., & XIE, Y. (1999). Low temperature vapor-phase preparation of TiO2 nanopowders *JOURNAL OF MATERIALS SCIENCE 34*.

Boi Shield Inc (1999-2009). Nanotechnology, from http://www.teamenviroclean.com/what_is_nanotechnology_

Bonhôte, P., Gogniat, E., Grätzel, M., & Ashrit, P. V. (1999). Novel electrochromic devices based on complementary nanocrystalline TiO2 and WO3 thin films. *Thin Solid Films, 350*(1-2), 269-275.

Buonsanti, R., Grillo, V., Carlino, E., Giannini, C., Curri, M. L., Innocenti, C., et al. (2006). Seeded Growth of Asymmetric Binary Nanocrystals Made of a Semiconductor TiO2 Rodlike Section and a Magnetic γ-Fe2O3 Spherical Domain. *Journal of the American Chemical Society, 128*(51), 16953-16970.

Burda, C., Chen, X., Narayanan, R., & El-Sayed, M. A. (2005). Chemistry and Properties of Nanocrystals of Different Shapes. *Chemical Reviews, 105*(4), 1025-1102.

Burda, C., Lou, Y., Chen, X., Samia, A. C. S., Stout, J., & Gole, J. L. (2003). Enhanced Nitrogen Doping in TiO2 Nanoparticles. *Nano Letters, 3*(8), 1049-1051.

Busca, G., Ramis, G., Lorenzelli, V., Rossi, P. F., La Ginestra, A., & Patrono, P. (2002). Phosphoric acid on oxide carriers. 1. Characterization of silica, alumina, and titania impregnated by phosphoric acid. *Langmuir, 5*(4), 911-916.

Cao, Y., Yang, W., Zhang, W., Liu, G., & Yue, P. (2004). Improved photocatalytic activity of Sn4+ doped TiO2 nanoparticulate films prepared by plasma-enhanced chemical vapor deposition. *New Journal of Chemistry, 28*(2), 218-222.

Chae, S. Y., Park, M. K., Lee, S. K., Kim, T. Y., Kim, S. K., & Lee, W. I. (2003). Preparation of Size-Controlled TiO2 Nanoparticles and Derivation of Optically Transparent Photocatalytic Films. *Chemistry of Materials, 15*(17), 3326-3331.

Chang, J. T., Lai, Y. F., & He, J. L. (2005). Photocatalytic performance of chromium or nitrogen doped arc ion plated-TiO2 films. *Surface and Coatings Technology, 200*(5-6), 1640-1644.

Chen, H.-R., Shi, J.-L., Hua, Z.-L., Ruan, M.-L., & Yan, D.-S. (2001). Parameter control in the synthesis of ordered porous zirconium oxide. *Materials Letters, 51*(3), 187-193.

Chen, J., & Poon, C.-s. (2009). Photocatalytic construction and building materials: From fundamentals to applications. *Building and Environment, 44*(9), 1899-1906.

Chen, X., Lou, Y., Dayal, S., Qiu, X., Krolicki, R., Burda, C., et al. (2005). Doped semiconductor nanomaterials

Journal of Nanoscience and Nanotechnology, 5(9), 1408-1420.

Chen, X., & Mao, S. S. (2007). Titanium Dioxide Nanomaterials: Synthesis, Properties, Modifications, and Applications. *Chemical Reviews, 107*(7), 2891-2959.

Cheng, H., Ma, J., Zhao, Z., & Qi, L. (2002). Hydrothermal Preparation of Uniform Nanosize Rutile and Anatase Particles. *Chemistry of Materials, 7*(4), 663-671.

Chien, S.-H., Liou, Y.-C., & Kuo, M.-C. (2005). Preparation and characterization of nanosized Pt/Au particles on TiO2-nanotubes. *Synthetic Metals, 152*(1-3), 333-336.

Choi, H. C., Ahn, H. J., Jung, Y. M., Lee, M. K., Shin, H. J., Kim, S. B., et al. (2004). Characterization of the Structures of Size-Selected TiO2 Nanoparticles Using X-ray Absorption Spectroscopy. *Applied Spectroscopy, 58*, 598-602.

Choi, W., Termin, A., & Hoffmann, M. R. (1994). The Role of Metal Ion Dopants in Quantum-Sized TiO2: Correlation between Photoreactivity and Charge Carrier Recombination Dynamics. *The Journal of Physical Chemistry, 98*(51), 13669-13679.

Christie, T., Douch, C., Winfield, B., & Thompson, B. (2000). Industrial Minerals in New Zealand. *New Zealand Mining, 1*(27), 14-25.

Chu, D., Qin, G., Yuan, X., Xu, M., Lu, J., & Zheng, P. (2008). Nanoporous TiO2 film electrode for electrocatalytic reduction of 2-pyridineethanol in ionic liquids. *Journal of Porous Materials, 15*(6), 661-665.

Chu, R., Yan, J., Lian, S., Wang, Y., Yan, F., & Chen, D. (2004). Shape-controlled synthesis of nanocrystalline titania at low temperature. *Solid State Communications, 130*(12), 789-792.

Ciesla, U., Schacht, S., Stucky, G. D., Unger, K. K., & Schüth, F. (1996). Formation of a Porous Zirconium Oxo Phosphate with a High Surface Area by a Surfactant-Assisted Synthesis. *Angewandte Chemie International Edition in English, 35*(5), 541-543.

Collins, S. D. (1997). Etch Stop Techniques for Micromachining. *Journal of The Electrochemical Society, 144*(6), 2242-2262.

Cot, F., Larbot, A., Nabias, G., & Cot, L. (1998). Preparation and characterization of colloidal solution derived crystallized titania powder. *Journal of the European Ceramic Society, 18*(14), 2175-2181.

Cozzoli, P. D., Comparelli, R., Fanizza, E., Curri, M. L., & Agostiano, A. (2003). Photocatalytic activity of organic-capped anatase TiO2 nanocrystals in homogeneous organic solutions. *Materials Science and Engineering: C, 23*(6-8), 707-713.

Cozzoli, P. D., Comparelli, R., Fanizza, E., Curri, M. L., Agostiano, A., & Laub, D. (2004). Photocatalytic Synthesis of Silver Nanoparticles Stabilized by TiO2

Nanorods: A Semiconductor/Metal Nanocomposite in Homogeneous Nonpolar Solution. *Journal of the American Chemical Society, 126*(12), 3868-3879.

Cozzoli, P. D., Fanizza, E., Comparelli, R., Curri, M. L., Agostiano, A., & Laub, D. (2004). Role of Metal Nanoparticles in TiO2/Ag Nanocomposite-Based Microheterogeneous Photocatalysis. *The Journal of Physical Chemistry B, 108*(28), 9623-9630.

Cozzoli, P. D., Fanizza, E., Curri, M. L., Laub, D., & Agostiano, A. (2005). Low-dimensional chainlike assemblies of TiO2 nanorod-stabilized Au nanoparticles. *Chemical Communications*(7), 942-944.

Cozzoli, P. D., Kornowski, A., & Weller, H. (2003). Low-Temperature Synthesis of Soluble and Processable Organic-Capped Anatase TiO2 Nanorods. *Journal of the American Chemical Society, 125*(47), 14539-14548.

Cservenyák, I., Kelsall, G. H., & Wang, W. (1996). Reduction of tiIV species in aqueous sulfuric and hydrochloric acids i. Titanium speciation. *Electrochimica Acta, 41*(4), 563-572.

D. V. Bavykin, J. M. F., F. C. Walsh, (2006). Protonated Titanates and TiO_{<FONT SIZE='-1'>2</FONT>} Nanostructured Materials: Synthesis, Properties, and Applications. *Advanced Materials, 18*(21), 2807-2824.

Dagan, G., & Tomkiewicz, M. (1993). Titanium dioxide aerogels for photocatalytic decontamination of aquatic environments. *The Journal of Physical Chemistry, 97*(49), 12651-12655.

Dhage, S. R., Pasricha, R., & Ravi, V. (2003). Synthesis of ultrafine TiO2 by citrate gel method. *Materials Research Bulletin, 38*(11-12), 1623-1628.

Diebold, U. (2003). The surface science of titanium dioxide. *Surface Science Reports, 48*(5-8), 53-229.

Dowling, A., Clift, R., Grobert, N., Hutton, D., Oliver, R., O'Neill, et al. (2004). *Nanoscience & Nanotechnologies: Opportunities & Uncertainities*.

Dr. M. C. Roco (2003). *The Future of National Nanotechnology Initiative*. Boston: National Science and Technology Council (NSTC).

Du, G. H., Chen, Q., Che, R. C., Yuan, Z. Y., & Peng, L. M. (Writer) (2001). Preparation and structure analysis of titanium oxide nanotubes [Article], *Applied Physics Letters*: American Institute of Physics.

Duncan, J. F., & Metson, J. B. (1982). Acid attack on New Zealand ilmenite: I. The mechanism of dissolution. *New Zealand Journal of Science, 25*, 103– 109.

Egerton, T. A., Kosa, S. A. M., & Christensen, P. A. (2006). Photoelectrocatalytic disinfection of E. coli suspensions by iron doped TiO2. *Physical Chemistry Chemical Physics, 8*(3), 398-406.

El-Hazek, N., Lasheen, T. A., El-Sheikh, R., & Zaki, S. A. (2007). Hydrometallurgical criteria for TiO2 leaching from Rosetta ilmenite by hydrochloric acid. *Hydrometallurgy, 87*(1-2), 45-50.

Enache, C. S., Schoonman, J., & Krol, R. V. (2004). The Photoresponse of Iron- and Carbon-Doped TiO2 (Anatase) Photoelectrodes. *Journal of Electroceramics, 13*(1), 177-182.

F Di Fonzo, C S Casari, V Russo, MF Brunella, A Li Bassi, & Bottani, C. E. (2009). Hierarchically organized nanostructured TiO2 for photocatalysis applications. *NANOTECHNOLOGY, **20***, 015604.

Fahmi, A., Minot, C., Silvi, B., & Causá, M. (1993). Theoretical analysis of the structures of titanium dioxide crystals. *Physical Review B, 47*(18), 11717.

Feng, X., Liu, J., Li, P., Zhang, Y., & Wei, Y. (2009). Inhibition effect of phosphate on the crystal grain growth of nanosized titania. *Rare Metals, 28*(4), 385-390.

Finkelstein, L. D., Kurmaev, E. Z., Korotin, M. A., Moewes, A., Schneider, B., Butorin, S. M., et al. (1999). Band approach to the excitation-energy dependence of x-ray fluorescence of TiO2. *Physical Review B, 60*(4), 2212.

Fitz, C. W., & Rose, H. F. (1983). Effects of phosphorus on nickel-molybdenum hydrodesulfurization/hydrodenitrogenation catalysts of varying metals content. *Industrial & Engineering Chemistry Product Research and Development, 22*(1), 40-44.

Francioso, L., Presicce, D. S., Epifani, M., Siciliano, P., & Ficarella, A. (2005). Response evaluation of TiO2 sensor to flue gas on spark ignition engine and in controlled environment. *Sensors and Actuators B: Chemical, 107*(2), 563-571.

Francisco, M. S. P., & Mastelaro, V. R. (2002). Inhibition of the Anatase-Rutile Phase Transformation with Addition of CeO2 to CuO-TiO2 System: Raman Spectroscopy, X-ray Diffraction, and Textural Studies. *Chemistry of Materials, 14*(6), 2514-2518.

Fujishima, A., & Honda, K. (1972). Electrochemical photolysis of water at a semiconductor electrode. *Nature, 238*, 37–38.

Fujishima, A., Rao, T. N., & Tryk, D. A. (2000). Titanium dioxide photocatalysis. *Journal of Photochemistry and Photobiology C: Photochemistry Reviews, 1*(1), 1-21.

Garcia, T., Solsona, B., Amoros, D. C., Solano, A. L., & Taylor, S. H. (2006). Total oxidation of volatile organic compounds by vanadium promoted palladium-titania catalysts: Comparison of aromatic and polyaromatic compounds. *Applied Catalysis B: Environmental, 62*(1-2), 66-76.

Garzella, C., Comini, E., Tempesti, E., Frigeri, C., & Sberveglieri, G. (2000). TiO2 thin films by a novel sol-gel processing for gas sensor applications. *Sensors and Actuators B: Chemical, 68*(1-3), 189-196.

Gennari, F. C., & Pasquevich, D. M. (1999). Enhancing Effect of Iron Chlorides on the Anatase-Rutile Transition in Titanium Dioxide. *Journal of the American Ceramic Society, 82*(7), 1915-1921.

GENS Nano Inc (2010). Nanotechnology Now, from http://www.greenearthnanoscience.com/

Gesenhues, U. (2001). Calcination of Metatitanic Acid to Titanium Dioxide White Pigments. *Chemical Engineering & Technology, 24*(7), 685-694.

Girgin, I. (1990). Leaching of ilmenite in HCl---H2O, HCl---CH3OH---H2O and HCl---CH3OH solutions. *Hydrometallurgy, 24*(1), 127-134.

Girgin, I. (**1990**). Leaching of ilmenite in HCl –H2O, HCl – CH3OH–H2O and HCl–CH3OH solutions. *Hydrometallurgy, 24*, 127– 134.

Gishti, K., Iannibello, A., Marengo, S., MorelliLi, G., & Tittarelli, P. (1984). On the role of phosphate anion in the MoO3-Al2O3 based catalysts. *Applied Catalysis, 12*(4), 381-393.

Grätzel, M. (2001). Sol-Gel Processed TiO2 Films for Photovoltaic Applications. *Journal of Sol-Gel Science and Technology, 22*(1), 7-13.

Grzmil, B., Grela, D., & Kic, B. (2008). Hydrolysis of titanium sulphate compounds. *Chemical Papers, 62*(1), 18-25.

Grzmil, B., Kic, B., & Rabe, M. (2004). Inhibition of the Anatase-Rutile Phase Transformation with Addition of K2O, P2O5, and Li2O. *Chemical Papers, 58* ((6)), 410–414.

Grzmil, B., Rabe, M., Kic, B., & Lubkowski, K. (2007). Influence of Phosphate, Potassium, Lithium, and Aluminium on the Anatase-Rutile Phase Transformation. *Industrial & Engineering Chemistry Research, 46*(4), 1018-1024.

Guarino, M., Costa, A., & Porro, M. (2008). Photocatalytic TiO2 coating to reduce ammonia and greenhouse gases concentration and emission from animal husbandries. *Bioresource Technology, 99*(7), 2650-2658.

Gun'ko, V. M., Blitz, J. P., Zarko, V. I., Turov, V. V., Pakhlov, E. M., Oranska, O. I., et al. (2009). Structural and adsorption characteristics and catalytic activity of titania and titania-containing nanomaterials. *Journal of Colloid and Interface Science, 330*(1), 125-137.

Gundiah, G., Mukhopadhyay, S., Tumkurkar, U. G., Govindaraj, A., Maitra, U., & Rao, C. N. R. (2003). Hydrogel route to nanotubes of metal oxides and sulfates. *Journal of Materials Chemistry, 13*(9), 2118-2122.

Gurav, A., Kodas, T., Pluym, T., & Xiong, Y. (1993). Aerosol Processing of Materials. *Aerosol Science and Technology, 19*(4), 411-452.

Hashimoto, K., Irie, H., & Fujishima, A. (2005). TiO2 Photocatalysis: A Historical Overview and Future Prospects. *Japanese Journal of Applied Physics, 44*(12), 8269–8285.

Hashimoto, T., Yoko, T., & Sakka, S. (1994). Sol-Gel Preparation and Third-Order Nonlinear Optical Properties of TiO2 Thin Films. *Bulletin of the Chemical Society of Japan, 67*(3), 653-660.

Hasin, P., Alpuche-Aviles, M. A., Li, Y., & Wu, Y. (2009). Mesoporous Nb-Doped TiO2 as Pt Support for Counter Electrode in Dye-Sensitized Solar Cells. *The Journal of Physical Chemistry C, 113*(17), 7456-7460.

Hay, J. N., & Raval, H. M. (1998). Preparation of Inorganic Oxides via a Non-Hydrolytic Sol-Gel Route. *Journal of Sol-Gel Science and Technology, 13*(1), 109-112.

Hay, J. N., & Raval, H. M. (2001). Synthesis of Organic−Inorganic Hybrids via the Non-hydrolytic Sol−Gel Process. *Chemistry of Materials, 13*(10), 3396-3403.

Hench, L. L., & West, J. K. (1990). The sol-gel process. *Chemical Reviews, 90*(1), 33-72.

Henrich, V. E. (1983). The nature of transition-metal-oxide surfaces. *Progress in Surface Science, 14*(2), 175-199.

Huang, D., Luo, G. S., & Wang, Y. J. (2005). Using phosphoric acid as a catalyst to control the structures of mesoporous titanium dioxide materials. *Microporous and Mesoporous Materials, 84*(1-3), 27-33.

Huang, Q., & Gao, L. (2003). A Simple Route for the Synthesis of Rutile TiO2 Nanorods. *Chemistry Letters, 32*(7), 638-639.

Huang, X., Yang, J., Zhang, W., Zhang, Z., & An, Z. (1999). Determination of the Critical Micelle Concentration of Cationic Surfactants: An Undergraduate Experiment. *Journal of Chemical Education, 76*(1), 93-null.

Hussein MK , Kolta GA , & El, T. S. (1976). Removal of iron from Egyptian ilmenite. *Egyptian Journal of Chemistry, 19*(19), 143-152.

Hwang, D. K., Moon, J. H., Shul, Y. G., Jung, K. T., Kim, D. H., & Lee, D. W. (2003). Scratch Resistant and Transparent UV-Protective Coating on Polycarbonate. *Journal of Sol-Gel Science and Technology, 26*(1), 783-787.

Hwu, Y., Yao, Y. D., Cheng, N. F., Tung, C. Y., & Lin, H. M. (1997). X-ray absorption of nanocrystal TiO2. *Nanostructured Materials, 9*(1-8), 355-358.

Iida, Y., & Ozaki, S. (1961). Grain Growth and Phase Transformation of Titanium Oxide During Calcination`. *Journal of the American Ceramic Society, 44*(2 JUN 2006), 120–127.

Imahashi, M., & Takamatsu, N. (1976). The dissolution of titanium minerals in hydrochloric acid and sulphuric acids. *Bulletin of the Chemical Society of Japan, 49*(6), 1549-1553.

Jang, H. D., & Kim, S. K. (2001). Controlled synthesis of titanium dioxide nanoparticles in a modified diffusion flame reactor. *Materials Research Bulletin, 36*(3-4), 627-637.

Jiang, B., Yin, H., Jiang, T., Yan, J., Fan, Z., Li, C., et al. (2005). Size-controlled synthesis of anatase TiO2 nanoparticles by carboxylic acid group-containing organics. *Materials Chemistry and Physics, 92*(2-3), 595-599.

Jianshu Lu, Luciana Pitta Bauermann, Peter Gerstel , Ute Heinrichs, Peter Kopold, Joachim Bill , et al. (2009). Synthesis and characterization of TiO2 nanopowders from peroxotitanium solutions. *Material of Chemistry & Physics*.

Jim Saxton (2007). Nanotechnology: The Future is Coming Sooner Than You Think, . *A JOINT ECONOMIC COMMITTEE STUDY*.

Joo, J., Kwon, S. G., Yu, T., Cho, M., Lee, J., Yoon, J., et al. (2005). Large-Scale Synthesis of TiO2 Nanorods via Nonhydrolytic Sol−Gel Ester Elimination Reaction and Their Application to Photocatalytic Inactivation of E. coli. *The Journal of Physical Chemistry B, 109*(32), 15297-15302.

Juan Yang, S. M., José M. F. Ferreira, (2000). Hydrothermal Synthesis of Nanosized Titania Powders: Influence of Peptization and Peptizing Agents on the Crystalline Phases and Phase Transitions. *Journal of the American Ceramic Society, 83*(6), 1361-1368.

Juan Yang, S. M., José M. F. Ferreira, (2001). Hydrothermal Synthesis of Nanosized Titania Powders: Influence of Tetraalkyl Ammonium Hydroxides on Particle Characteristics. *Journal of the American Ceramic Society, 84*(8), 1696-1702.

Judd, B. T. (1986).

Jung, K., & Park, S. (2001). Effect of calcination temperature and addition of silica, zirconia, alumina on the photocatalytic activity of titania. *Korean Journal of Chemical Engineering, 18*(6), 879-888.

Kathirvelu, S., D'Souza, L., & Dhurai, B. (2008). Nanotechnology applications in textiles. *Indian Journal of Science and Technology, 1(5),* 1-10.

Karvinen, S. (2003). The effects of trace elements on the crystal properties of TiO2. *Solid State Sciences, 5*(5), 811-819.

Kasuga, T., Hiramatsu, M., Hoson, A., Sekino, T., & Niihara, K. (1998). Formation of Titanium Oxide Nanotube. *Langmuir, 14*(12), 3160-3163.

Kavan, L., Rathouský, J., Grätzel, M., Shklover, V., & Zukal, A. (2001). Mesoporous thin film TiO2 electrodes. *Microporous and Mesoporous Materials, 44-45*, 653-659.

Kemp, T. J., & McIntyre, R. A. (2006). Transition metal-doped titanium(IV) dioxide: Characterisation and influence on photodegradation of poly(vinyl chloride). *Polymer Degradation and Stability, 91*(1), 165-194.

Kim, C.-S., Moon, B. K., Park, J.-H., Choi, B.-C., & Seo, H.-J. (2003). Solvothermal synthesis of nanocrystalline TiO2 in toluene with surfactant. *Journal of Crystal Growth, 257*(3-4), 309-315.

Kim, D. H., Woo, S. I., Moon, S. H., Kim, H. D., Kim, B. Y., Cho, J. H., et al. (2005). Effect of Co/Fe co-doping in TiO2 rutile prepared by solid state reaction. *Solid State Communications, 136*(9-10), 554-558.

Kim, D. J., Hahn, S. H., Oh, S. H., & Kim, E. J. (2002). Influence of calcination temperature on structural and optical properties of TiO2 thin films prepared by sol-gel dip coating. *Materials Letters, 57*(2), 355-360.

Kim, K. D., & Kim, H. T. (2001). Synthesis of TiO2 nanoparticles by hydrolysis of TEOT and decrease of particle size using a two-stage mixed method. *Powder Technology, 119*(2-3), 164-172.

Kim, K. D., Kim, S. H., & Kim, H. T. (2005). Applying the Taguchi method to the optimization for the synthesis of TiO2 nanoparticles by hydrolysis of TEOT in micelles. *Colloids and Surfaces A: Physicochemical and Engineering Aspects, 254*(1-3), 99-105.

Kim, S. J., Park, S. D., Jeong, Y. H., & Park, S. (1999). Homogeneous Precipitation of TiO2 Ultrafine Powders from Aqueous TiOCl2 Solution. *Journal of the American Ceramic Society, 82*(4), 927-932.

Klosek, S., & Raftery, D. (2001). Visible Light Driven V-Doped TiO2 Photocatalyst and Its Photooxidation of Ethanol. *The Journal of Physical Chemistry B, 105*(14), 2815-2819.

Koleske, J. V. (1995). *Paint and coating testing manual: fourteenth edition of the Gardner-Sward handbook*: ASTM.

Kominami, H., Kato, J.-i., Murakami, S.-y., Kera, Y., Inoue, M., Inui, T., et al. (1999). Synthesis of titanium(IV) oxide of ultra-high photocatalytic activity: high-temperature hydrolysis of titanium alkoxides with water liberated homogeneously from solvent alcohols. *Journal of Molecular Catalysis A: Chemical, 144*(1), 165-171.

Kormann, C., Bahnemann, D. W., & Hoffmann, M. R. (2002). Preparation and characterization of quantum-size titanium dioxide. *The Journal of Physical Chemistry, 92*(18), 5196-5201.

Kroger, F. A. (1964). The Chemistry of Imperfect Crystals.North-Holland, Amsterdam; Interscience (Wiley), New York, 1964. xvi + 1039 pp. *Science, 145*(3627), 40-41.

Kukovecz, Á., Hodos, M., Kónya, Z., & Kiricsi, I. (2005). Complex-assisted one-step synthesis of ion-exchangeable titanate nanotubes decorated with CdS nanoparticles. *Chemical Physics Letters, 411*(4-6), 445-449.

Lafond, V., Mutin, P. H., & Vioux, A. (2004). Control of the Texture of Titania−Silica Mixed Oxides Prepared by Nonhydrolytic Sol−Gel. *Chemistry of Materials, 16*(25), 5380-5386.

Lasheen, T. A. I. (2005). Chemical benefication of Rosetta ilmenite by direct reduction leaching. *Hydrometallurgy, 76*(1-2), 123-129.

Lazaro, M. J., Echegoyen, Y., Alegre, C., Suelves, I., Moliner, R., & Palacios, J. M. (2008). TiO2 as textural promoter on high loaded Ni catalysts for methane decomposition. *International Journal of Hydrogen Energy, 33*(13), 3320-3329.

Lee, I. Y., Lee, J. B., Park, K. K., & Hong, J. H. (2009). Deactivation of V2O5/Sulfated TiO2 Catalyst Used in Diesel Engine for NOX Reduction with Urea. *Chemical Engineering Transactions, 17*, 67-72.

Lee, S., Jeon, C., & Park, Y. (2004). Fabrication of TiO2 Tubules by Template Synthesis and Hydrolysis with Water Vapor. *Chemistry of Materials, 16*(22), 4292-4295.

Lewis, J. M., & Kydd, R. A. (1991). Adsorption mechanism of phosphoric acid on. gamma. -alumina. *Journal Name: Journal of Catalysis; (United States); Journal Volume: 132:2*, Medium: X; Size: Pages: 465-471.

Li, & Ishigaki, T. (2004). Controlled One-Step Synthesis of Nanocrystalline Anatase and Rutile TiO2 Powders by In-Flight Thermal Plasma Oxidation. *The Journal of Physical Chemistry B, 108*(40), 15536-15542.

Li, B., Wang, X., Yan, M., & Li, L. (2002). Preparation & Characterization of nano-Tio2 Powder. *Materials Chemistry & Physics*.

Li, G. L., & Wang, G. H. (1999). Synthesis of nanometer-sized TiO2 particles by a microemulsion method. *Nanostructured Materials, 11*(5), 663-668.

Li, W., Ni, C., Lin, H., Huang, C. P., & Shah, S. I. (Writer) (2004). Size dependence of thermal stability of TiO2 nanoparticles [Article], *Journal of Applied Physics*: American Institute of Physics.

Li, W., Wang, Y., Lin, H., Shah, S. I., Huang, C. P., Doren, D. J., et al. (2003). Band gap tailoring of Nd[sup 3+]-doped TiO[sub 2] nanoparticles. *Applied Physics Letters, 83*(20), 4143-4145.

Li, Y.-L., & Ishigaki, T. (2002). Synthesis and structural characterization of titanium oxides and composites by thermal plasma oxidation of titanium carbide. *Thin Solid Films, 407*(1-2), 79-85.

Lichtenthaler, H. K. (1988). *Applications of chlorophyll fluorescence in photosynthesis research, stress physiology, hydrobiology and remote sensing*.: Kluwer Academic Publishers.

Lim, H. A. (2003). Bioinformatics, Nanotechnology & SARS. *Symbiosis*, 26-29.

Lim, K. T., Hwang, H. S., Ryoo, W., & Johnston, K. P. (2004). Synthesis of TiO2 Nanoparticles Utilizing Hydrated Reverse Micelles in CO2. *Langmuir, 20*(6), 2466-2471.

Lin, F. (2006). Preparation and Characterization of Polymer TiO2 Nanocomposites via In-situ Polymerization: University of Waterloo.

Lin, H. M., Hsu, T. Y., Tung, C. Y., & Hsu, C. M. (1995). Hydrogen sulfide detection by nanocrystal PT doped TiO2-based gas sensors. *Nanostructured Materials, 6*(5-8), 1001-1004.

Linsebigler, A. L., Lu, G., & Yates, J. T. (2002). Photocatalysis on TiO2 Surfaces: Principles, Mechanisms, and Selected Results. *Chemical Reviews, 95*(3), 735-758.

Liu, Y., Liu, C.-y., & Zhang, Z.-y. (2008). Effects of carboxylic acids on the microstructure and performance of titania nanocrystals. *Chemical Engineering Journal, 138*(1-3), 596-601.

Luca, V., Djajanti, S., & Howe, R. F. (1998). Structural and Electronic Properties of Sol-Gel Titanium Oxides Studied by X-ray Absorption Spectroscopy. *The Journal of Physical Chemistry B, 102*(52), 10650-10657.

Ma, R., Fukuda, K., Sasaki, T., Osada, M., & Bando, Y. (2005). Structural Features of Titanate Nanotubes/Nanobelts Revealed by Raman, X-ray Absorption Fine Structure and Electron Diffraction Characterizations. *The Journal of Physical Chemistry B, 109*(13), 6210-6214.

MacKenzie, K. J. D. (1975). Calcination of titania: V, Kinetics and mechanism of the anatase-rutile transformation in the presence of additives *Transactions and Journal of the British Ceramic Society, 74*(**no. 3**), 77-84.

Madhusudan Reddy, K., Gopal Reddy, C. V., & Manorama, S. V. (2001). Preparation, Characterization, and Spectral Studies on Nanocrystalline Anatase TiO2. *Journal of Solid State Chemistry, 158*(2), 180-186.

Mahmoud, M. H. H., Afifi, A. A. I., & Ibrahim, I. A. (2004). Reductive leaching of ilmenite ore in hydrochloric acid for preparation of synthetic rutile. *Hydrometallurgy, 73*(1-2), 99-109.

Martin, S. T., Morrison, C. L., & Hoffmann, M. R. (1994). Photochemical Mechanism of Size-Quantized Vanadium-Doped TiO2 Particles. *The Journal of Physical Chemistry, 98*(51), 13695-13704.

Maurizio Addamo, V. A., Agatino Di Paola, Elisa Garcıa-Lopez,, Vittorio Loddo, G. M., Raffaele Molinari,, & Leonardo Palmisano, M. S. (2004). Preparation, Characterization, and Photoactivity of Polycrystalline Nanostructured TiO2 Catalysts. *Journal Physical Chemistry B, 108*, 3303-3310.

Miao, L., Tanemura, S., Toh, S., Kaneko, K., & Tanemura, M. (2004a). Fabrication, characterization and Raman study of anatase-TiO2 nanorods by a heating-sol-gel template process. *Journal of Crystal Growth, 264*(1-3), 246-252.

Miao, L., Tanemura, S., Toh, S., Kaneko, K., & Tanemura, M. (2004b). Heating-sol-gel template process for the growth of TiO2 nanorods with rutile and anatase structure. *Applied Surface Science, 238*(1-4), 175-179.

Miao, Z., Xu, D., Ouyang, J., Guo, G., Zhao, X., & Tang, Y. (2002). Electrochemically Induced Sol−Gel Preparation of Single-Crystalline TiO2 Nanowires. *Nano Letters, 2*(7), 717-720.

Millenium Inorganic Chemicals (2007-2009). Titanium Dioxide Manufacturing Process, from http://www.millenniumchem.com/Products+and+Services/Products+by+Type/Titanium+Dioxide+-+Paint+and+Coatings/r_TiO2+Fundamentals/Titanium+Dioxide+Manufacturing+Processes_EN.htm

Mills, A., & Le Hunte, S. (1997). An overview of semiconductor photocatalysis. *Journal of Photochemistry and Photobiology A: Chemistry, 108*(1), 1-35.

Mindat.org (2009). Ilmenite mineral information and data, from http://www.mindat.org/min-2013.html

Mohammad, B., Modirshahla, N., Mohammad Shokri, H. E., & Zeininezhad, A. (2008). The effect of particle size and crystal structure of titanium dioxide nanoparticles on the photocatalytic properties. *Journal of Environmental Science and Health Part A*.

Morris, D., Dou, Y., Rebane, J., Mitchell, C. E. J., Egdell, R. G., Law, D. S. L., et al. (2000). Photoemission and STM study of the electronic structure of Nb-doped TiO2. *Physical Review B, 61*(20), 13445.

Morris, J., & Willis, J. (2007). Nanotechnology White Paper. *U.S. Environmental Protection Agency*(EPA 100/B-07/001), pg 5.

Murray, C. B., Kagan, C. R., & Bawendi, M. G. (2000). SYNTHESIS AND CHARACTERIZATION OF MONODISPERSE NANOCRYSTALS AND CLOSE-PACKED NANOCRYSTAL ASSEMBLIES. *Annual Review of Materials Science, 30*(1), 545-610.

Nabivanets, B. I., & Kudritskaya, L. N. (1967). A study on the polymerization of titanium (IV) in hydrochloric acid solution. *Russian Journal of Inorganic Chemistry, 1.2*(5), 616.

National Nanotechnology Initiatives (2001). What is Nanotechnology, Applications and Products: Putting Technology to Use, from http://www.nano.gov/html/facts/whatIsNano.html, http://www.nano.gov/html/facts/nanoapplicationsandproducts.html

Nedeljkovic, J. M., Saponjic, Z. V., Rakocevic, Z., Jokanovic, V., & Uskokovic, D. P. (1997). Ultrasonic spray pyrolysis of TiO2 nanoparticles. *Nanostructured Materials, 9*(1-8), 125-128.

Nian, J.-N., & Teng, H. (2006). Hydrothermal Synthesis of Single-Crystalline Anatase TiO2 Nanorods with Nanotubes as the Precursor. *The Journal of Physical Chemistry B, 110*(9), 4193-4198.

Niederberger, M., Bartl, M. H., & Stucky, G. D. (2002). Benzyl Alcohol and Titanium Tetrachloride A Versatile Reaction System for the Nonaqueous and Low-Temperature Preparation of Crystalline and Luminescent Titania Nanoparticles. *Chemistry of Materials, 14*(10), 4364-4370.

O'Regan, B., & Gratzel, M. (1991). A low-cost, high-efficiency solar cell based on dye-sensitized colloidal TiO2 films. *Nature, 353*(6346), 737-740.

Oh, S.-M., Kim, S.-S., Lee, J. E., Ishigaki, T., & Park, D.-W. (2003). Effect of additives on photocatalytic activity of titanium dioxide powders synthesized by thermal plasma. *Thin Solid Films, 435*(1-2), 252-258.

Oh, S. W., Park, S. H., & Sun, Y. K. (2006). Hydrothermal synthesis of nano-sized anatase TiO2 powders for lithium secondary anode materials. *Journal of Power Sources, 161*(2), 1314-1318.

Olanipekun, E. (1999). A kinetic study of the leaching of a Nigerian ilmenite ore by hydrochloric acid. *Hydrometallurgy, 53*(1), 1-10.

Oskam, G., Nellore, A., Penn, R. L., & Searson, P. C. (2003). The Growth Kinetics of TiO2 Nanoparticles from Titanium(IV) Alkoxide at High Water/Titanium Ratio. *The Journal of Physical Chemistry B, 107*(8), 1734-1738.

Ovenstone, J., & Yanagisawa, K. (1999). Effect of Hydrothermal Treatment of Amorphous Titania on the Phase Change from Anatase to Rutile during Calcination. *Chemistry of Materials, 11*(10), 2770-2774.

Pan, J. M., & Madey, T. E. (1993). The encapsulation of Fe on TiO2(110). *Catalysis Letters, 20*(3), 269-274.

Parida, K. M., & Pattnayak, P. K. (1996). Studies on PO3-4/ZrO2: I. Effect of H3PO4on Textural and Acidic Properties of ZrO2. *Journal of Colloid and Interface Science, 182*(2), 381-387.

Park, D. G., & Burlitch, J. M. (2002). Nanoparticles of anatase by electrostatic spraying of an alkoxide solution. *Chemistry of Materials, 4*(3), 500-502.

Pattnayak, P. K., & Parida, K. M. (2000). Studies on PO43-/ZrO2: II. Effect of Phosphate Concentration and Activation Temperature on the Catalytic Properties of Zirconia. *Journal of Colloid and Interface Science, 226*(2), 340-345.

Peill, N. J., Bourne, L., & Hoffmann, M. R. (1997). Iron(III)-doped Q-sized TiO2 coatings in a fiber-optic cable photochemical reactor. *Journal of Photochemistry and Photobiology A: Chemistry, 108*(2-3), 221-228.

Peng, T., Zhao, D., Dai, K., Shi, W., & Hirao, K. (2005). Synthesis of Titanium Dioxide Nanoparticles with Mesoporous Anatase Wall and High Photocatalytic Activity. *The Journal of Physical Chemistry B, 109*(11), 4947-4952.

Peng, X., & Chen, A. (2004). Aligned TiO2 nanorod arrays synthesized by oxidizing titanium with acetone. *Journal of Materials Chemistry, 14(16),* 2542-2548.

Pesty, F., Steinruck, H. P., & Madey, T. E. (1995). Thermal stability of Pt films on TiO2(110): evidence for encapsulation. *Surface Science, 339*(1-2), 83-95.

Phillips, L. G., & Barbano, D. M. (1997). The Influence of Fat Substitutes Based on Protein and Titanium Dioxide on the Sensory Properties of Lowfat Milks. *Journal of Dairy Science, 80*(11), 2726-2731.

Pierre, A. C., & Pajonk, G. M. (2002). Chemistry of Aerogels and Their Applications. *Chemical Reviews, 102*(11), 4243-4266.

Popov, A. P., Priezzhev, A. V., Lademann, J., & Myllyla, R. (2005). TiO2 nanoparticles as an effective UV-B radiation skin-protective compound in sunscreens. *Journal of Physics D: Applied Physics, 38*(15), 2564-2570.

Porter, J. F., Li, Y. G., & Chan, C. K. (1999). The effect of calcination on the microstructural characteristics and photoreactivity of Degussa P-25 TiO2. *Journal of Materials Science, 34*(7), 1523-1531.

Qian, L., Du, Z.-L., Yang, S.-Y., & Jin, Z.-S. (2005). Raman study of titania nanotube by soft chemical process. *Journal of Molecular Structure, 749*(1-3), 103-107.

Qu, J., Zhang, X., Wang, Y., & Xie, C. (2005). Electrochemical reduction of CO2 on RuO2/TiO2 nanotubes composite modified Pt electrode. *Electrochimica Acta, 50*(16-17), 3576-3580.

Ramakrishna, G., & Ghosh, H. N. (2003). Optical and Photochemical Properties of Sodium Dodecylbenzenesulfonate (DBS)-Capped TiO2 Nanoparticles Dispersed in Nonaqueous Solvents. *Langmuir, 19*(3), 505-508.

Ramis, G., Rossi, P. F., Busca, G., Lorenzelli, V., La Ginestra, A., & Patrono, P. (2002). Phosphoric acid on oxide carriers. 2. Surface acidity and reactivity toward olefins. *Langmuir, 5*(4), 917-923.

Ranade, M. R., Navrotsky, A., Zhang, H. Z., Banfield, J. F., Elder, S. H., Zaban, A., et al. (2002). Energetics of Nanocrystalline TiO2. *Proceedings of the National Academy of Sciences of the United States of America, 99*(9), 6476-6481.

Ranjit, K. T., & Viswanathan, B. (1997). Synthesis, characterization and photocatalytic properties of iron-doped TiO2 catalysts. *Journal of Photochemistry and Photobiology A: Chemistry, 108*(1), 79-84.

Ratajska, H. (1992). The effect of certain promoters on TiO2 crystal structure transformation. *Journal of Thermal Analysis and Calorimetry, 38*(9), 2109-2114.

Ruiz, A. M., Dezanneau, G., Arbiol, J., Cornet, A., & Morante, J. R. (2004). Insights into the Structural and Chemical Modifications of Nb Additive on TiO2 Nanoparticles. *Chemistry of Materials, 16*(5), 862-871.

Ruiz, A. M., Sakai, G., Cornet, A., Shimanoe, K., Morante, J. R., & Yamazoe, N. (2003). Cr-doped TiO2 gas sensor for exhaust NO2 monitoring. *Sensors and Actuators B: Chemical, 93*(1-3), 509-518.

Sahoo, C., Gupta, A. K., & Pal, A. (2005). Photocatalytic degradation of Methyl Red dye in aqueous solutions under UV irradiation using Ag+ doped TiO2. *Desalination, 181*(1-3), 91-100.

Sakai, N., Ebina, Y., Takada, K., & Sasaki, T. (2004). Electronic Band Structure of Titania Semiconductor Nanosheets Revealed by Electrochemical and Photoelectrochemical Studies. *Journal of the American Chemical Society, 126*(18), 5851-5858.

Samantaray, S. K., & Parida, K. (2001). Studies on anion-promoted titania: 3. Effect of concentration and source of phosphate ion, method of preparation, and activation temperature on redox, acid-base, textural and catalytic properties of titania. *Journal of Molecular Catalysis A: Chemical, 176*(1-2), 151-163.

Sato, H., Ono, K., Sasaki, T., & Yamagishi, A. (2003). First-Principles Study of Two-Dimensional Titanium Dioxides. *The Journal of Physical Chemistry B, 107*(36), 9824-9828.

Sberveglieri, G. (1995). Recent developments in semiconducting thin-film gas sensors. *Sensors and Actuators B: Chemical, 23*(2-3), 103-109.

Schwarz, J. A., Contescu, C., & Contescu, A. (1995). Methods for Preparation of Catalytic Materials. *Chemical Reviews, 95*(3), 477-510.

Scolan, E., & Sanchez, C. (1998). Synthesis and Characterization of Surface-Protected Nanocrystalline Titania Particles. *Chemistry of Materials, 10*(10), 3217-3223.

Seagle, S. R. (2000). *Titanium and Titanium Alloys*: John Wiley & Sons, Inc.

Seifried, S., Winterer, M., & Hahn, H. (2000). Nanocrystalline Titania Films and Particles by Chemical Vapor Synthesis. *Chemical Vapor Deposition, 6*(5), 239-244.

Selhofer, H., & Muller, R. (1999). Comparison of pure and mixed coating materials for AR coatings for use by reactive evaporation on glass and plastic lenses. *Thin Solid Films, 351*(1-2), 180-183.

Seo, D.-S., Lee, J.-K., & Kim, H. (2001). Preparation of nanotube-shaped TiO2 powder. *Journal of Crystal Growth, 229*(1-4), 428-432.

Serpone, N., Lawless, D., Khairutdinov, R., & Pelizzetti, E. (2002). Subnanosecond Relaxation Dynamics in TiO2 Colloidal Sols (Particle Sizes Rp = 1.0-13.4 nm). Relevance to Heterogeneous Photocatalysis. *The Journal of Physical Chemistry, 99*(45), 16655-16661.

Shah, S. I., Li, W., Huang, C. P., Jung, O., & Ni, C. (2002). Study of Nd3+, Pd2+, Pt4+, and Fe3+ dopant effect on photoreactivity of TiO2 nanoparticles. *Proceedings of the National Academy of Sciences of the United States of America, 99*(Suppl 2), 6482-6486.

Shanmugam, S., & Gedanken, A. (2007). Carbon-Coated Anatase TiO2 Nanocomposite as a High-Performance Electrocatalyst Support. *Small, 3*(7), 1189-1193.

Shannon, R. D., & Pask, J. A. (1965). Kinetics of the Anatase-Rutile Transformation. *Journal of the American Ceramic Society, 48*(8), 391-398.

Sinha, H. N. (1984). *Hydrochloric acid leaching of ilmenite* (No. 3053). Melbourne (Australia): Australasian Institute of Mining and Metallurgy.

Sorantin, P. I., & Schwarz, K. (2002). Chemical bonding in rutile-type compounds. *Inorganic Chemistry, 31*(4), 567-576.

Spurr, R. A., & Myers, H. (2002). Quantitative Analysis of Anatase-Rutile Mixtures with an X-Ray Diffractometer. *Analytical Chemistry, 29*(5), 760-762.

Stashans, A., Lunell, S., & Grimes, R. W. (1996). Theoretical study of perfect and defective TiO2 crystals. *Journal of Physics and Chemistry of Solids, 57*(9), 1293-1301.

Sugimoto, T., Okada, K., & Itoh, H. (1997). Synthetic of Uniform Spindle-Type Titania Particles by the Gel-Sol Method. *Journal of Colloid and Interface Science, 193*(1), 140-143.

Sugimoto, T., Zhou, X., & Muramatsu, A. (2002). Synthesis of Uniform Anatase TiO2 Nanoparticles by Gel-Sol Method: 1. Solution Chemistry of Ti(OH)n(4-n)+ Complexes. *Journal of Colloid and Interface Science, 252*(2), 339-346.

Sugimoto, T., Zhou, X., & Muramatsu, A. (2003). Synthesis of uniform anatase TiO2 nanoparticles by gel-sol method: 4. Shape control. *Journal of Colloid and Interface Science, 259*(1), 53-61.

Swamy, V., Kuznetsov, A., Dubrovinsky, L. S., Caruso, R. A., Shchukin, D. G., & Muddle, B. C. (2005). Finite-size and pressure effects on the Raman spectrum of nanocrystalline anatase Ti O2. *Physical Review B, 71*(18), 184302.

T. Aarthi, Prashanthi Narahari, & Madras, G. (2007). Photocatalytic degradation of Azure and Sudan dyes using nano TiO2. *Journal of Hazardous Material, 149*, 725-734.

T. Kasuga, M. H., A. Hoson, T. Sekino, K. Niihara, (1999). Titania Nanotubes Prepared by Chemical Processing. *Advanced Materials, 11*(15), 1307-1311.

Tang, H., Lévy, F., Berger, H., & Schmid, P. E. (1995). Urbach tail of anatase TiO2. *Physical Review B, 52*(11), 7771.

Tang, H., Prasad, K., Sanjines, R., & Levy, F. (1995). TiO2 anatase thin films as gas sensors. *Sensors and Actuators B: Chemical, 26*(1-3), 71-75.

Tang, J., Redl, F., Zhu, Y., Siegrist, T., Brus, L. E., & Steigerwald, M. L. (2005). An Organometallic Synthesis of TiO2 Nanoparticles. *Nano Letters, 5*(3), 543-548.

Taverner, A. E., Gulino, A., Egdell, R. G., & Tate, T. J. (1995). A photoemission study of electron states in Sb-ion implanted TiO2(110). *Applied Surface Science, 90*(3), 383-387.

Tian, Z. R., Voigt, J. A., Liu, J., Mckenzie, B., & Xu, H. (2003). Large Oriented Arrays and Continuous Films of TiO2-Based Nanotubes. *Journal of the American Chemical Society, 125*(41), 12384-12385.

TiPE (2003-2008). Advanced Nano Photo Energy Technology, from http://www.tipe.com.cn/index.htm

Trentler, T. J., Denler, T. E., Bertone, J. F., Agrawal, A., & Colvin, V. L. (1999). Synthesis of TiO2 Nanocrystals by Nonhydrolytic Solution-Based Reactions. *Journal of the American Chemical Society, 121*(7), 1613-1614.

Tsuchida, H., Narita, E., Takeuchi, H., Adachi, M., & Okabe, T. (1982). Manufacture of high pure titanium(IV) oxide by the chloride process: I. Kinetic study on leaching of ilmenite ore in concentrated hydrochloric acid solution. *Bulletin of the Chemical Society of Japan, 55*(6), 1934-1938.

Turkoglu, M., & Yener, S. (1997). Design and in vivo evaluation of ultrafine inorganic-oxide-containing-sunscreen formulations. *International Journal of Cosmetic Science, 19*(4), 193-201.

Uekawa, N., Kajiwara, J., Kakegawa, K., & Sasaki, Y. (2002). Low Temperature Synthesis and Characterization of Porous Anatase TiO2 Nanoparticles. *Journal of Colloid and Interface Science, 250*(2), 285-290.

Valentine, A. M. (2006). *Titanium: Inorganic & Coordination Chemistry*: John Wiley & Sons, Ltd.

van Dyk, J. P., Vegter, N. M., & Pistorius, P. C. (2002). Kinetics of ilmenite dissolution in hydrochloric acid. *Hydrometallurgy, 65*(1), 31-36.

Vioux, A. (1997). Nonhydrolytic Solâˆ'Gel Routes to Oxides. *Chemistry of Materials, 9*(11), 2292-2299.

Viswanath, R. N., & Ramasamy, S. (1998). Study of TiO2 nanocrystallites in TiO2-SiO2 composites. *Colloids and Surfaces A: Physicochemical and Engineering Aspects, 133*(1-2), 49-56.

Von Kraemer, S., Wikander, K., Lindbergh, G., Lundblad, A., & Palmqvist, A. E. C. (2008). Evaluation of TiO2 as catalyst support in Pt-TiO2/C composite cathodes for the proton exchange membrane fuel cell. *Journal of Power Sources, 180*(1), 185-190.

Vorkapic, D., & Matsoukas, T. (1999). Reversible Agglomeration: A Kinetic Model for the Peptization of Titania Nanocolloids. *Journal of Colloid and Interface Science, 214*(2), 283-291.

Vukicevic, U., Ziemian, S., Bismarck, A., & Shaffer, M. S. P. (2008). Self-cleaning anatase nanorods: photocatalytic removal of structure directing agents and subsequent surface modification. *Journal of Materials Chemistry, 18*(29), 3448-3453.

Wang, C.-C., Zhang, Z., & Ying, J. Y. (1997). Photocatalytic decomposition of halogenated organics over nanocrystalline titania. *Nanostructured Materials, 9*(1-8), 583-586.

Wang, M., Guo, D.-j., & Li, H.-l. (2005). High activity of novel Pd/TiO2 nanotube catalysts for methanol electro-oxidation. *Journal of Solid State Chemistry, 178*(6), 1996-2000.

Wang, Y. Q., Hu, G. Q., Duan, X. F., Sun, H. L., & Xue, Q. K. (2002). Microstructure and formation mechanism of titanium dioxide nanotubes. *Chemical Physics Letters, 365*(5-6), 427-431.

Wang, Y. Q., Yu, X. J., & Sun, D. Z. (2007). Synthesis, characterization, and photocatalytic activity of TiO2-xNx nanocatalyst. *Journal of Hazardous Materials, 144*(1-2), 328-333.

Wang, Z., Helmersson, U., & Käll, P.-O. (2002). Optical properties of anatase TiO2 thin films prepared by aqueous sol-gel process at low temperature. *Thin Solid Films, 405*(1-2), 50-54.

Wei, H., Wu, Y., Lun, N., & Zhao, F. (2004). Preparation and photocatalysis of TiO2 nanoparticles co-doped with nitrogen and lanthanum. *Journal of Materials Science, 39*(4), 1305-1308.

Wei, M., Konishi, Y., Zhou, H., Sugihara, H., & Arakawa, H. (2004). A simple method to synthesize nanowires titanium dioxide from layered titanate particles. *Chemical Physics Letters, 400*(1-3), 231-234.

Welham, N. J., & Llewellyn, D. J. (1998). Mechanical enhancement of the dissolution of ilmenite. *Minerals Engineering, 11*(9), 827-841.

Wen-Yu Wang, A. I., Young Ku (2008). Photocatalytic degradation of Acid Red 4 using a titanium dioxide membrane supported on a porous ceramic tube. *Water Research*, 1 - 8.

Wen, B.-M., Liu, C.-Y., & Liu, Y. (2005). Solvothermal synthesis of ultralong single-crystalline TiO2 nanowires. *New Journal of Chemistry, 29*(7), 969-971.

Wen, B., Liu, C., & Liu, Y. (2005a). Bamboo-Shaped Ag-Doped TiO2 Nanowires with Heterojunctions. *Inorganic Chemistry, 44*(19), 6503-6505.

Wen, B., Liu, C., & Liu, Y. (2005b). Depositional Characteristics of Metal Coating on Single-Crystal TiO2 Nanowires. *The Journal of Physical Chemistry B, 109*(25), 12372-12375.

Wen, C. Z., Jiang, H. B., Qiao, S. Z., Yang, H. G., & Lu, G. Q. Synthesis of high-reactive facets dominated anatase TiO2. *Journal of Materials Chemistry, 21*(20), 7052-7061.

West, R. H., Beran, G. J. O., Green, W. H., & Kraft, M. (2007). First-Principles Thermochemistry for the Production of TiO2 from TiCl4. *The Journal of Physical Chemistry A, 111*(18), 3560-3565.

Wight, A. P., & Davis, M. E. (2002). Design and Preparation of Organic−Inorganic Hybrid Catalysts. *Chemical Reviews, 102*(10), 3589-3614.

Wikipedia (2009a). Citric acid. from Wikimedia Foundation, Inc.: http://en.wikipedia.org/wiki/Citric_acid

Wikipedia (2009b). Titanium dioxide. http://en.wikipedia.org/wiki/Tio2

Wu, J.-J., & Yu, C.-C. (2004). Aligned TiO2 Nanorods and Nanowalls. *The Journal of Physical Chemistry B, 108*(11), 3377-3379.

Wu, J.-M., Shih, H. C., & Wu, W.-T. (2005). Electron field emission from single crystalline TiO2 nanowires prepared by thermal evaporation. *Chemical Physics Letters, 413*(4-6), 490-494.

Wu, J.-M., Shih, H. C., Wu, W.-T., Tseng, Y.-K., & Chen, I. C. (2005). Thermal evaporation growth and the luminescence property of TiO2 nanowires. *Journal of Crystal Growth, 281*(2-4), 384-390.

Wu, M., Long, J., Huang, A., Luo, Y., Feng, S., & Xu, R. (1999). Microemulsion-Mediated Hydrothermal Synthesis and Characterization of Nanosize Rutile and Anatase Particles. *Langmuir, 15*(26), 8822-8825.

Wu, Z. Y., Ouvrard, G., Gressier, P., & Natoli, C. R. (1997). Ti and O K edges for titanium oxides by multiple scattering calculations: Comparison to XAS and EELS spectra. *Physical Review B, 55*(16), 10382.

Xia, H.-B., Liu, X.-Y., & Zhang, K.-Q. (2008). Nano-Architecture by Molecular Structure-Directing Agent. *Chemistry of Materials, 20*(7), 2432-2434.

Xiao-Lin Li, Q. P., Jia-Xiang Yi, Xun Wang, Yadong Li, (2006). Near Monodisperse TiO_{<FONT SIZE='-1'>2</FONT>} Nanoparticles and Nanorods. *Chemistry - A European Journal, 12*(8), 2383-2391.

Xiao, X., Liao, D., Zhang, H., & Chen, H. (2007). Synthesis of TiO2 nano-particles and their photocatalytic activity for formaldehyde and methyl orange degradation. *Frontiers of Chemical Engineering in China, 1*(2), 178-183.

Xinjian Feng, J. Z., Lei Jiang, (2005). The Fabrication and Switchable Superhydrophobicity of TiO_{<FONT SIZE='-1'>2</FONT>} Nanorod Films13. *Angewandte Chemie International Edition, 44*(32), 5115-5118.

Xu, J.-C., Lu, M., Guo, X.-Y., & Li, H.-L. (2005). Zinc ions surface-doped titanium dioxide nanotubes and its photocatalysis activity for degradation of methyl orange in water. *Journal of Molecular Catalysis A: Chemical, 226*(1), 123-127.

Xu, J., Ge, J.-P., & Li, Y.-D. (2006). Solvothermal Synthesis of Monodisperse PbSe Nanocrystals. *The Journal of Physical Chemistry B, 110*(6), 2497-2501.

Xu, K. (2007). Preparation and Characterization of Nano-ZnFe2O4/TiO2 Films. *Journal of Natural Gas Chemistry, 16*(1), 100-105.

Xun, W., Jing, Z., Qing, P., & Yadong, L. (2005). A general strategy for nanocrystal synthesis, *Nature* (Vol. 437, pp. 121-124): Nature Publishing Group.

Y. Lan, X. P. G., H. Y. Zhu, Z. F. Zheng, T. Y. Yan, F. Wu, S. P. Ringer, D. Y. Song, (2005). Titanate Nanotubes and Nanorods Prepared from Rutile Powder. *Advanced Functional Materials, 15*(8), 1310-1318.

Yan, X., He, J., G. Evans, D., Duan, X., & Zhu, Y. (2005). Preparation, characterization and photocatalytic activity of Si-doped and rare earth-doped TiO2 from mesoporous precursors. *Applied Catalysis B: Environmental, 55*(4), 243-252.

Yang, J., Mei, S., & Ferreira, J. M. F. (2001). Hydrothermal synthesis of TiO2 nanopowders from tetraalkylammonium hydroxide peptized sols. *Materials Science and Engineering: C, 15*(1-2), 183-185.

Yang, P., Zhao, D., Margolese, D. I., Chmelka, B. F., & Stucky, G. D. (1999). Block Copolymer Templating Syntheses of Mesoporous Metal Oxides with Large Ordering Lengths and Semicrystalline Framework. *Chemistry of Materials, 11*(10), 2813-2826.

Yang, S., & Gao, L. (2005a). Fabrication and Characterization of Nanostructurally Flowerlike Aggregates of TiO2 via a Surfactant-free Solution Route: Effect of Various Reaction Media. *Chemistry Letters, 34*(7), 1044-1045.

Yang, S., & Gao, L. (2005b). A Facile and One-pot Synthesis of High Aspect Ratio Anatase Nanorods Based on Aqueous Solution. *Chemistry Letters, 34*(7), 972-973.

Yang, S., & Gao, L. (2005c). Low-temperature Synthesis of Crystalline TiO2 Nanorods: Mass Production Assisted by Surfactant. *Chemistry Letters, 34*(7), 964-965.

Yang, T. Y., Lin, H. M., Wei, B. Y., Wu, C. Y., & Lin, C. K. (2003). UV Enhancement of the Gas sensing Properties of nano-TiO2. *Reviews on Advanced Material Science, 4*, 48-54.

Yao, B. D., Chan, Y. F., Zhang, X. Y., Zhang, W. F., Yang, Z. Y., & Wang, N. (2003). Formation mechanism of TiO[sub 2] nanotubes. *Applied Physics Letters, 82*(2), 281-283.

Ye, X., Sha, J., Jiao, Z., & Zhang, L. (1997). Thermoanalytical characteristic of nanocrystalline brookite-based titanium dioxide. *Nanostructured Materials, 8*(7), 919-927.

Yin, H., Wada, Y., Kitamura, T., Kambe, S., Murasawa, S., Mori, H., et al. (2001). Hydrothermal synthesis of nanosized anatase and rutile TiO2 using amorphous phase TiO2. *Journal of Materials Chemistry, 11*(6), 1694-1703.

Yin, H., Wada, Y., Kitamura, T., Sumida, T., Hasegawa, Y., & Yanagida, S. (2002). Novel synthesis of phase-pure nano-particulate anatase and rutile TiO2 using TiCl4 aqueous solutions. *Journal of Materials Chemistry, 12*(2), 378-383.

Yongping, L., Shangang, D., & Fuan, G. (2002). The Research of Modification of Interior Wall Paint by Nano-TiO2. *Architectural Decoration and Finishing Materials*.

Yoshida, R., Suzuki, Y., & Yoshikawa, S. (2005). Syntheses of TiO2(B) nanowires and TiO2 anatase nanowires by hydrothermal and post-heat treatments. *Journal of Solid State Chemistry, 178*(7), 2179-2185.

Yu-de, W., Chun-lai, M., Xiao-dan, S., & Heng-de, L. (2003). Synthesis and characterization of mesoporous TiO2 with wormhole-like framework structure. *Applied Catalysis A: General, 246*(1), 161-170.

Yu, J., Wang, G., Cheng, B., & Zhou, M. (2007). Effects of hydrothermal temperature and time on the photocatalytic activity and microstructures of bimodal mesoporous TiO2 powders. *Applied Catalysis B: Environmental, 69*(3-4), 171-180.

Yu, J., Yu, J. C., Leung, M. K. P., Ho, W., Cheng, B., Zhao, X., et al. (2003). Effects of acidic and basic hydrolysis catalysts on the photocatalytic activity and microstructures of bimodal mesoporous titania. *Journal of Catalysis, 217*(1), 69-78.

Yu, J. C., Zhang, L., Zheng, Z., & Zhao, J. (2003). Synthesis and Characterization of Phosphated Mesoporous Titanium Dioxide with High Photocatalytic Activity. *Chemistry of Materials, 15*(11), 2280-2286.

Yu, J. G., Yu, H. G., Cheng, B., Zhao, X. J., Yu, J. C., & Ho, W. K. (2003). The Effect of Calcination Temperature on the Surface Microstructure and Photocatalytic Activity of TiO2 Thin Films Prepared by Liquid Phase Deposition. *The Journal of Physical Chemistry B, 107*(50), 13871-13879.

Yuan, Z.-Y., & Su, B.-L. (2004). Titanium oxide nanotubes, nanofibers and nanowires. *Colloids and Surfaces A: Physicochemical and Engineering Aspects, 241*(1-3), 173-183.

Yue, Y., & Gao, Z. (2000). Synthesis of mesoporous TiO2 with a crystalline framework. *Chemical Communications*(18), 1755-1756.

Zaban, A., Aruna, S. T., Tirosh, S., Gregg, B. A., & Mastai, Y. (2000). The Effect of the Preparation Condition of TiO2 Colloids on Their Surface Structures. *The Journal of Physical Chemistry B, 104*(17), 4130-4133.

Zhang, H., & Banfield, J. F. (1998). Thermodynamic analysis of phase stability of nanocrystalline titania. *Journal of Material Chemistry, 8*(9), 2073.

Zhang, H., & Banfield, J. F. (2000). Understanding Polymorphic Phase Transformation Behavior during Growth of Nanocrystalline Aggregates: Insights from TiO2. *The Journal of Physical Chemistry B, 104*(15), 3481-3487.

Zhang, L., Zhu, Y., He, Y., Li, W., & Sun, H. (2003). Preparation and performances of mesoporous TiO2 film photocatalyst supported on stainless steel. *Applied Catalysis B: Environmental, 40*(4), 287-292.

Zhang, Q., & Gao, L. (2003). Preparation of Oxide Nanocrystals with Tunable Morphologies by the Moderate Hydrothermal Method: Insights from Rutile TiO2. *Langmuir, 19*(3), 967-971.

Zhang, Q., Gao, L., & Guo, J. (2000a). Effect of hydrolysis conditions on morphology and crystallization of nanosized TiO2 powder. *Journal of the European Ceramic Society, 20*(12), 2153-2158.

Zhang, Q., Gao, L., & Guo, J. (2000b). Effects of calcination on the photocatalytic properties of nanosized TiO2 powders prepared by TiCl4 hydrolysis. *Applied Catalysis B: Environmental, 26*(3), 207-215.

Zhang, R., Gao, L., & Zhang, Q. (2004). Photodegradation of surfactants on the nanosized TiO2 prepared by hydrolysis of the alkoxide titanium. *Chemosphere, 54*(3), 405-411.

Zhang, Y. X., Li, G. H., Jin, Y. X., Zhang, Y., Zhang, J., & Zhang, L. D. (2002). Hydrothermal synthesis and photoluminescence of TiO2 nanowires. *Chemical Physics Letters, 365*(3-4), 300-304.

Zhao, Y., Li, F., Zhang, R., Evans, D. G., & Duan, X. (2002). Preparation of Layered Double-Hydroxide Nanomaterials with a Uniform Crystallite Size Using a New Method Involving Separate Nucleation and Aging Steps. *Chemistry of Materials, 14*(10), 4286-4291.

Zhihua Zhang, X. Z., Shuhua Liu, Dongfei Li, Mingyong Han, (2005). Aminolysis Route to Monodisperse Titania Nanorods with Tunable Aspect Ratio13. *Angewandte Chemie International Edition, 44*(22), 3466-3470.

Zhu, J., Yang, J., Bian, Z.-F., Ren, J., Liu, Y.-M., Cao, Y., et al. (2007). Nanocrystalline anatase TiO2 photocatalysts prepared via a facile low temperature nonhydrolytic sol-gel reaction of TiCl4 and benzyl alcohol. *Applied Catalysis B: Environmental, 76*(1-2), 82-91.

Zhu, Y. C., & Ding, C. X. (1999). Oriented growth of nano-TiO2 whiskers. *Nanostructured Materials, 11*(3), 427-431.

Zimmermann, R., Steiner, P., Claessen, R., Reinert, F., & Hüfner, S. (1998). Electronic structure systematics of 3d transition metal oxides. *Journal of Electron Spectroscopy and Related Phenomena, 96*(1-3), 179-186.